

Broad-spectrum Antiviral Nanoparticles: a morphological CryoEM Study on the Interaction of Nanoparticles and Viruses

THÈSE N° 7906 (2017)

PRÉSENTÉE LE 4 AOÛT 2017

À LA FACULTÉ DES SCIENCES ET TECHNIQUES DE L'INGÉNIEUR

LABORATOIRE DES NANOMATÉRIAUX SUPRAMOLÉCULAIRES ET INTERFACES - CHAIRE CONSTELLUM

PROGRAMME DOCTORAL EN SCIENCE ET GÉNIE DES MATÉRIAUX

ÉCOLE POLYTECHNIQUE FÉDÉRALE DE LAUSANNE

POUR L'OBTENTION DU GRADE DE DOCTEUR ÈS SCIENCES

PAR

Marie MÜLLER

acceptée sur proposition du jury:

Prof. C. Hébert, présidente du jury
Prof. F. Stellacci, directeur de thèse
Prof. D. Lembo, rapporteur
Prof. B. Rothen-Rutishauser, rapporteuse
Prof. V. Tileli, rapporteuse



ÉCOLE POLYTECHNIQUE
FÉDÉRALE DE LAUSANNE

Suisse
2017

Abstract

Viral infections affect millions of people every year, yet broad-spectrum virucidal therapies are not available. Antiviral substances in current use act on specific viral mechanisms against only a small number of viruses. Virustatic materials interfere with the viral infection cycle before the cells become infected. By targeting highly conserved attachment receptors, they can be broad-spectrum and non-toxic. However, their reversible virus binding renders them ineffective *in-vivo* and therapeutically irrelevant. Broad-spectrum virucidal substances that irreversibly inhibit viral infectivity do exist, but are too toxic for therapeutic applications. An ideal antiviral method would be broad-spectrum, virucidal instead of virustatic and therefore irreversible, and non-toxic.

The scientific literature describes gold-nanoparticles (NPs) with 2-mercaptoethanesulfonate (MES) ligands as virustatic since these NPs only bind reversibly to viral attachment ligands. In our research group, we postulated that by lengthening the ligands to 11-mercapto-1-undecanesulfonate (MUS), their binding would be stronger and induce a force on the viruses sufficient to damage the virus irreversibly. Virological testing indicated that these MUS NPs do exhibit a virucidal effect against a wide range of viruses.

The present study was able to show the structural damage to viruses in their near-native state imaged in cryo-electron microscopy (cryoEM). We found that while virustatic MES NPs attach only in small numbers to the viruses virucidal MUS NPs avidly attach to viruses and show a clear progression towards fully NP-covered viruses, which we interpret as the morphology of the virucidal endpoint.

The analysis of the immediate interaction of virucidal NPs and viruses showed that virucidal NPs bind to proteins vital to the viral infection cycle:

- (1) Virucidal NPs bind to glycoproteins on the viral envelope that exert a force onto the viral envelope leading to envelope breakage.
- (2) Virucidal NPs attach to released viral capsids that break upon interaction with virucidal NPs and become fully NP covered, which is the morphology of the virucidal endpoint.

This project provided an opportunity to advance the field of NPs – based antivirals. It is the first study to provide a solution-state visualisation of the interaction of viruses and virucidal NPs. The study further offers important insight to the association of single NPs with viral proteins of the envelope and virus capsid as well as their effect upon them, and offers a new approach for the future of broad-spectrum non-toxic virucidal therapies.

Keywords

Nanoparticles, Viruses, CryoEM, CryoET, broad-spectrum antivirals, virustatic, virucidal, HSPG, HSV

Kurzdarstellung

Virusinfektionen betreffen jedes Jahr Millionen Menschen, dennoch gibt es bisher keine breitband-antiviralen Therapien. Existierende antivirale Substanzen sind spezifisch für bestimmte Wirkungsmechanismen und nur für wenige Viren verfügbar. Virustatische Wirkstoffe hingegen hemmen die Viren bevor die Zellen infiziert werden. Indem sie evolutionär konservierte Viren-Bindungsrezeptoren blockieren, können sie eine Vielzahl von Viren inhibieren und sind dabei von geringer Zelltoxizität. Da sie aber nur reversibel an Viren binden, sind sie leider *in-vivo* ineffizient und damit therapeutisch irrelevant. Es gibt Substanzen, die breitgefächert viele Viren inhibieren indem sie irreversibel ihre Infektiosität hemmen, also viruzid wirken. Sie sind jedoch zu toxisch für eine therapeutische Anwendung. Eine ideale antivirale Therapie wäre breitbandwirksam, nicht toxisch und viruzid.

In der wissenschaftlichen Literatur wurden antivirale Gold-Nanopartikel mit 2-Mercaptoethansulfonat (MES) beschrieben. Da sie aber nur reversibel an die Viren binden sind sie virustatisch. In unserer Forschungsgruppe haben wir festgestellt, dass bei Verlängerung der Liganden der Nanopartikel zu 11-mercapto-1-undecansulfonat (MUS) deren Bindung an die Viren stark genug wird um diese irreversibel zu schädigen. Virologische Versuche ergaben, dass diese MUS Nanopartikel einen viruziden Effekt gegen eine große Bandbreite von Viren aufweisen.

In der vorliegenden Studie konnten Nanopartikel-induzierte Schäden an Viren cryo-elektronen-mikroskopisch dargestellt werden. Wir konnten zeigen das virustatische MES Nanopartikel nur in geringer Zahl an Viren binden. Viruzide MUSOT Nanopartikel hingegen binden zahlreich und in zunehmendem Maße an die Viren bis diese vollkommen von Nanopartikeln umgeben sind, wir interpretieren dies als die Morphologie des viruziden Endpunkts.

Eine Analyse der initialen Nanopartikel -Virus Interaktion zeigt, dass viruzide Nanopartikel an Proteinen binden, welche essentiell für den viralen Infektionszyklus sind:

- (1) Viruzide Nanopartikel binden sich an virale Zuckerproteine, welche eine Kraft auf die Virushülle ausüben und ein Brechen dieser bewirken.
- (2) Viruzide Nanopartikel binden zahlreich und stark an die dann freigesetzten Virus-kapside, welche durch diese Interaktion mit den Nanopartikel aufbrechen und vollständig von Nanopartikeln umgeben werden und somit wieder die Morphologie des viruziden Endpunkts aufweisen.

Dieses Projekt konnte Fortschritte im Bereich von antiviralen Nanopartikel erreichen. Es ist die erste Studie die eine Interaktion der Viren und der viruziden Nanopartikel in Lösung bildlich darstellen konnte. Die Studie bietet wichtige Einblicke in die Bindungsprozesse von einzelnen Nanopartikel mit viralen Proteinen von Viruskapsid und Virushülle, sowie deren Auswirkungen. Sie bietet einen neuen Ansatz für die Zukunft von Breitband-, nicht-toxischen viruziden Therapien.

Schlagwörter

Nanopartikel, Viren, CryoEM, CryoET, Breitband Antivirale Therapien, virustatisch, viruzid, HSPG, HSV

Acknowledgements

I would like to deeply thank everyone who has been involved in this endeavour for the amazing time in the last years, who has helped, supported, surprised, inspired me on the way though these crazy years. I would like to thank.....

Prof. Francesco Stellacci without whom none of this there would even have been possible, for all his support, ideas, discussions, opportunities.

My jury, Prof. David Lembo, Prof. Barbara Rothen-Rutishauser, Prof. Vasiliki Tileli, and Prof. Cécile Hébert, for kindly accepting to evaluate my work.

Paulo Henrique Jacob Silva – simply for everything – for motivation, discussions, keeping a good grip to the ground and staying sound in crazy times

My cryo sister Pelin Güven Zekiye for wonderful long cryo nights and weekends at the microscope, for the wonderful time learning together and making it through everything that comes whichever way.

Davide Demurtas and Ricardo-Guerrero-Ferreira for introducing me to the most amazing technique ever!

All the virus people: Valeria Cagno, Nicholas Dorma, Özgün Kocabiyik, Emma-Rose Janecek for all discussions, explanations, help, support and last minutes craziness.

The entire SUNMIL group with all current and past members for inspirations, distraction and wonderful discussions day and night. Special thanks go to the night workers Zhi Luo and Huayan Yang for never being alone, ever far after midnight.

To Marta Marta Diez Castelnou for her constructive criticism.

All the welcoming, incredibly helpful people from BIOP, CIME, GR-CE.

My family - the lovely girls for training me for night shifts and flooding me with endorphins.

To Karsten my dear for making this time even possible for me and the girls – für den besten 2000% Papa der ganzen Welt.

In keiner Sprache kann ich auch nur ansatzweise ausdrücken wie dankbar ich meiner Familie bin, der kleinen, großen und der ganz großen. Es ist so wundervoll, das es Euch gibt. An Maike, an Micha, an Matti, an Omi und Opi und Kika, an ganz Freesenort und alle lieben Menschen die dazu gehören, an Sebastian und Anna, an Wolf und Madeleine. Vielen Dank für die Liebe und Hilfe alles fertigzustellen, für die vielen Reisen und die Hilfe mit den Kleinen.

Lausanne, le 17 Mai 2014

Table of contents

Abstract.....	1
Kurzdarstellung	3
Acknowledgements	5
Table of contents	7
List of Figures	11
List of Tables.....	15
Abbreviations	17
Chapter 1 Viruses and Antivirals	19
1.1 Viral diseases	19
1.2 Vaccines	20
1.3 Herpes infection and treatment.....	21
1.4 Antivirals currently in clinical use	23
1.5 Towards broad-spectrum antivirals	24
Chapter 2 Electron microscopy characterisation of viruses	33
2.1 The development of electron microscopy for biological specimen.....	33
2.2 Cryo electron microscopy of viruses	35
2.3 Towards a three-dimensional structure of viruses	38
2.4 Cryo electron tomography and the resolution revolution	38
2.5 Cryo electron microscopy to elucidate structure and function of herpes simplex viruses.....	40
2.6 Electron microscopy in antiviral research	45

Chapter 3	Materials and Methods	49
3.1	Nanoparticle Synthesis and characterisation	49
3.1.1	Ligand synthesis	49
3.1.2	Nanoparticle synthesis	49
3.1.3	Nanoparticle characterisation	50
3.2	Cyclodextrins	52
3.3	Virus culture and antiviral testing	52
3.3.1	Cell culture	52
3.3.2	Pseudo Human Papilloma virus -16 (HPV)	53
3.3.3	Herpes simplex virus type 1 and 2 (HSV1 & HSV2)	53
3.3.4	Viral inhibition assay (Dose response) and Virucidal assay on HPV, HSV1 and HSV2	53
3.4	Transmission electron microscopy	57
3.4.1	Dry transmission electron microscopy	57
3.4.2	Cryo electron microscopy and tomography	57
Chapter 4	Overall virus – nanoparticle association	59
4.1	Cryo electron microscopy of HPV-NP-interaction	59
4.2	Cryo electron microscopy of Herpesviridae	60
4.3	Cryo electron microscopy of HSV2-NP interaction	61
4.4	Cryo electron tomography of HSV2-NP interaction	68
4.5	Cryo electron microscopy of HSV1-NP interaction	70
4.6	Discussion	74
4.6.1	Association of nanoparticles with viruses	76
4.6.2	Morphology of nanoparticle treated viruses	78
4.6.3	Summary	79

Chapter 5	An in-depth study of the nanoparticle virus interaction.....	81
5.1	Cryo electron microscopy of nanoparticle association to viral envelopes.....	81
5.2	Cryo electron microscopy and tomography of the interaction of nanoparticle with viral capsids.....	86
5.3	Discussion	89
5.3.1	Nanoparticle interaction with viral envelopes.....	90
5.3.2	Hypothesized mechanism for virucidal NP action	93
Chapter 6	Conclusion.....	99
6.1	Achieved results	99
6.2	Future development	100
6.2.1	A deeper mechanistic study	100
6.2.2	Towards application as a pharmaceutical active agent	101
References	105
Curriculum Vitae	113

List of Figures

Figure 1-1: Infectious diseases on the rise, Graphic reproduced from Dye et al. ³ (left); Global number of human infectious disease outbreaks, Graphic reproduced from Smith et al. ⁴ (right).	19
Figure 1-2: Poliomyelitis cases registered in 2016, Graphic from http://polioeradication.org/polio-today/polio-now/ .	21
Figure 1-3: Based on the viral life cycle different general targets for antiviral substances have been identified and developed. Graphic reproduced from Flint et al. ⁵	24
Figure 1-4: HSV1 entry cascade, Graphic reproduced from Shukla et al. ³⁸	26
Figure 1-5: Schematic representation of the effect of high dilution upon a virus treated with a virustatic antiviral material (top) and on a virus treated with a virucidal antiviral material (bottom).	28
Figure 1-6: Schematic representation of the hypothesized virustatic and virucidal effect exerted by Au-NPs functionalized with short MES or long MUS ligands, Graphic reproduced from Cagno et al. (submitted) ⁷⁷ .	29
Figure 1-7: Comparison of virustatic and virucidal action of heparin, Graphic reproduced rearranged from Cagno et al. (submitted) ⁷⁷ .	30
Figure 1-8: Virucidal activity of MUS:OT NPs onto a range of different viruses, Graphic reproduced rearranged from Cagno et al. (submitted) ⁷⁷ .	30
Figure 2-1: HSV1 negatively stained and immunogold labelled for glycoprotein B (left) and glycoprotein D (right), Graphic reproduced and modified from Stannard et al. ⁸⁸ . The Scale bars are 100 nm.	34
Figure 2-2: Herpesvirus egress, Graphics reproduced from Mettenleiter et al. ⁹⁵	35
Figure 2-3: Electron micrographs of viruses in their frozen-hydrated state, Graphics reproduced from Adrian et al. ⁹⁷	36
Figure 2-4: Schematic representation of cryoEM principle, Graphic modified and reproduced from Newcomb et al. ¹⁰⁴	37
Figure 2-5: Four-dimensional data representation of time-lapse electron tomography of the first 15 seconds of endocytosis, Graphic reproduced from Kukulski et al. ¹²⁵	40
Figure 2-6: CryoEM image (a) and reconstruction (b) of HSV1 capsid and tegument; (c) reconstruction of HSV1 capsid; Graphics reproduced from Zhou et al. ^{126,127}	41
Figure 2-7: CryoEM images and reconstructions of HSV1 capsids showing the portal protein, Graphics reproduced from respective sources.	42

Figure 2-8: CryoET tomographic reconstruction of HSV1 virions, Graphic reproduced from Grünewald et al. ¹⁷	43
Figure 2-9: HSV1 virion entry and fusion into a synaptosome, Graphic reproduced from Maurer et al. ¹³⁶	43
Figure 2-10: Herpes 'life-cycle' illustration, Graphic reproduced from Maurer et al. ¹³⁷	44
Figure 2-11: CryoET sub-volume averaging of HSV1-gB on vesicles showing two different conformations, Graphics reproduced and merged from Mordehai et al. ⁴⁰	45
Figure 2-12: Dry negatively stained TEM of HPV-16 Pseudovirus treated with 0.1 mg/ml MUSOT 131008 for 1h at 37°C, (Sample preparation by V. Cagno, imaging by M. Valino; the scale bars are 100 nm).	46
Figure 2-13: Dry TEM images of HSV2 after treatment with 0.2mg/ml MUSOT 131008 NPs for 1h at 37°C, Graphic reproduced from V. Cagno et al. (submitted) ⁷⁷ .	50
Figure 3-2: Schematic representation of β -Cyclodextrin with MUS functionalisation; Graphic reproduced and modified from Haldar et al. ¹⁴⁵	52
Figure 3-3: Virucidal assay of HSV1 with 230516 NPs over a time frame of 1h.	56
Figure 3-4: NP enumeration on virus envelopes in ImageJ.	57
Figure 3-5: Measurement of NP distance from viral envelope as well as NP particle to particle distance in ImageJ.	58
Figure 4-1: CryoEM of HPV-NP association.	60
Figure 4-2: CryoEM micrographs and diameter of capsid only and fully enveloped viruses in HSV1 and two HSV2 batches	61
Figure 4-3: Representative CryoEM images for the different general classes of NP- virus association as observed in incubation durations, ranging from 5 min to 2h. The scale bars are 100 nm.	62
Figure 4-4: Quantification of NP-HSV2 association for different NPs at a concentration of 0.2mg/ml incubated with NPs from 5 min to 90 min at 37°C.	63
Figure 4-5: Quantification of NP-HSV2 association for different NPs at a concentration of 0.2mg/ml incubated with NPs for 0.5 min at RT before plunging into liquid ethane.	64
Figure 4-6: Quantification of NP-HSV2 association for different NPs at a concentration of 0.2mg/ml incubated with NPs for 0.5 min to 90 min.	65
Figure 4-7: Representative pictures of virus morphologies identified in CryoEM.	66
Figure 4-8: CryoEM quantification of different virus morphologies after 30sec incubation of HSV2a with 0.2mg/ml NPs	68
Figure 4-10: Grouped (22) z-slice montage of a CryoET reconstruction of HSV2 incubated for 1h with MUSOT 131008 particles.	69
Figure 4-11: Grouped (13) z-slice montage of a CryoET reconstruction of HSV2 incubated for 1h with MUSOT 131008 particles.	69
Figure 4-12: Grouped (10) z-slice montage of a CryoET reconstruction of HSV2 incubated for 30sec with MUSOT 131008 particles.	70

Figure 4-13: Representative images of different envelope morphologies counted in HSV1 samples treated with different NPs	71
Figure 4-14: Representative CryoEM micrographs of the respective most represented classes in the interaction of HSV1 with non-virus inhibiting EG2OH, virustatic MES and virucidal MUSOT 131008 and 200515.	71
Figure 4-15: Quantification of HSV1-NP association and morphologies after incubation with MUSOT NPs for 30sec	72
Figure 4-16: CryoEM quantification of HSV1 association and morphology upon immediate treatment with MES or MUSOT 131008.	73
Figure 4-17: Comparison of capsid, enveloped and fully covered virus diameter for HSV1 and HSV2	74
Figure 4-18: Stages of virus-NP association.	77
Figure 5-1: CryoEM images of MUSOT200515 (0.2mg/ml) immediate association to HSV1 envelopes	82
Figure 5-2: Membrane protrusions after treatment with MUSOT 200515 NPs for 0.5min	83
Figure 5-3: CryoEM image of 0.5 min MUSOT 131008 treated HSV2 with well resolved viral glycoproteins.	84
Figure 5-4: HSV1 enveloped virus 30sec after incubation with 0.2mg/ml MUSOT 131008 showing a virus capsid expelled out of the virus envelope.	85
Figure 5-5: CryoEM of breaking and broken capsids	86
Figure 5-6: Grouped z-slice montage of a CryoET reconstruction of HSV2 incubated for 30sec with MUSOT 200515 particles	88
Figure 5-7: Grouped z-slice montage of a CryoET reconstruction of HSV2 incubated for 30sec with MUSOT 200515 particles.	88
Figure 5-8: Schematic representation of the aforepresented CryoEM of an HSV1 virion after 30sec of treatment with 0.02mg/ml of MUSOT 131008	92
Figure 5-9: Left: Membrane fusion pore reproduced from Maurer et al. ⁴⁰	93
Figure 5-10: CryoEM micrographs of the hypothesized mechanism for the action of virucidal NPs on viruses	94
Figure 5-11 Hypothesised sequence of NP-capsid association events leading to the eventual breakage and full NP coverage of broken capsids.	96
Figure 5-12: Hypothesized virucidal mechanism	97
Figure 6-1: Dose response and virucidal assay testing the temperature influence on NP-virus pre-incubation.	100
Figure 6-2: CryoEM imaging and quantification of HSV2 capsid morphology immediately after treatment with CDS2	102
Figure 6-3: Diagrams of counts of the CryoEM HSV1 morphology after treatment with the virustatic CD1 and virucidal CDS2 for 0.5 min at RT	103

List of Tables

<i>Table 1: Basic NP characterisation</i>	51
<i>Table 2: Dose response and virucidal assay of HSV2 to NPs</i>	54
<i>Table 3: Dose response and virucidal assay for HSV1</i>	55
<i>Table 4: Summary of antiviral and virucidal properties of NPs and Cyclodextrins</i>	56

Abbreviations

2D	Two-dimensional
3D	Three-dimensional
CD	Cyclodextrin
cryoEM	Cryo-electron microscopy
DNA	Deoxyribonucleic acid
EM	Electron microscopy
FDA	Food and Drug Administration
FFU	Focus forming units
GAG	Glycosaminoglycans
gX	Glycoprotein x
HBV	Hepatitis B Virus
HPV	Human Papilloma Virus
HSPG	Heparan sulfate proteoglycans
HSV	Herpes simplex virus
MES	2- mercaptoethanesulfonate
MOI	Multiplicity of infection
MUS	11-mercaptoundecanoic sulfonic acid
NP	Nanoparticle
OT	1-octanethiol
pfu	Plaque forming units
RSV	Respiratory syncytial virus
RT	Room temperature

Chapter 1 Viruses and Antivirals

Viral diseases affect billions and kill millions of people worldwide every year. Although effective vaccines against some viruses have been developed, and, with smallpox and rinderpest, two of them are even considered eradicated, it has not been possible to develop vaccines against all viruses. In this chapter I will outline the state of the art in the development of antiviral substances, including their current shortcomings and detail approaches to develop broad-spectrum antiviral substances.

1.1 Viral diseases

About 20% of worldwide mortality are caused by infectious diseases¹ and to a great extent by viruses. Not all viruses are pathogenic: disease occurs when our immune system is not able to keep a pathogenic virus in check. Diseases can range from a minor cold to deadly epidemics. Smil et al. calculated the risk for ‘massively fatal discontinuities’ worldwide and rated that a pandemic is more likely to change the course of humanity in the next 50 years than other events such as war and famine². Dye et al quantified that 84% of all international health hazards between 2001 and 2013 were infectious diseases³. Globally a rise in human infectious diseases can be noted, about half of which can be attributed to viral diseases⁴.

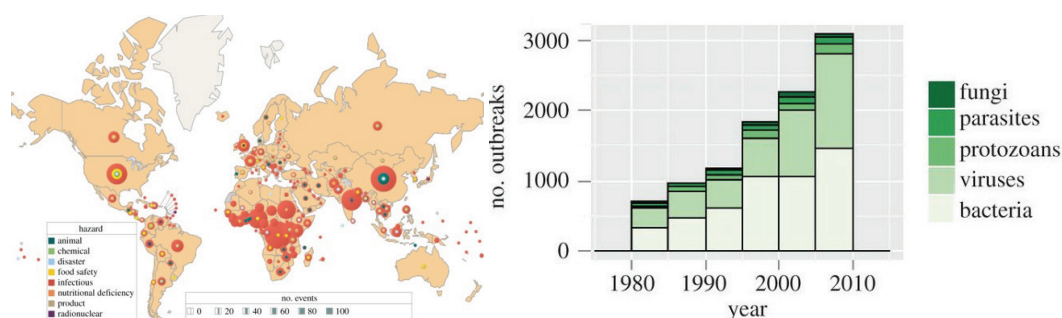


Figure 1-1: Infectious diseases on the rise: International health hazards by country 2001-2013; 84% were outbreaks of infectious diseases, Graphic reproduced from Dye et al.³ (left); Global number of human infectious disease outbreaks from 1980 to 2010, Graphic reproduced from Smith et al.⁴ (right).

1.2 Vaccines

Our best defence against viruses are vaccines. Vaccines stimulate a protective immune response and tap into our immunologic memory. Two different forms of vaccination exist: active and passive vaccines. Passive immunisation instils the products of the immune response: the antibodies; be it delivered by mother's milk, humanized antibodies or convalescent serum⁵. Active vaccines are a modified form of a pathogen such as inactivated viruses, subunit proteins, attenuated microorganisms or viruses or conjugates that modify the polysaccharide outercoats of bacteria. For a more efficient immune response the production of neutralizing antibodies has to be induced. Vaccines have to protect against the disease, be safe with minimal side effects, be long lasting and affordable⁶. For combating diseases, effectively and to avoid pandemics, it is important to attain a critical level of immunity in a population to generate herd immunity. This herd immunity threshold depends on the basic reproduction number of the virus, the number of secondary cases generated by a typical infectious individual⁷. The herd immunity threshold is generally above 75%, for smallpox it is 80-85%, for measles 93-95%⁸. Above this threshold the risk of infection for individuals who have no immunity against the pathogen is lowered by the presence of immune individuals.

To fully eradicate a viral disease several criteria have to be met: it must only replicate in one host and the vaccination must confer lifelong immunity⁹. These criteria apply, for example, to smallpox that was declared eradicated in 1980¹⁰. Polio has also been largely eradicated with the exception of Nigeria, Afghanistan and Pakistan. Today 97% of children are reached by essential vaccines. Measles for example could potentially be eradicated as well, but in 2012 still 157000 children died from measles, a fully preventable infectious disease. The vast majority of cases occurred in the developing world in areas of insufficient vaccine coverage, but cases also occur in European small wealthy communities that are in only little danger of a fatal disease outcome⁹.

Herd immunity cannot be reached everywhere, especially in remote regions of the world that lack a well-structured health care system⁹. Only a limited number of vaccines can be administered orally, most vaccines have to be injected by trained health care personnel. This problem is amplified by the cold-chain-problem – attenuated vaccines are especially thermally unstable and although great efforts have been taken to stabilize vaccines with sugars¹¹ or silk: these remains at a research level and have not been approved yet^{12,13}.



Figure 1-2: Poliomyelitis cases registered in 2016, Polio was eradicated from almost the entire world except Afghanistan, Pakistan And Nigeria with 37 cases of wild type polio in total in 2016; Graphic from <http://polioeradication.org/polio-today/polio-now/>.

Despite advances in vaccine production, such as the use of cell cultures and the development of novel additives such as oil-in-water adjuvants, in case of a pandemic it would not be possible to produce enough vaccines to limit the spread of the infection. Post-exposure prophylaxis is only possible in rabies and only highly effective if administered in the first 24 hours of infection¹⁴.

There is a lack of vaccines to address emerging diseases such as severe acute respiratory syndrome (SARS), Middle east respiratory corona virus (MERS-CoV), avian and swine flu, influenza and re-emerging diseases such as Dengue, Ebola or West Nile virus and most haemorrhagic fevers¹⁵. Additionally, vaccines are difficult to design against viruses with a high mutation frequency such as HIV and Influenza. For example, the development of vaccines against herpes simplex have failed, because not only an antibody response, but also a T-cell response has to be elicited to confer immunity¹⁶. In cases in which no vaccination is amendable antiviral therapies are necessary to keep the viruses in check.

1.3 Herpes infection and treatment

Herpes simplex viruses are members of the family of herpesviridae, subfamily alphaherpesvirinae, genus simplexvirus. These are enveloped viruses that contain their double stranded DNA in an icosahedral capsid surrounded by tegument proteins and the viral envelope¹⁷.

Herpes infections can lead to different clinical manifestations spanning from asymptomatic infections to life threatening conditions.

Herpes simplex virus (HSV) infections are ubiquitous. In 2004 57% of all adults in the US were HSV1 seropositive and 17% HSV2 seropositive¹⁶, other estimates suggest infection rates as high as 90%¹⁸. While HSV1 is mostly associated with a commonly mild orolabial disease, HSV2 is more often associated with a genital disease. Regardless the type, the viruses most commonly infect skin and mucosal membranes¹⁹. The primary infection shows a lytic infection cycle in epithelia and fibroblasts that usually resolves within a week, but additionally the viruses are retrogradely transported from the skin to the innervating neurons of the sensory ganglia, where life-long latent infection with frequent virus reactivation and mucocutaneous shedding is established. The viruses are spread from person to person via infected secretions²⁰.

Although herpes infections are mild in otherwise healthy patients, they are potentially fatal for neonates²¹ or immunocompromised patients²². Neonates acquire the infection usually during birth from their mother and the prognosis highly depends on the location of the infection with a rather good prognosis for skin, eye and mouth infections, with increasing severity for CNS or disseminated multi-organ infections²⁰. CNS infections from reactivation of the virus in the brain or herpes simplex keratitis present a major cause for blindness²³. Immunocompromised patients present all kinds of clinical HSV manifestations often necessitating long-term antiviral treatment.

The most widely used antiviral treatment for herpes simplex infections is acyclovir, a guanosine analogue that is phosphorylated intracellularly by HSV1 thymidine Kinase (HSV1-TK) and acts as a chain terminator of the viral DNA polymerase²⁴. Antiviral treatment can shorten the duration of the episode and decrease viral shedding, for example in the case of HSV2 shedding has reportedly been reduced by 60-80%¹⁶.

Prolonged treatment as in the case of immunocompromised patients builds the perfect ground for the development of resistances. Most frequently, HSV1-TK mutates to no longer phosphorylate Acyclovir²⁵ or the viral DNA polymerase mutates to not take acyclovir as a chain terminator. In such cases the only antiviral left is Foscarnet: it inhibits the HSV DNA polymerase directly, but imparts significant kidney and bone toxicity²⁰. The development of new antivirals for herpes simplex and many other viruses is an active area of research.

1.4 Antivirals currently in clinical use

Antivirals are designed targeting either viral or cellular host proteins. As obligate intracellular parasites, viruses hinge on the hosts' molecular functions, so antivirals have to be developed carefully to limit side effects on the host²⁶. As of March 2014, 50 antivirals that directly affect the viruses have been approved²⁷. For HIV, more than 25 antiviral compounds are on the market¹⁰. Other antivirals target the viruses for hepatitis B and C, influenza and herpes. The substances have been developed in mechanism-based screens, cell-based screens based on natural products, chemical libraries or combinatorial chemical libraries, often with high throughput screening methods. Moreover in-silico screening designs molecules to fit into the active site of the viral enzymes. This has been successfully applied to develop LEDGINs, antivirals that block the HIV integrase^{28,29}. This technique might further prove useful in the development of antiviral substances for viruses that are hard to grow in culture, such as Hepatitis B Virus (HBV) and Human Papilloma Virus (HPV). Further challenges in the development of antiviral substances are posed by viruses for which only limited animal models exists or dangerous viruses such as Ebola or Lassa⁵.

With increasing knowledge about the viral life cycle, antiviral substances have been developed for every crucial step of the viral replication cycle ranging from the viral attachment, over penetration and uncoating, to mRNA and protein synthesis as well as DNA or RNA replication to the assembly and eventual release of the viral particles as shown in Figure 1-3.

The high replication count of viruses including their high mutation rate poses a problem to antivirals: they have to not only completely block replication of the viruses but also avoid the fast development of resistances. RNA viruses show a mutation frequency of 1 in 10⁴-10⁵ nucleotides, resulting in 1 mutation per replication. DNA replication includes exonucleases and error control producing less frequent mutations. Therefore, DNA viruses evolve more slowly and develop resistances more slowly. Indeed, this proved especially important in the case of HIV where therapeutic approaches using single antiviral substances rapidly lead to the development of resistances⁵. Antiviral combination therapy successfully overcame this hurdle for HIV; there are now multiple approved drugs and drug combinations²⁷.

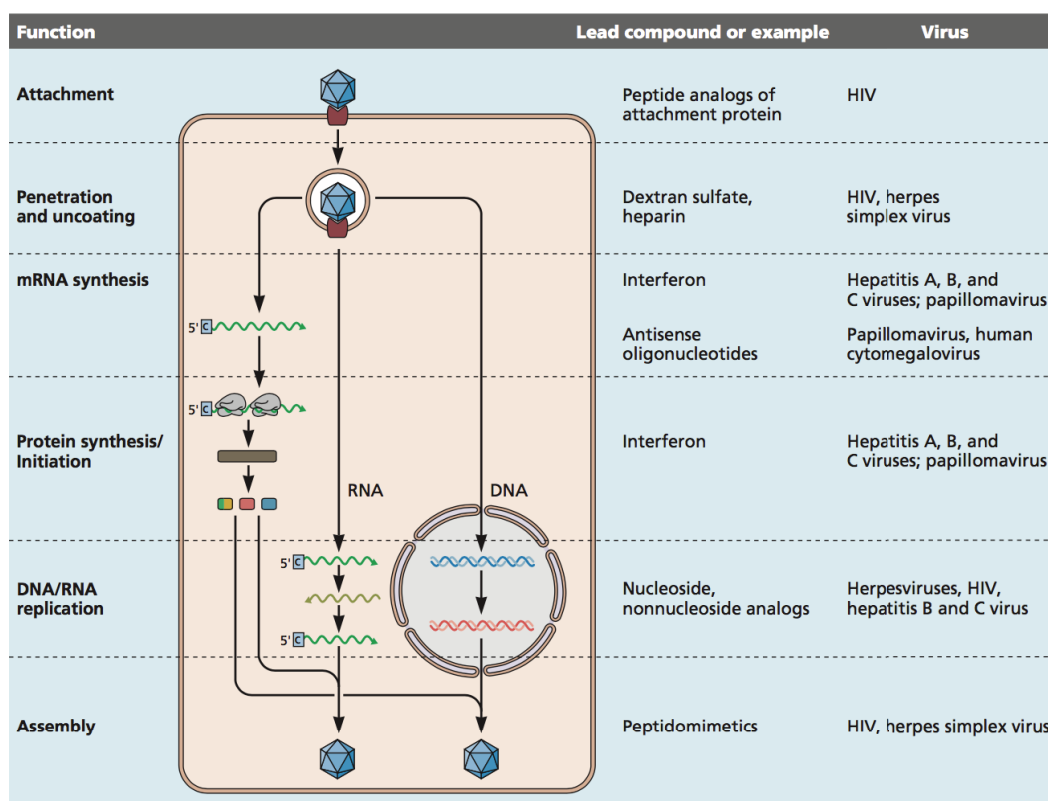


Figure 1-3: Based on the viral life cycle different general targets for antiviral substances have been identified and developed. Graphic reproduced from Flint et al.⁵

Another hurdle in the application of antivirals is that short acute infections with fast progression further limit the time window in which a specific antiviral substance can successfully be administered. The higher the virus load upon beginning antiviral therapy the more difficult³⁰. Here new virus identification systems would be very important to immediately be able to test which virus causes the infection to treat accordingly³¹.

1.5 Towards broad-spectrum antivirals

Diverse emerging viruses as well as clinical situation where viruses cannot be identified quickly enough necessitate not a specific but rather a broad-spectrum antiviral approach as comparable to broad-spectrum antibiotics. The paradigm of 'one-drug-one-bug' has to be changed towards a broader approach to respond to the increasing diversity of viruses causing diseases in humans, including the broad variety of zoonoses posing a constant threat to global health³². A broad-spectrum antiviral would not only present a tool for emerging or novel pathogens, but also if multiple viruses or genotypes of viruses are implicated in an infection²⁷. Broad-spectrum antivirals targeting host factors used for viral replication or used

in viral restriction have been proposed²⁷, but when targeting host factors the very high risk of side-effects has to be taken into consideration. At present ribavirin is the only broad-spectrum antiviral that has been Food and Drug Administration (FDA) approved. It is a guanosine analog, but its exact mechanism remains elusive and extensive side effects limit its use.³²

A different approach towards the development of broad-spectrum antivirals is to target a common, highly-conserved, essential region or mechanism of viruses, which would additionally pose a higher barrier to the development of resistances²⁷. The attachment and entry to the cell represent such a step in the viral life cycle³³. Viruses of different classes share common attachment factors bearing negatively charged groups such as sialic acid or Heparan Sulfate Proteo Glycans (HSPG)³⁴.

HSPG are built of a glycosaminoglycan (GAG) and are categorized based on their core protein as either syndecans composed of transmembrane proteins interacting with the cytoskeleton or as glypicans that are glycosyl-phosphatidylinositol (GPI)-anchored proteins³⁵. HSPG can be found on almost all cells as well as in the extracellular matrix. They are implicated in various biological functions such as blood coagulation or wound healing³⁶. Its abundance and importance in the function of eukaryotic cells makes HSPG an ideal viral attachment factor^{37,38}.

Human diseases in which HSPG is implicated include HSV³⁹, Dengue virus, HIV, Cytomegalovirus, Vaccinia virus, Hepatitis C virus, HPV, Respiratory syncytial virus and Varicella zoster virus³⁶. The viruses express glycoproteins with domains rich in basic amino acids to bind to the negatively charged HSPG³⁷. Domains rich in Lysine and arginine have been published for the L1 capsid protein of HPV, glycoprotein120 of HIV and glycoproteins B, C and D of HSV-1³⁵. Mutations in these amino acids reduce the attachment of HSV1 virions to cells³⁴. The first binding event of the viruses to the glycoproteins usually presents the beginning of a cascade leading to the internalisation of the virus as shown in the example of HSV1 entry into cells in Figure 1-4. The glycoproteins B and C mediated adhesion to HSPG is followed by glycoprotein D binding to one of three entry receptors: HVEM a TNF-receptor, Nectin immunoglobulins or O-sulfated heparan. Following this, viral fusion supported by gB and gH-gL is induced⁴⁰.

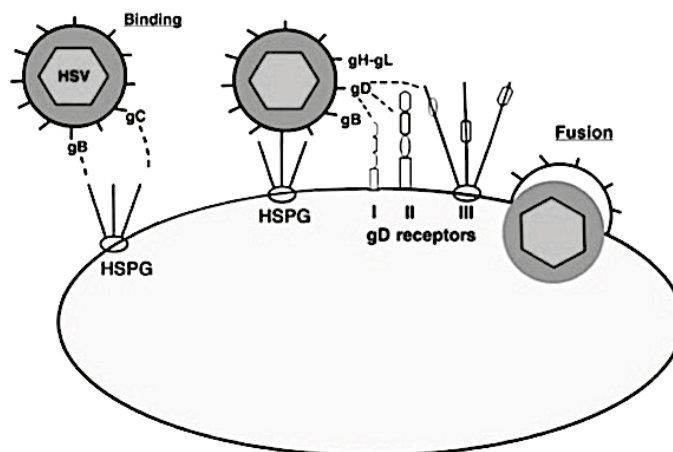


Figure 1-4: HSV-1 entry cascade from the initial binding of HSPG by the virus' glycoproteins B or C to the binding to entry receptors such as HVEM, nectins or O-sulfated heparan by glycoprotein D that induces the fusion of virus and cellular membrane. Graphic reproduced from Shukla et al.³⁸

HSPG thus presents a pivotal point in the initiation of the viral entry cascade of several viruses; it is therefore a promising target to design broad-spectrum antiviral substances. The receptor-virus interactions could be prevented in two ways: by either blocking the adhesion by blocking the viral glycoproteins with heparin or polyanions, or by blocking all HSPGs on the cells with polycations. The first approach seems to be the more promising one, as in the second approach, the risk of not only blocking the virus from adhering to the cells but also blocking several of the cellular functions of HSPG is high³⁷. Several different heparins and heparin derivatives have been proposed to block adhesion of heparan sulfate binding dependent viruses⁴¹. Native heparin is a very potent anticoagulant, so care has to be taken to develop antiviral derivatives lacking the anticoagulant activity. HSPG binding peptides⁴², heparin and sulfated polysaccharides^{35,43-45}, sulfonic acid decorated polymers⁴⁶ as well as dendrimers^{47,48} have been studied and showed potent *in-vitro* antiviral activity. These promising *in-vitro* results unfortunately could not be translated into successful *in-vivo* activity. Three polyanionic HIV microbicides (Carrageenan, cellulose sulfate, Pro2000 naphthalene sulfonate) successfully passed Phase 2b 'proof of concept' trials, but failed in large scale phase III clinical trials intended to test the substances full efficacy^{49,50}. The cellulose sulfate trial had to be stopped based on concerns of enhanced infection⁵¹.

Rider et al. proposed that not only the high degree of sulfonation, but also structural features are highly important to elicit a potent antiviral activity⁴¹. Nanoparticles (NPs) present an adjustable versatile system where various surface structures and chemistries can be engineered. Nanotherapeutic antiviral approaches range from Heparin nanoassemblies

^{52,53} to nanoparticulate delivery systems for antiviral drugs⁵⁴ to the direct application of silver and gold NPs as antiviral agents. Silver NPs (AgNPs) have been proposed as potential Anti-viral Agents^{55,56}. Lara et al. tested the antiviral action of commercially available PVP-coated 30-50 nm AuNPs and proposed a binding to the HIV glycoprotein⁵⁷, but even after 1h at 5mg/ml, the residual infectivity in a virucidal assay was only about 30%. Later experiments on cervical tissues were successful at lower concentrations⁵⁸, but considering that AgNPs have been shown to be toxic at concentrations above 6µg/ml, a potential antiviral application of these NPs seems currently rather unlikely. Other attempts with PVP-coated silver NPs on respiratory syncytial virus (RSV) also only showed a reduction in infectivity of 44%⁵⁹ or a 50% reduction in transduction efficiency upon treatment with silica-NPs⁶⁰.

A more targeted approach using sulfonate functionalisation was tested by different groups. A Pt and a Pd metal-thiolate complexes with 2-mercaptoethanesulfonate (MES) showed antiviral activity⁶¹. Baram-Pinto et al.⁶² synthesized AuNPs capped with MES and were able to inhibit *in-vitro* HSV1 infections of a viral load of 2500 plaque forming units (pfu) by 97%. The same group tested MES-capped AuNPs against HSV-1 and could again prove an antiviral effect in a plaque reduction assay. The free MES and plain gold NP in contrast showed no inhibition, suggesting that the structure of the sulfonate ligands plays an important role in the antiviral efficacy. Bowman et al. studied multivalent AuNPs functionalized with a derivative of a C-C chemokine receptor type 5 (CCR5) antagonist. CCR5 is an essential co-receptor in HIV infection. They proved that the multivalent presentation of a monovalently inactive molecule on AuNPs could be an active antiviral⁶³. Bastian et al. confirmed this hypothesis and enhanced the antiviral potency of an antiviral peptide triazole by presenting it on large AuNPs⁶⁴.

Our group, as well as others⁶⁵ proposed that this lack of effectiveness of the proposed antivirals targeting the interaction of HSPG and viruses is due to the only virustatic nature of the interaction and a poor virucidal effect.

Virustatic materials act on the initiation of the viral replication cycle outside of the cells. Targeting a common and highly conserved mechanism such as heparan sulfate or sialic acid binding, they can be broad-spectrum antiviral as well as potentially non-toxic to the cell as no cellular mechanisms should be affected. However, a merely virustatic interaction is reversible. It can be compared to a competitive effect: Once the competitor, the antiviral, is

diluted out, the virus is liberated in its fully infective form. This could explain why the aforementioned antiviral substances presented as highly effective *in-vitro*, but non-effective in humans, where bodily fluids readily dilute the virustatic antiviral and release an again fully infective virus.

An ideal antiviral would thus be a **virucidal** substance that causes irreversible inactivation⁶⁶ of the virus that cannot be reverted by dilution as schematically represented in Figure 1-5.

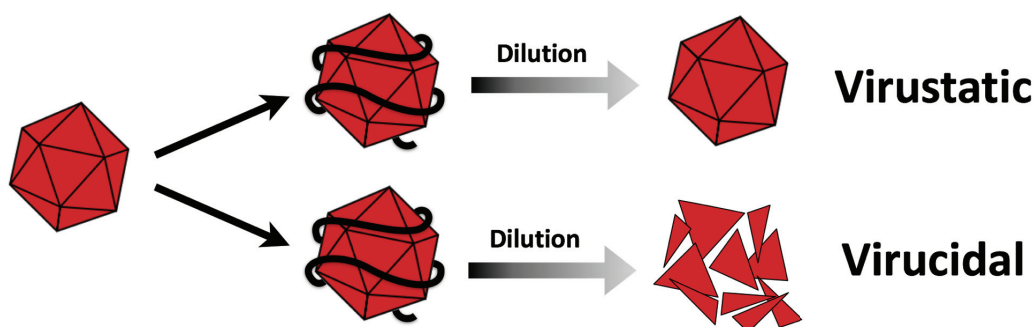


Figure 1-5: Schematic representation of the effect of high dilution upon a virus treated with a virustatic antiviral material (top) and on a virus treated with a virucidal antiviral material (bottom). A virustatic material can upon high dilution be diluted off the virus and releases a fully infective virus. A virucidal material irreversibly alters a virus, so that even when the active substance is diluted off the virus the virus remains non-infective.

Most of the published research (201 of 313 papers as of April 2017) on virucidal substances focusses on the development and testing⁶⁷ of disinfectants⁶⁸ such as glutaraldehyde⁶⁹, detergents^{70,71}, non-alcoholic substances⁷², alcohols and strong acids⁷³. Though those substances are highly effective, their high toxicity to humans renders them inappropriate to be used as a drug. Other published virucidal materials are also limited by their low tolerability^{74,75}. Not only should the general toxicity be carefully tested, in the case of e.g. topical antivirals the danger in toxicity is further enhanced as a damaged mucus layer or cell is more susceptible to infections than an intact cell.⁶⁵

A successful drug candidate ought thus to combine the beneficial properties of a virustatic material being broad-spectrum efficient at low toxicity, but simultaneously irreversibly block the viruses' infectivity. Our research group developed a method to engineer NPs such as to render a virustatic material into a virucidal material. As introduced above, sulfonated ligands have been shown to exert an antiviral effect onto viruses using HSPG as their attachment ligand to cells. Previous research on sulfonated NPs as antiviral agents only studied short rigid ligands that we presume to bind only weakly to a limited number of receptors on

the viral surface resulting in a solely virustatic effect. Consequently, we hypothesized that a virustatic sulfonated NP could be engineered into a virucidal NP by introducing longer ligands enabling strong multivalent binding on the viruses that would irreversibly inhibit viral infectivity by inducing local distortions in the virus structure. Figure 1-6 schematically illustrates this hypothesis. Short, rigid 2-mercaptoethylenesulfonate (MES) ligands were proposed to bind only weakly and reversibly to viruses, whereas long, mobile 11-mercaptopundecanoic sulfonic acid (MUS) could bind multivalently to viruses to induce distortions in the virus. Studies on local distortions induced in membranes when NP bind⁷⁶ strongly support this concept.

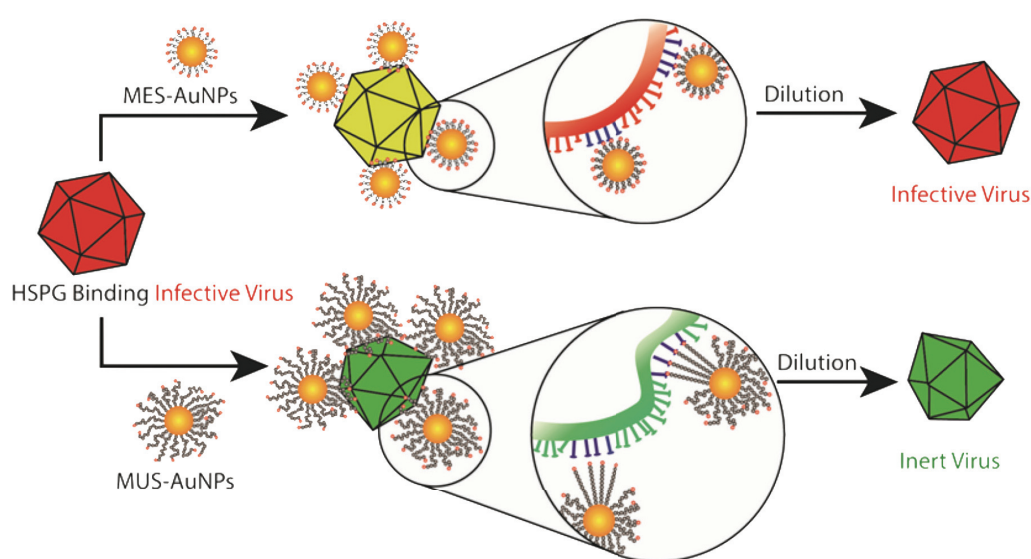


Figure 1-6: Schematic representation of the hypothesized virustatic and virucidal effect exerted by Au-NPs functionalized with short MES or long MUS ligands, Graphic reproduced from Cagno et al. (submitted)⁷⁷.

In the study, heparin, short ligand and long ligand NPs have been compared regarding their antiviral and virustatic effect on a range of HSPG-binding dependent viruses. HSV, RSV and Dengue and Zika virus have been tested as examples of enveloped viruses, HPV as an example for a non-enveloped virus. As long ligand NPs, we chose MUS:OT particles coated with a 2:1 mixture of MUS and 1-octanethiol (OT) that have been shown to be biocompatible, water soluble and protein resistant^{78,79,80}.

From the dose response, which can be seen in the graphs below, it can be concluded that all tested substances exert an antiviral effect on HSV-2. Control samples such as only the ligand or different non-sulfonated NPs did not yield a reduction in infection. The particles showed no toxicity at the concentrations tested. To test for a virucidal effect, a sample is incubated

with virus at a concentration above the EC₉₀. The EC₉₀ is the effective concentration at which an effect has been exerted onto at least 90% of the viruses, in our case the inhibition of the virus. In the virucidal assay, the active substance and the virus are pre-incubated at an EC₉₀ concentration and diluted sequentially to ascertain that the antiviral effect is not merely competitive, but irreversible. The bottom graphs in Figure 1-7 show that both heparin and MES do not show a virucidal effect, the virus infectivity is fully recovered after dilution; MUS:OT particles on the other hand reduce the virus titer by 5 logs showing a clear virucidal effect.

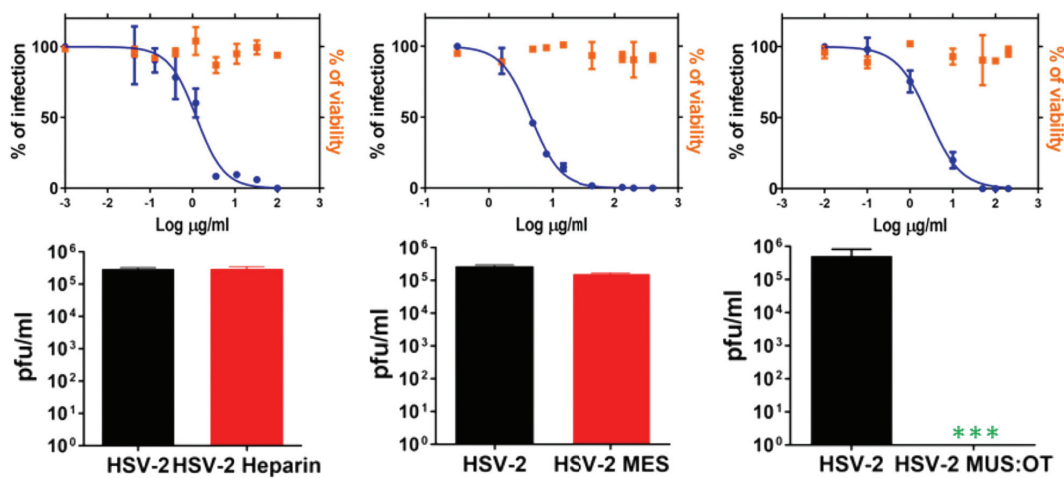


Figure 1-7: Comparison of virustatic and virucidal action of heparin, MES-NPs and MUSOT NPs on HSV-2: the top graphs show the dose response curves, the bottom graphs show the virucidal activity, Graphic reproduced rearranged from Cagno et al. (submitted) ⁷⁷.

A comparably high virucidal effect could be measured for several other HSPG-dependent viruses, as shown graphically in Figure 1-8. Tests on adeno-associated virus serotypes AAV2 and AAV5 indicated that the virucidal activity is indeed specific to HSPG binding viruses. While a clear virucidal effect was measured for AAV2 that binds cellular HSPG, no virus inhibition could be measured for AAV5, a sialic acid binding virus.

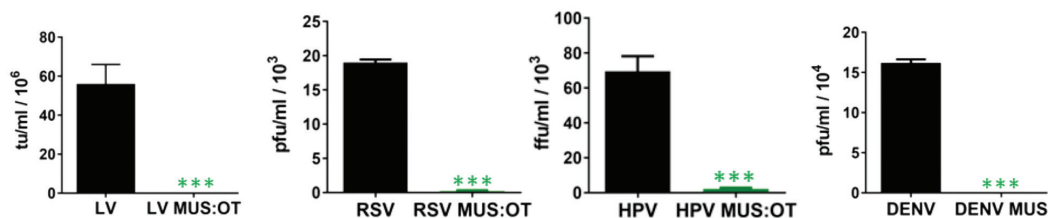


Figure 1-8: Virucidal activity of MUS:OT NPs onto a range of different viruses: Lentiviruses, Respiratory syncytia virus, human papilloma virus and Dengue virus; Graphic reproduced rearranged from Cagno et al. (submitted) ⁷⁷.

Later, molecular dynamics simulations of the binding of short versus long ligand sulfonate NPs were performed on HPV-16 capsids. It was shown that the NP's sulfonates bind to the positively charged HSPG binding arginine residues of the capsid proteins. While short ligand MES-NPs only bind to single residues, long-ligand MUS:OT particles bind multivalently and exert a stress onto the viral capsid that generates a force of ~ 125 pN.

Moving the system more towards potential applications *in-vivo* the virucidal effects could be repeated in a post-treatment approach where cells were beforehand infected with viruses and then treated with NPs. A further step towards a real-life application was taken testing the NPs on EpiVaginal tissues, tissue culture system to model vaginal mucosa. MUSOT NP were both virucidal and non-toxic. A final test has been taken synthesizing the effective ligand shell onto an iron core NP that proved as effective as its gold counterpart.

Taken together the results suggest that a highly efficient broad-spectrum virucidal system has been designed. The question though of how the interaction of these NPs with more complex capsids or viral envelopes looks and if this can lead to a better understanding of the molecular processes involved will be answered in this thesis.

Chapter 2 Electron microscopy characterisation of viruses

In this chapter I am presenting an overview of the development of techniques to elucidate the structure of viruses, from the first crystallographic approaches to negative staining in electron microscopy (EM). I will finish this chapter with advances in cryo electron microscopy (CryoEM) from 2D representations of viruses to 3D reconstructions of single virus particles to viruses in their cellular environment. In my description, I will illustrate the steps taken on herpes viruses, the determination of their capsid structure to the more complex enveloped structure to studies of its infection process.

2.1 The development of electron microscopy for biological specimen

Starting from the setup of the first electron microscope by Ernst Ruska in 1931⁸¹ there was great interest in imaging biological samples. Ruska's brother, Helmut, successfully obtained the first image of dried tobacco mosaic virus in 1939⁸², but imaging biological samples poses major challenges to the EM community. Biological samples are not only soft, sensitive materials, but they also contain a lot of water and are, being composed of mostly light elements such as Carbon, Hydrogen, Nitrogen, not electron-dense enough to be imaged in an EM. Therefore, both fixation and contrasting methods had to be developed to increase resolution of EM images taken of biological specimens.

In 1945 Williams and Wyckoff imaged tobacco mosaic viruses increasing contrast by depositing a thin layer of metal over the sample and coined the term metal shadowing⁸³. The first human pathogen visualized was influenza in 1946⁸⁴. The metal shadowing technique was later enhanced by Heinmets et al. who developed rotary metal shadowing in 1949 to gain a better understanding of the sample shape⁸⁵. Brenner and Horne developed the basic negative staining technique⁸⁶ by mixing the viruses with a preparation of 1% phosphotungstic acid and could resolve structural details that had previously been described by X-ray crystallography. Today a range of negative stains is used, such as the cationic uranyl acetate or anionic

stains such as ammonium molybdate and sodium phosphotungstate. They are classically used at concentrations of 1-2% in water to 'support or embed' the sample⁸⁷. With the development of antibody-labelling of gold colloids⁸⁸ it became possible to locate specific proteins with electron dense gold particles. Stannard et al. studied the distribution of different glycoproteins on the surface of herpes simplex virus 1⁸⁸. As depicted in Figure 2-1 glycoproteins on the surface of HSV1 virions show different shapes as well as different distributions on the viral surface.

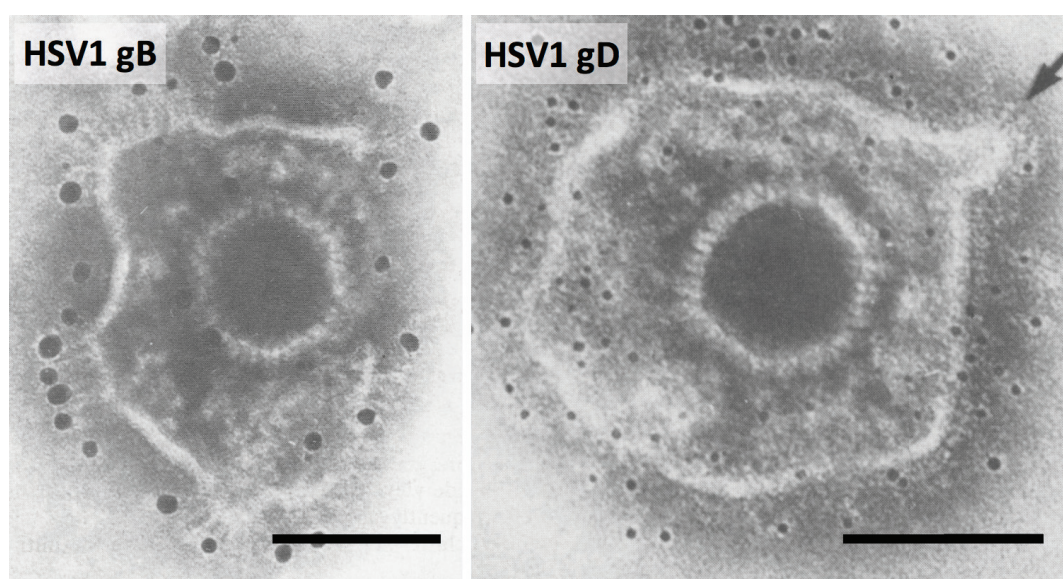


Figure 2-1: HSV1 negatively stained and immunogold labelled for glycoprotein B (left) and glycoprotein D (right), Graphic reproduced and modified from Stannard et al.⁸⁸. The Scale bars are 100 nm.

Today, negative staining is used as a readily available technique for a quick assessment of sample composition, purity or aggregations. Goldsmith et al. described the importance of EM as a rapid technique, that in contrast to molecular diagnostics did not require prior knowledge of the nature of the sample and hence offers an unbiased view of the sample contents⁸⁹, which proved especially important in the detection of e.g. infections in 1972 when Norovirus was first described⁹⁰ or at the first description of corona virus as causative agent of the Severe Acute Respiratory Syndrome SARS in 2002⁹¹. Negative staining remains pivotal also in virus surveillance to identify unknown diseases or terrorist attacks⁸⁹.

Techniques to examine samples that were too thick to be imaged in a thin film, such as tissue samples or whole cells, were significantly advanced in the 1950s with the development of efficient microtomy techniques⁹² epoxy as embedding medium⁹³ as well as heavy metal stains for tissue sections⁹⁴. Samples are fixed, washed, stained with Osmium tetroxide,

washed, stained with uranyl acetate, washed, dewatered in washes of increasing ethanol concentration to be then embedded in resin. Cured samples are then cut in an ultra-microtome to obtain 50-70 nm thick sections of the tissue sample that can be imaged in TEM to gain insight of the virus interactions in tissues, for example to study the infection cycle of herpes simplex⁹⁵ or the human immunodeficiency virus⁹⁶.

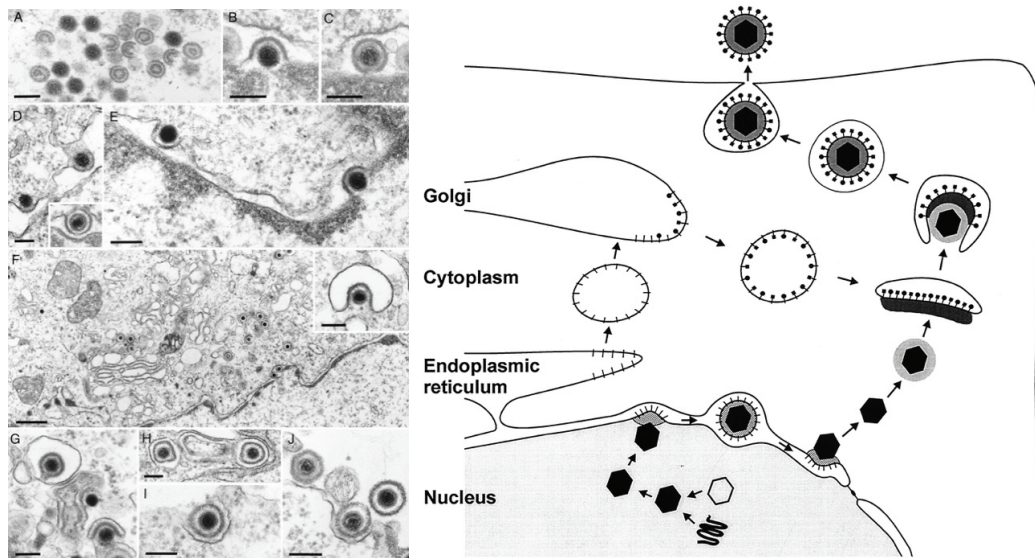


Figure 2-2: Herpesvirus egress studied in epoxy embedded cells showing that an inside the nucleus assembled virus capsid is shuttled through the nuclear membrane by engulfing and acquires its viral membrane in the Golgi apparatus to then be exocytosed off the cell Left: EM ; Right: schematic representation of the process ; Scale bars 100 nm. Graphics reproduced from Mettenleiter et al. ⁹⁵

2.2 Cryo electron microscopy of viruses

A paradigm shift for the electron microscopy of viruses was introduced by Adrian and Dubochet in 1984⁹⁷. They developed the method of CryoEM to image samples in their native solution state without the introduction of further fixation or stains. Figure 2-3 shows the first published electron micrographs imaged in CryoEM.

A drop of a suspension containing viruses is suspended over an EM grid, frozen rapidly into its vitreous state, transferred into the microscope avoiding heating over the devitrification temperature of approximately -135°C and imaged while taking care to preserve the sample structure. The frozen layer has to be sufficiently thin (below 300 nm) to obtain enough contrast, therefore small mesh uncoated carbon grids or grids covered with a perforated carbon film were utilized. The hydrophilicity of the grid is important for an even and thin spread of the liquid. Appropriate cryogens such as liquid ethane or propane are crucial to avoid a Leidenfrost effect as in the case of liquid nitrogen at room temperature⁹⁸. The Leidenfrost

effect of forming a thin gas layer on the sample has an insulating effect that would slow the cooling of the sample so much as to enable the formation of ice crystals. Vitreous ice is obtained by rapid cooling (10^{-4} s for a thin-layer vitrification) to avoid even the first nucleation steps⁹⁹. The vitrified water is described as a supercooled liquid without a visible internal structure and without scattering. The state of the sample is thus referred to as frozen hydrated state¹⁰⁰. Devitrification, the formation of ice crystals, happens when the samples are warmed during the transfer, stressed under a strong electron beam or upon mechanical stress¹⁰¹.

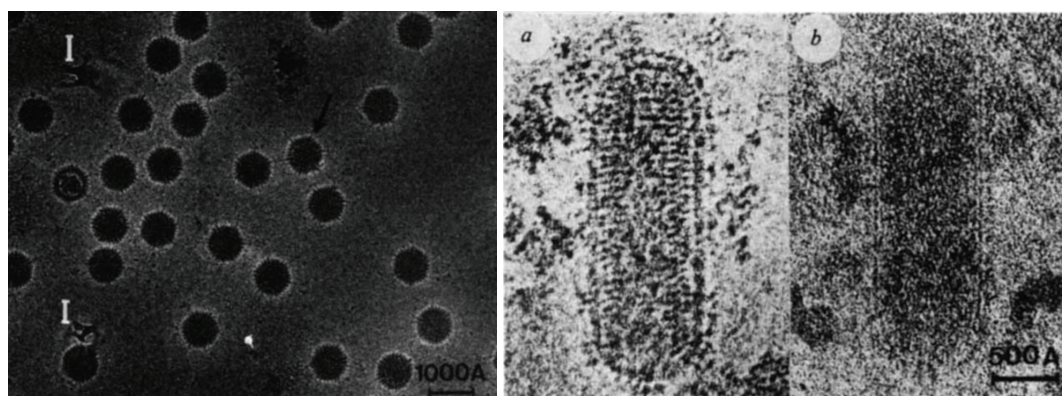


Figure 2-3: Electron micrographs of viruses in their frozen-hydrated state; Left: Adenovirus type 2 at a magnification of 12,500x with a total dose of about 10 electrons per \AA^2 at about 8 μm underfocus in an ice layer of a thickness of 120 nm, adenovirus spikes are highlighted by black arrows, ice contaminations are marked with an I; Right: Vesicular stomatitis virus imaged at two different defocus values (a) 4 μm and (b) 0.7 μm showing global details at high defocus and fine details at low defocus; Graphics reproduced from Adrian et al.⁹⁷

In electron microscopy, contrast is generated by amplitude and phase contrast. Amplitude contrast is produced as heavy atoms scatter electrons. Phase contrast is generated when a scattered electron wave and an unscattered electron wave interfere. The amplitude contrast in biological specimens is very low, so CryoEM relies on phase contrast for high resolution acquisitions. A compromise has to be met to interpret both the overall aspects of the viruses at high defocus as well as fine details at lower defocus as depicted in Figure 2-3 on the right. Erickson et al. recommend a moderately under-focused image as the best compromise between resolution and contrast for biological specimen¹⁰². Compared to a sample at room temperature, electron damage is reduced by imaging at -175°C ¹⁰³ and images can be acquired at doses of 10 electrons per \AA^2 . The phenomenon of bubbles emerging from samples at higher electron doses could be explained by the formation of volatile fragments induced by the beam that are hindered from escaping¹⁰⁰. The sample distribution in solution resembles that of the suspended liquid, but is different for every virus or sample depending on their

hydrophilicity as well as their dimensions. The virus dimensions measured were also well comparable to previously reported X-ray diffraction sizes⁹⁷.

Dubochet's innovations made CryoEM of thin films a simple and powerful method that has since widely been applied, but the basic principle to prepare a vitrified thin film has not changed as illustrated in Figure 2-4.

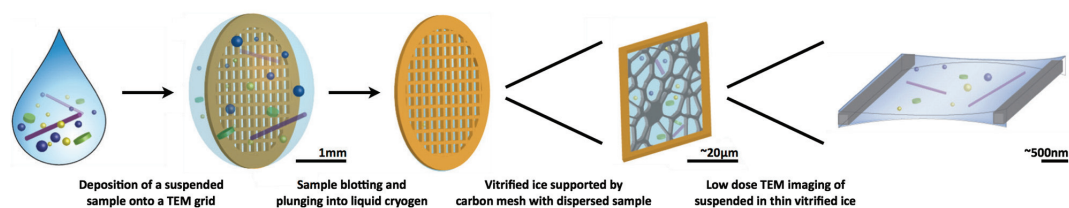


Figure 2-4: Schematic representation of cryoEM principle, Graphic modified and reproduced from Newcomb et al.¹⁰⁴

The advantages of enabling a visualisation of fragile structures, directly in the solvent, without drying the sample, and at lesser flattening largely outweigh certain limitations that have to be taken into consideration in CryoEM. The still high radiation sensitivity of the samples necessitates the use of low dose techniques, hence inducing a lower signal to noise ratio. The limitations imposed by the imaging in phase contrast have already been mentioned. Additional challenges in sample handling further render CryoEM anything but a trivial technique. The samples have to consistently be cooled to avoid heating and the consequent formation of cubic or hexagonal ice⁹⁹; moreover it is important to take great care during sample preparation to avoid contaminations from air (condensation of air humidity on the samples and in liquid nitrogen or liquid ethane) or from liquid ethane directly, that can form droplets on the vitrified ice surface¹⁰⁵. Although samples are imaged suspended in their solvent, interactions at the air-liquid interface cannot be excluded and poor handling might still lead to drying of the sample. Classically humidified chambers are utilized for the blotting process to avoid full or partial drying of the sample inducing excessive buffer concentration. High salt concentrations in the ice for example induce a grainy structure and cryoprotectants such as sugars can lead to blurry images. The uniform formation of a thin ice layer additionally poses its own set of challenges ranging from sample preparation to the choice and treatment of the holey carbon grid¹⁰⁶. Despite these challenges, tremendous progress has been made using CryoEM especially because the image presents a full two-dimensional projection through the specimen and not only a representation of the surface as in most negative staining techniques.

2.3 Towards a three-dimensional structure of viruses

The first three-dimensional input on the structure of single viruses brought about by Watson and Crick in 1956, who determined that the genetic material in small spherical viruses could only accommodate a limited number of proteins, thus the protein coat was composed most likely of identical subunits arranged in an icosahedral fashion to best accommodate the DNA¹⁰⁷. Steve Harrisons crystallized the first virus – Tomato bushy stunt virus¹⁰⁸ and Michael Rossman later crystallized human rhinovirus 14 and highlighted functional relationships with other picornaviruses¹⁰⁹.

Crystallisation has provided a lot of insight into virus structures, but it is limited to regular virus capsids that can crystalize: to study the structure of viruses as a whole, electron microscopy was necessary. Although the advances in metal shadowing and negative staining had greatly enhanced the quality of the information that could be obtained from biological specimen in EM, these samples still had to be dehydrated, adsorbed to a supporting film and be covered with an electron-dense material limiting the information that could be gained about the original material; molecular flattening, selective sample orientation, positive staining or partial staining are only some of the further artefacts that can be encountered⁸⁷.

For regular viruses algorithms for single particle reconstruction elevated CryoEM from a low-resolution technique to a versatile tool for structural biology¹¹⁰. As of April 2017, 94 full virus structures acquired from single particle reconstruction were published and listed in the EMDataBank with resolution below 4 Å. Algorithms to reconstruct 3D density maps of single particles from thousands of 2D projection images have proven successful for symmetrical samples such as non-enveloped viruses or viral capsids where e.g. an icosahedral symmetry can be imposed. For less structurally homogeneous samples, calculations without imposed symmetry remain challenging¹¹¹.

2.4 Cryo electron tomography and the resolution revolution

A different methodology is necessary to probe the structure of extremely heterogeneous samples, flexible, short-lived samples or membrane bound proteins. In cryo electron tomography (CryoET) a sample is rotated around a fixed axis to acquire the specimen at different tilt angles usually from -70 to 70° with increments of 1 to 2° or increments in relation to the cosine of the tilt angles¹¹². The total electron exposure must be minimized to about 1 electron

per \AA^2 per image and is adapted to the respective tomography setup and the sample sensitivity. Today samples up to a thickness of $1\text{ }\mu\text{m}$ can be imaged, but sample thickness and the attainable resolution are inversely related. Fiducial markers (colloidal gold particles of 10-20 nm in diameter) are classically imaged with the samples to accurately realign tilt series. In a marker-free alignment, other identifiable features of the sample or cross-correlation can be utilized. Tomogram reconstruction is classically performed in a weighted back-projection method¹¹¹. As the tilt series are only acquired at $\pm 70^\circ$, the missing wedge can lead to elongation of the tomograms in the direction of the electron beam¹¹³. Further sub-volume averaging of regions of interest between tomograms can further enhance information on the structure of single molecules of interest in their natural context¹¹⁸.

Integrative approaches, such as the structure determination of the 26S proteasome holo-complex, by fitting crystal structures with the help of residue specific crosslinking and proteomic techniques into a low resolution CryoEM, can produce understanding of the sequence of events of the protein action¹¹⁴.

Advances in the field, including the development of energy filters, phase plates¹¹⁵ as well as advances in sample preparation (more stable gold grids, graphene films) and especially the development of new direct electron detectors¹¹⁶ and faster automated readouts lead to a 'resolution revolution'¹¹⁷. Consequently, it was possible to obtain a high-resolution structure of the 26S proteasome by CryoEM in weeks instead of years as for the 2012 published 26S proteasome structure¹¹⁸.

Proteins or viruses, however, do not naturally function intracellularly in an isolated manner, but in a densely-crowded environment. For bulky samples cryo-ultramicrotomy (CEMO-VIS) was developed, where a sample is first vitrified and then cut into TEM thin sections to observe bulkier samples in CryoEM. The method was first published by Bernhard et al. in 1965 on frozen sections and further developed on vitrified samples¹¹⁹. The work on vitrified samples improved the resolution, but despite improvements including cryo-protectants such as sugars it still suffers from systematic sectioning artefacts, such as deformation, crevasses, chatter and surface deformations that can clearly be ascribed to the cutting direction and hence be identified. However, artefacts caused by dehydration and chemical fixation remain more difficult to identify. Sectioning tools have been greatly advanced by serial block face imaging¹²⁰ and focussed ion beam (FIB) -milling of thick sample slices imaged by SEM¹²¹.

This has been applied both to resin embedded as well as high pressure frozen brain samples¹²². Hence, to gain more high resolution insight on protein function, FIB milling was further developed to prepare tomography samples to study proteins inside their “close-to-living-state”¹²³.

Recent integrative approaches that use cryo-light microscopy to identify regions of interest for later CryoET further enable a direct functional correlation between molecules within their cellular context¹²⁴. Kukulski et al. applied this for example to the study of the plasma membrane reshaping during endocytosis in time-resolved electron tomography¹²⁵.

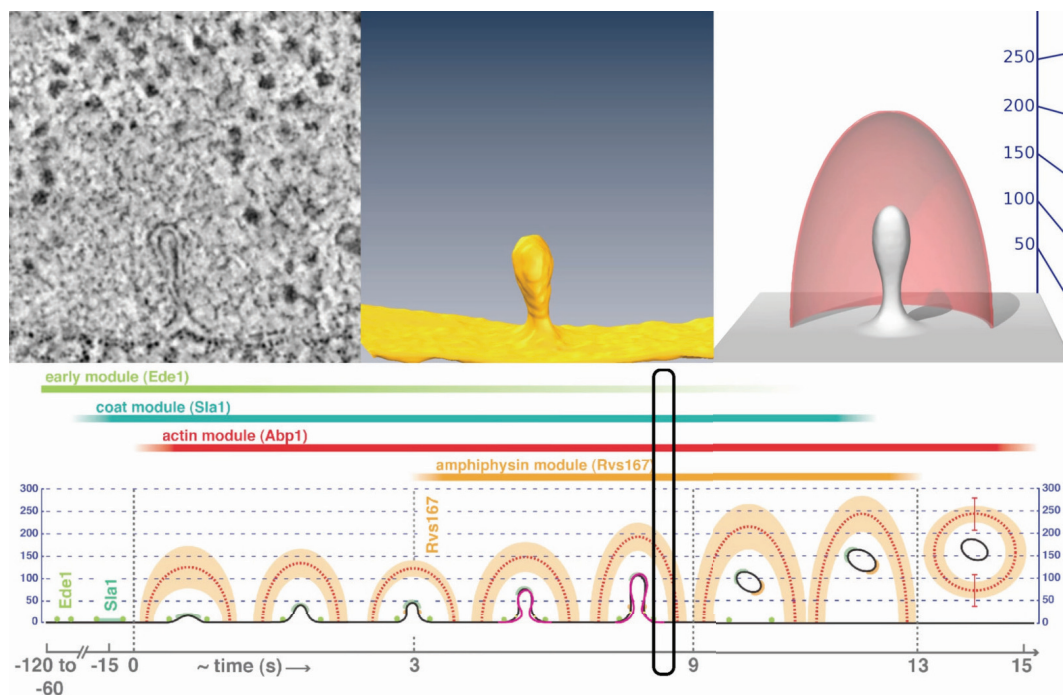


Figure 2-5: Four-dimensional data representation of time-lapse electron tomography of the first 15 seconds of endocytosis showing on the top left representative tomographic slices of the stages, in the top middle an isosurface representation of said stage, in the top right image a 3D surface rendering of the membrane and the actin-network volume, bottom temporal representation of the endocytosis development over time including the respective fluorescence markers utilized to identify the respective stages; Graphic reproduced from Kukulski et al.¹²⁵

2.5 Cryo electron microscopy to elucidate structure and function of herpes simplex viruses

From the first negative staining micrographs of viruses and the imaging of the infection mechanism inside cells, the field of herpes simplex microscopy has advanced substantially. Herpes simplex virus 1 presents a perfect example where an ample number of the new ‘close-to-native’ imaging techniques have been applied to gain combined information of dynamic

processes at EM resolution. Avoiding harsh sample preparation methods such as fixation, dehydration, embedding or staining of the sample is important, especially to understand ultrastructural processes in a mixed hydrophobic-hydrophilic environment. Several groups worked on HSV1 as a model virus for complex herpesviridae such as varicella-zoster virus, Epstein Barr virus, cytomegalievirus or kaposi's sarcoma-associated herpesvirus.

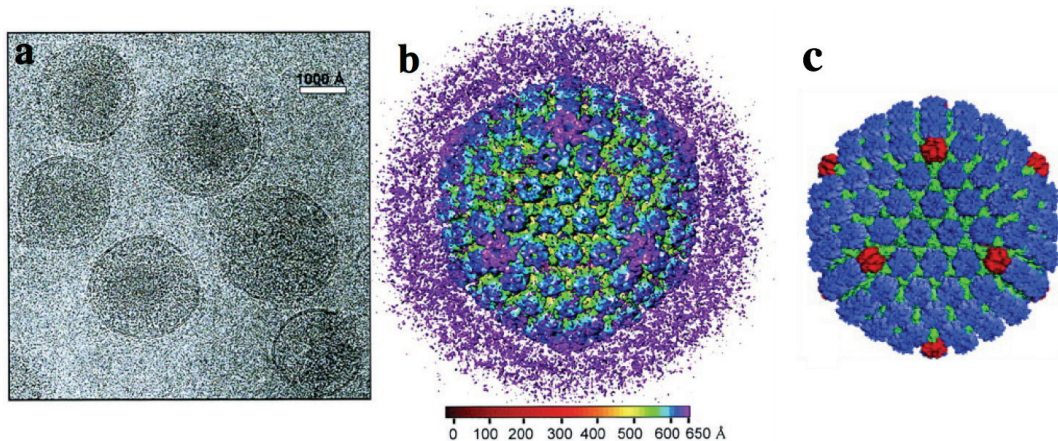


Figure 2-6: CryoEM image (a) and reconstruction (b) of HSV1 capsid and tegument; (c) reconstruction of HSV1 capsid; Graphics reproduced from Zhou et.al.^{126,127}

Zhou et al produced the first 3D reconstruction of HSV1¹²⁶. Figure 2-6 presents a CryoEM micrograph of several HSV1 (a) as well as their reconstruction that reached a resolution of 20 Å. The virus consists of its envelope, tegument proteins, its icosahedral capsid and double stranded DNA. The icosahedral capsid is mainly built of 995 molecules of VP5, the major capsid protein that is arranged in 12 pentons (12) and 150 hexons¹²⁸. Comparing the capsid structure of isolated capsids and capsids inside a full virion, Zhou et al. proposed an important role of the proteins in DNA packing and cytoplasmic transport; also, they suggested that the DNA inside the capsid is arranged in a spool model indicating that the genetic material would pass through a single-entry port. Shortly after, they also published the first 8.5 Å resolution map of the HSV1 purified capsids¹²⁷.

The postulated single entry port was further investigated by Cardone et al. using immunolabeled gold against the portal protein, providing a first orientation for the capsid reconstruction (Figure 2-7)¹²⁹. For objects of lower symmetry, a reconstruction approach without imposing symmetry is important. Advances in Zernike-Phase-contrast enabled Rochat et al. to reconstruct virions without symmetry enforcement and could show that portal protein UL6 (responsible for injection and ejection of DNA into and from the viruses) is situated

beneath the capsid proteins on one of the 5-fold vertices of the icosahedral capsid and presents a 12-fold symmetry, similar to one described before for the tail of bacteriophages¹³⁰. The protein is 19 nm long, its bottom diameter was reported as 16 ± 1.1 nm, the diameter of the part of the protein pointing outwards was measured to be 5.0 ± 0.7 nm¹³¹. In a CryoET approach using sub-volume averaging of regions of interest between tomograms, Schmid et al. showed similarities between the structure of the portal protein of HSV2 and the tail structures of bacteriophages¹⁸. The internal pressure to accommodate the full genome inside of the capsid is ~ 18 atm was measured to be at the same order of magnitude as that of bacteriophages¹³². Accordingly, capsids of herpes viruses and phages are well-reinforced by stabilising proteins as characterized by Sae-Ueng et al. by means of CryoEM and Atomic Force microscopy (AFM)¹³³.

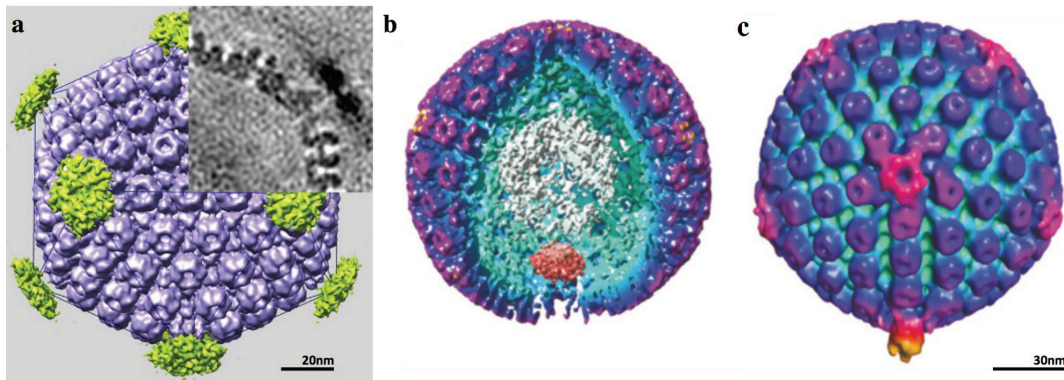


Figure 2-7: CryoEM images and reconstructions of HSV1 capsids showing the portal protein: (a) Immunogold aided symmetry imposed reconstruction of HSV1 with its portal protein¹²⁹, (b) HSV1 capsid partly resected to show portal vertex¹³⁰, (c) HSV1 capsid with portal attached proteins showing similarities to bacteriophage tail organisation¹⁸. Graphics reproduced from respective sources.

From capsid structures, researchers advanced to the study of complete virus particles, including those with envelopes and associated glycoproteins. In a non-symmetry driven CryoET approach Grünwald et al. showed that neither tegument- nor glycoproteins are evenly distributed in or on the virions. Also, the capsid did appear slightly asymmetric, indicating a proximal and a distal pole that, based on their different distribution of tegument and envelope glycoproteins, suggest different functionalities¹⁷.

Of the 12 different glycoproteins (gX) on the surface of HSV2, five are directly involved in the virus entry process to lower the kinetic barrier to induce membrane fusion¹³⁴: gB, gC, gD, gH and gL. Stannard et al.⁸⁸ had described shape and distribution of gC, gD and gB in negatively stained electron micrographs labelled with immunogold. gC appeared as thin 24 nm long spikes that randomly distributed on the virus surface, while gD was 8 to 10 nm long

and tended to cluster on the virus envelope, without a clear pattern. gB was measured as 14 nm long spikes that formed clusters and were often seen at membrane protrusions.

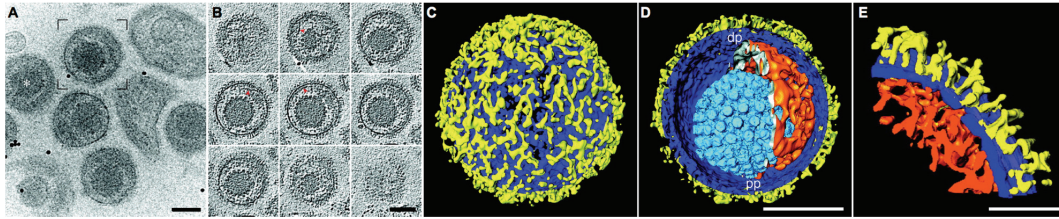


Figure 2-8: CryoET tomographic reconstruction of HSV1 virions showing (a) untitled virions with 10 nm gold fiducial markers and (b) Parallel averaged planes of the reconstructed tomogram of one virion with red highlighted filaments in the tegument protein layer, (c) segmented surface rendering of a virion tomogram with the viral envelope in blue and envelope embedded glycoproteins in yellow, (d) cutaway image with the light blue capsid proteins and orange tegument proteins, dp and pp indicate the location of the distal and proximal pole of the virus, (e) zoom on the tegument – envelope – glycoprotein organisation; Scale bars are 100 nm; Graphic reproduced from Grünewald et al.¹⁷

The ‘molecular gymnastics’¹³⁵ of the different glycoproteins on the HSV envelope have further been studied in native 3D intermediates of membrane fusion published by Maurer et al. by CryoET of cells upon virus entry. First, gC binds HSPGs on the cell surface, then gD binds one of three receptors: herpes virus entry mediator (HVEM), nectin-1 or modified heparan sulfate. Thereafter the gH-gL complex approaches the two membranes and gB initiates membrane fusion. Based on glycoprotein densities in cryoET reconstructions, Maurer et al. suggest a more detailed view of the process, proposing that conformational changes in gD upon binding induce the flip-out of a gH/gL complex to the plasma membrane to connect the viral and the plasma membrane and that gB is recruited later to stabilize the fusion pore.

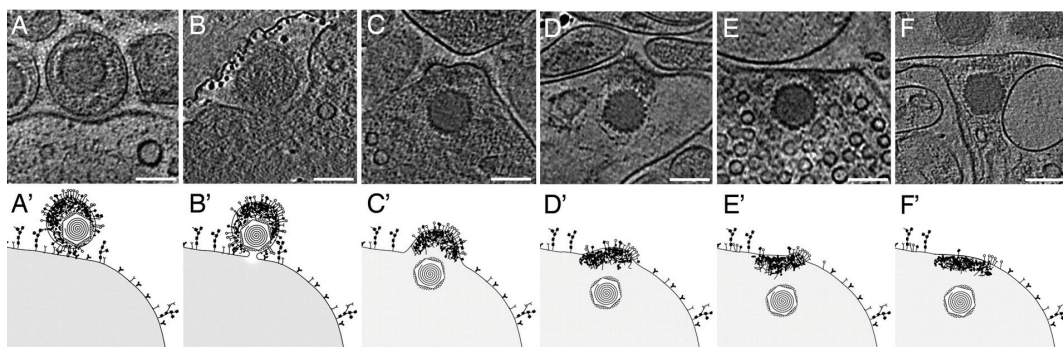


Figure 2-9: HSV1 virion entry and fusion into a synaptosome showing slices of 2/7-12.8 nm thickness of tomographic reconstructions of different stages of virus entry with schematic drawings in the bottom row; (A) Virus attachment, (B) Fusion pore formation at proximal side of the virion, (C) capsid entering the cell, membranes fuse but retain curvature and glycoprotein studding, (D) tegument protein initially remains at the place of virus entry, (E and F) cell membrane flattens again and viral glycoproteins are spread on the membrane, Scale bars are 100 nm; Graphic reproduced from Maurer et al.¹³⁶

Furthermore, they suggested a functional arrangement of the glycoproteins at the proximal pole that appears to serve as the entry pole. At this pole, proteins are less densely packed, minimizing steric hindrance of the glycoproteins. This is in contrast to the densely packed 'glycoprotein 'cap' that forms during the virus assembly on the distal pole¹³⁶.

The full infection cycle of HSV1 has been revisited in close-to-native EM approaches (Cemovis, cemovis correlated with fluorescence and soft-x-ray microscopy, live cell imaging correlated to cryoEM and ET) to understand HSV1 action in its native environment in all parts of its 'life cycle' as presented in Figure 2-10.

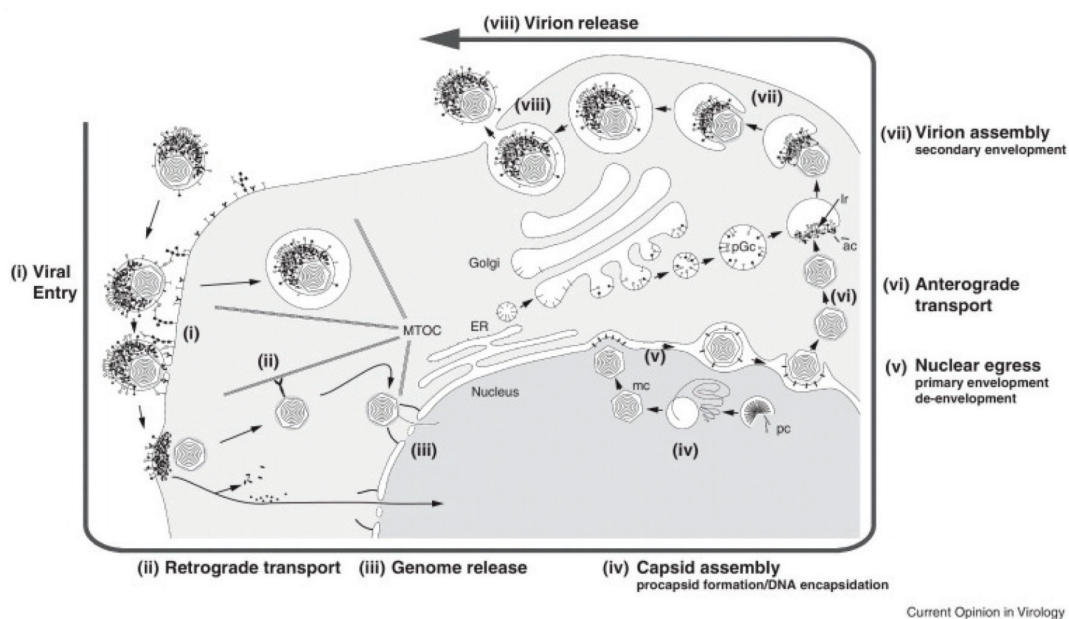


Figure 2-10: Herpes 'life-cycle' illustration showing the full infection cycle from viral entry to the intracellular release of the capsid that is retrogradely transported via the microtubule network to the nucleus to inject its DNA. Alternatively, viral entry starts by endocytosis and the viruses fuse out of the endosome into the cell. Following transcription and genome replication pro-capsids are formed and DNA is enclosed inside the nucleus from which capsids egress by envelopment and de-envelopment through the nuclear membrane. Capsids are then anterogradely transported close to the cell surface for the assembly of the full virion with tegument and glycosylated envelopment by binding to vesicles produced in the Golgi apparatus. Finally, viruses are released by fusion of the virus containing vesicle with the cell-membrane. Graphic reproduced from Mordehai et al.¹³⁷

The herpes life-cycle based on 'close-to-native' acquisition underlines the importance of glycoproteins as well as their sequential activation. The concerted action of the fusion machinery is generally well-agreed on and understanding of this mechanism has been advanced as presented above¹³⁶. Yet, the pivotal action of gB remained poorly understood. Positions in the protein sequence tolerating insertion only partially matched with the crystal structure obtained by Heldwein et al. in 2006¹³⁸. The structure presents only the post-fusion confor-

mation of the protein as did another EM reconstruction of gB based on the membrane interaction of two glycoprotein ectodomain forms¹³⁹. Indeed, Mordehai et al.⁴⁰ studied the full-length HSV1-gB molecule to probe its native, less stable conformation integrated in membranes. Presenting the protein on lipid vesicles of different diameter yielded not only the previously known post-fusion structure, but also a shorter, more condensed form of the protein extending only 10 and not 14 nm from the envelope. Fitting of the known gB domains into the new condensed conformation yielded a structure that matched well with the pattern of tolerated and non-tolerated insertions in the gB genome. This fit of the condensed form showed a different arrangement of the gB domains most strikingly that of the hydrophobic fusion loops, which are responsible for the interaction with the cells' membrane in the two different conformations as depicted in Figure 2-11.

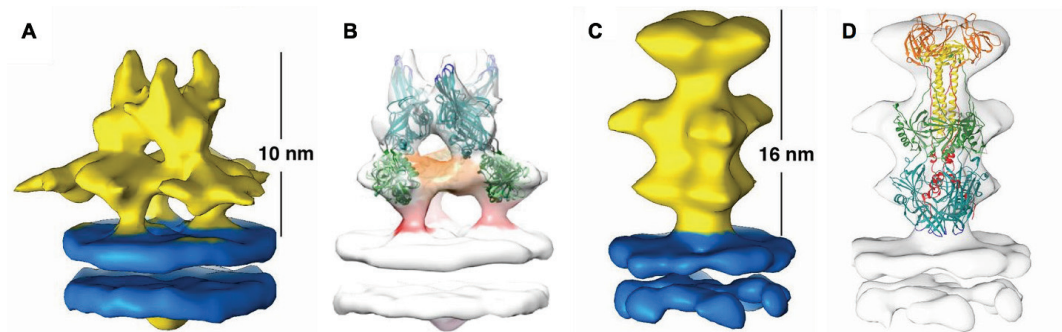


Figure 2-11: CryoET sub-volume averaging of HSV1-gB on vesicles showing two different conformations: short pre-fusion conformation (A, B) and elongated post-fusion conformation (C, D); (A, C) isosurface representation of the protein parts inside (blue) and outside (yellow) of the membrane; (B, D) Fitting of domains identified in crystal structures of HSV1-gB into the isosurfaces as determined form; Graphics reproduced and merged from Mordehai et al.⁴⁰

2.6 Electron microscopy in antiviral research

To summarize, EM has provided invaluable insight into the workings of viruses, opening more possibilities to interfere in these processes with antiviral substances. To date, most research on antivirals is conducted using molecular biology or virology methods, though EM can provide a more direct insight into the workings of antiviral substances. Up to now, microscopy studies have been limited to single images of negatively stained or resin embedded viruses after interaction with an antiviral substance^{65,75,140}.

In order to understand the effect of the broad-spectrum virucidal NPs presented in Chapter 1 that were developed in our research group we undertook initial negative staining EM experiments on two HSPG dependent viruses: HPV and HSV2.

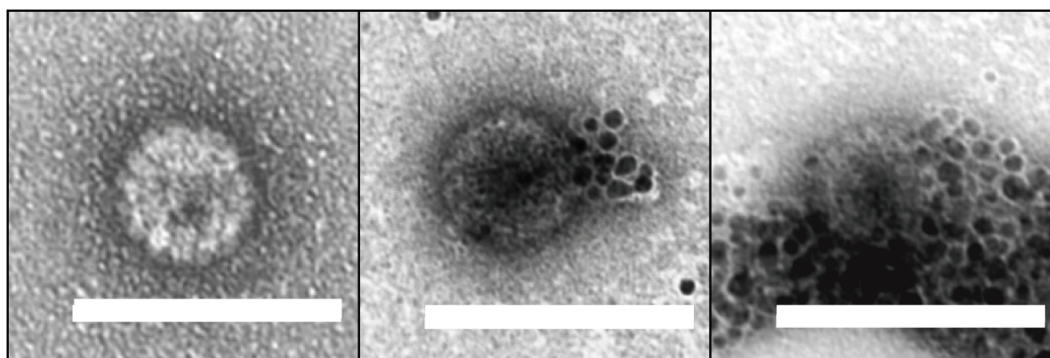


Figure 2-12: Dry negatively stained TEM of HPV-16 Pseudovirus treated with 0.1 mg/ml MUSOT 131008 for 1h at 37°C, (Sample preparation by V. Cagno, imaging by M. Valino; the scale bars are 100 nm).

Dry negatively stained TEM imaging revealed clearly visible 80 nm HPV virus capsids with occasionally well-resolved capsomers. Samples treated with MUSOT 131008 NPs showed that a considerable fraction of the viruses co-localized with the NPs as shown in Figure 2-12. A comparable association of viruses and NPs can be observed when treating HSV2 with MUSOT 131008 NPs as illustrated in Figure 2-13. HSV displayed a similar NP-association seen in the case of HPV, but additionally collapsed viruses were imaged as shown in the last picture of Figure 2-13 and appeared in a considerable fraction of the grid scanned.

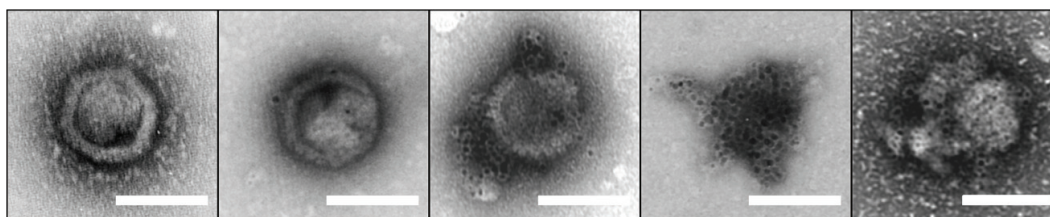


Figure 2-13: Dry TEM images of HSV2 after treatment with 0.2 mg/ml MUSOT 131008 NPs for 1h at 37°C. The viruses exhibit different amounts of NPs associated ranging from none to deflated viruses with many NPs (Sample preparation by V. Cagno, imaging by M. Valino; the scale bars are 100 nm).

As mentioned above negative staining has a lot of advantages: it is simple and fast to provide a first high contrast glance into the sample morphologies. On the other hand, it has significant limitations, especially in the case of sensitive samples such as viruses. Although uranyl acetate provides a certain fixation to the viruses upon drying onto the carbon surface on the grid, the viruses flatten and distort. Additionally, the images obtained show the electron dense stain and not directly of the light elements that make up the viruses. Certain areas of the sample become as electron dense as the metallic core of the NPs, rendering it difficult to clearly identify the NPs on the viruses. Additionally, this type of sample preparation is prone to form NP aggregates upon drying: the possibility that NPs merely aggregate onto

the viruses during sample preparation, instead of actually interacting in the solvated state must be taken into account for any interpretation of images that use negative staining. To address these concerns, CryoEM allows for an imaging of complex structures in their near to native solvated state. Although CryoEM presents its own sets of challenges and limitations as explained above, we regard it as the only tool to enable a true view into the association and morphology of the viruses upon interaction with our broad-spectrum antiviral NPs in solution.

This study uses EM to verify whether the treatment of viruses with broad-spectrum antiviral NPs can be correlated to detectable morphological damage to the viruses. To this end we examined the differences between the association of virustatic and virucidal NPs to different HSPG-dependent viruses in their near-native solution state using cryoEM. *Research question 1: Can the treatment of viruses with antiviral or virucidal NPs be correlated to detectable morphologies or morphological damage to the viruses?* By employing qualitative and quantitative assessments of the treated virus populations we aimed to establish differential association characteristics and morphologies of virustatic and virucidal NPs on viruses. In a further exploratory examination of the association of single NPs onto viruses we aimed to identify determinants of the interaction of virucidal NPs with viruses. *Research question 2: Can a mechanism for the interaction of virucidal NPs with viruses be hypothesised?*

This project provided an opportunity to advance the field of NP – based antivirals. It is the first study to provide a solution-state visualisation of the interaction of viruses and different types of NPs, to demonstrate, using CryoEM, that the virucidal effect depends on the type of monolayer that covers the NPs. This study further offers important insight on the association of single NPs with viral proteins of envelope and capsid and their effect upon them.

Chapter 3 Materials and Methods

All chemicals were purchased from Sigma Aldrich unless otherwise noted.

3.1 Nanoparticle Synthesis and characterisation

3.1.1 Ligand synthesis

The ligand 11-mercapto-1-undecanesulfonate (MUS) was synthesized by Paulo H. Jacob Silva synthesized based on the method described in Verma et. al.¹⁴¹ through an adapted synthesis protocols described in Jacob-Silva et al.¹⁴². HS-(CH₂)₆-(OCH₂CH₂)₂-OH (EG₂OH) was ordered from Prochimia Surfaces, Poland. Sodium 2-mercaptoethanesulfonate and 1-Octanethiol were purchased from Sigma Aldrich.

3.1.2 Nanoparticle synthesis

There are many methods to synthesize monolayer protected metallic NPs¹⁴³. In this thesis, NPs were synthesized via “direct” methods: the gold precursor was reduced in the presence of the ligands that compose the monolayer.

Generally, tetrachloroaurate H₂HAuCl₄·3H₂O was dissolved in ethanol with an equimolar amount of the thiolate ligand mixture: after 15 min, a saturated ethanolic solution of sodium borohydride (NaBH₄) was added dropwise. The product was isolated via decantation, washed with solvents (ethanol and acetone), followed by water-washes using centrifuge-assisted dialysis filters (Amicon® Ultra-15 Centrifugal Filter Devices (10k or 30k NMWL). This method enabled the synthesis of sulfonated particles (mixed with 1-Octanethiol or not) with size distributions between 1-4 nm (see Table 1). These particles were synthesized by Paulo H. Jacob Silva and Ahmet Bekdemir. The EG₂OH NPs were synthesized by Barbara Sanavio following this same procedure, outlined in Cagno et al. (submitted)⁷⁷.

3.1.3 Nanoparticle characterisation

For the NP characterisation, classically two techniques are used: transmission electron microscopy (TEM) to measure the diameter of the gold core of the NP and Nuclear Magnetic Resonance (NMR) to determine the ligand ratio in the shell of mixed ligand NPs.

To obtain the NP core size 5 μ l of a 0.02 mg/ml solution of NPs were drop-cast onto a carbon coated TEM grid and dried for at least 30 min. TEM images of the NPs were acquired in a Tecnai Spirit BioTWIN at a magnification of 100,000x and subsequently processed with a self-written macro in ImageJ to yield a size distribution of at least 1000 NPs.

To characterize the ligand ratio of mixed ligand NPs 1 to 5 mg of NPs are decomposed in 0.6 ml of etching solution of Iodine (purchased from Acros) in MeOD-d₄ (15 mg in 100 ML). The ligand ratio was determined in ¹H-NMR and calculated from the NMR peaks as described in Jacob-Silva et al.¹⁴². Figure 3-1 shows the NMR spectrum of iodine-etched MUSOT 131008 NPs: the peak at 0.9 ppm corresponds to the methyl terminal of 1-Octanethiol and the other peaks contain signal from both ligands. The ratio was determined with the values from the integration of each region and the knowledge of the chemical shifts of both ligands.

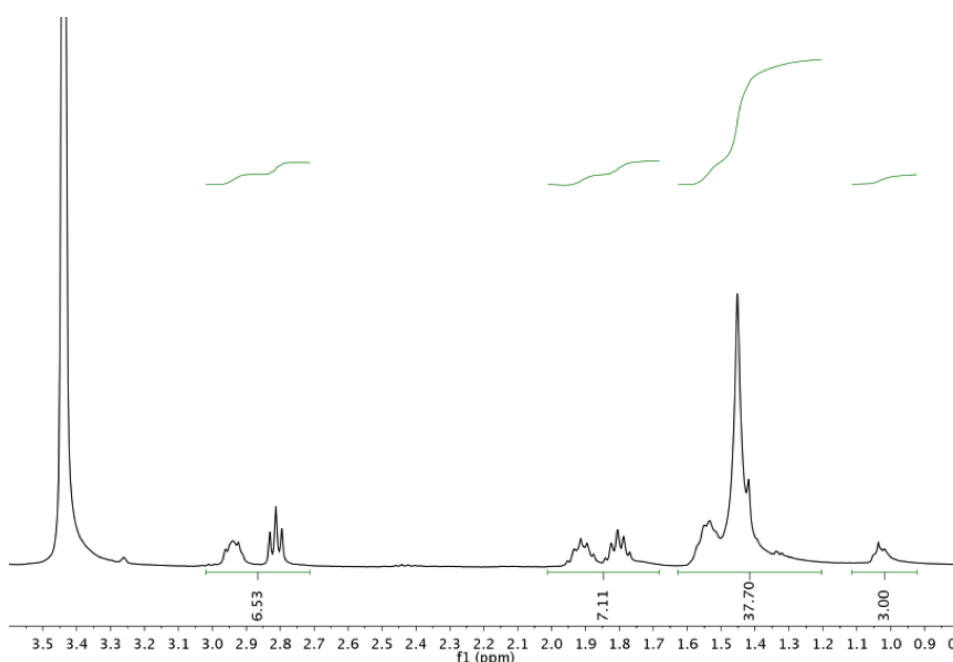
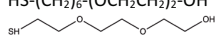
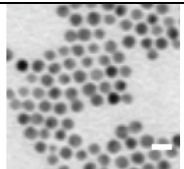
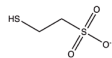
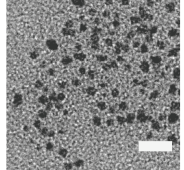
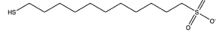
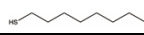
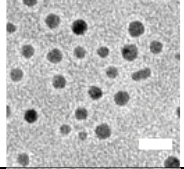
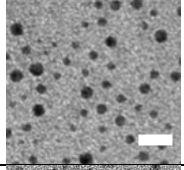
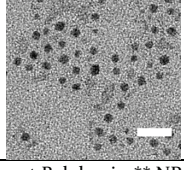


Figure 3-1: ¹H-NMR of decomposed MUSOT 131008 NPs, Graphic reproduced from V. Cagno et al. (submitted)
77.

Table 1 summarizes the results of the TEM and NMR NP characterisation showing that the main difference in the NP characteristics is their ligand shell composition. The molecular weight of ligand functionalized NPs has been calculated using Analytical Ultracentrifugation (AUC) based on Carney et al.¹⁴⁴ where both total volume and total mass of the NP depend on the respective radii of the NP core and the NP shell and their respective densities.

Table 1: Basic NP characterisation

Name	Ligand	Ligand ratio [%OT]*	Representative TEM [Scale bar 10 nm] **	Core diameter [nm]	Mol weight [kDa]
EG ₂ OH	$\text{HS}-(\text{CH}_2)_6-(\text{OCH}_2\text{CH}_2)_2-\text{OH}$ 	-		6.2 ± 0.8 ***	1660
MES	2-mercaptoethanesulfonate 	-		2.6 ± 0.8 nm ***	120
MUSOT BS	11-mercapto-1-undecanesulfonate  + 1-octanethiol 	25		3.3 ± 0.8	330
MUSOT 131008	"	34		2.8 ± 0.6 ***	220
MUSOT 200515	"	29		2.14 ± 0.5	125

*NMR performed by Paulo H. Jacob Silva, Pelin Z. Guven and Ahmet Bekdemir, ** NP dry sample preparation Marie Mueller, imaging by Urzula Cendrowska and Pelin Z. Guven, Image processing Marie Mueller, *** TEM and size quantification reproduced from V. Cagno et al. (submitted)⁷⁷.

3.2 Cyclodextrins

β -Cyclodextrins are 7 membered sugar ring molecules with an inner diameter of 7.8 Å, an outer diameter of 15.3 Å at a height of 7.9 Å. ¹⁴⁵ CD1 is the commercially available β -Cyclodextrin, sulfated sodium salt (CAS Number 37191-69-8) with a molecular weight of 2357.9-2650.0 g/mol.

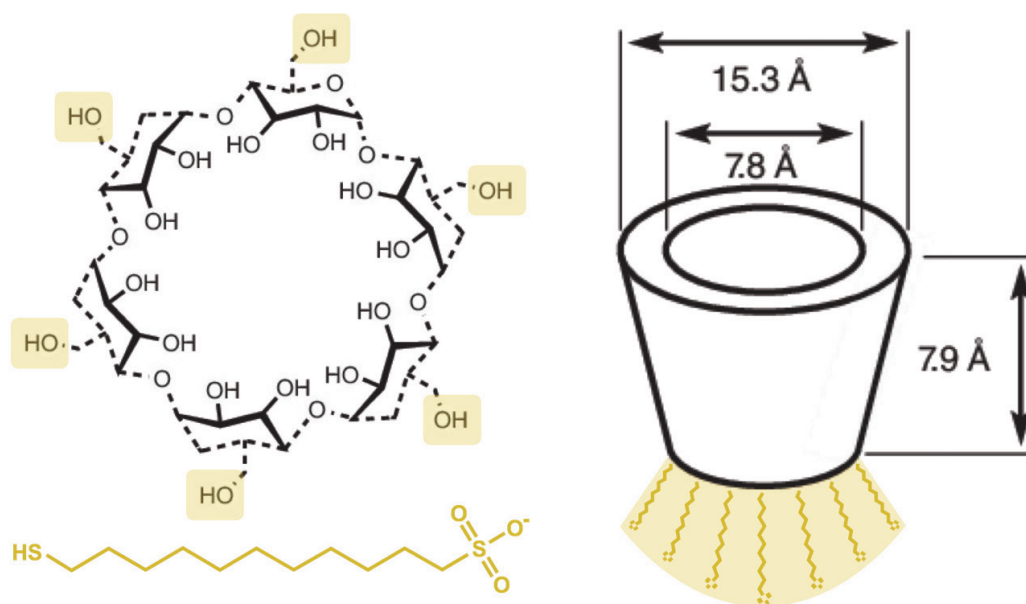


Figure 3-2: Schematic representation of β -Cyclodextrin with MUS functionalisation; Graphic reproduced and modified from Haldar et al.¹⁴⁵

In addition to the commercially available Cyclodextrin in which the sulfonates are directly bound to the sugar ring, Samuel Jones synthesized two further sulfonated cyclodextrins (CD₂ and CDS₂) with an eleven-carbon chain linker between the ring and the sulfonate group identical to the ligands on the NPs. Figure 3-2 shows schematically where the cyclodextrins have been functionalized.

3.3 Virus culture and antiviral testing

3.3.1 Cell culture

HeLa (human cervical carcinoma cell line) and Vero (African green monkey fibroblastoid kidney cells) were purchased from ATCC (American Type Culture Collection, Rockville, MD). All cell culture media as well as supplements were purchased from Thermo Fisher Scientific Inc. Waltham USA.

Both cell lines were cultured in Dulbecco's Modified Eagle Medium with high glucose 25mM, sodium pyruvate 1mM, L-glutamine 4mM supplemented with 10% FBS-South America-Origin. They were grown at 37°C with 5% CO₂ at a humidity of 80%.

3.3.2 Pseudo Human Papilloma virus -16 (HPV)

HPV pseudoviruses were grown by transfecting 293TT cells with a plasmid expressing the papilloma virus major (L1) and minor (L2) capsid protein and a reporter plasmid expressing GFP. Mature capsids were harvested the next day, clarified and then purified on an Optiprep gradient. The sample purity was tested in an SDS gel and by titration on 293TT cells for GFP expression. Samples were stocked frozen at -80°C at a titer of 10⁶ focus forming units per ml. This sample preparation has been performed by V. Cagno.

3.3.3 Herpes simplex virus type 1 and 2 (HSV1 & HSV2)

Clinical isolates¹⁴⁶ were kindly shared by Prof. Lembo (University of Torino, Italy) and were further propagated on Vero cells.

3.3.4 Viral inhibition assay (Dose response) and Virucidal assay on HPV, HSV1 and HSV2

The antiviral effect of the substances was tested in a plaque reduction assay. Vero cells were plated in 24-well plates a day in advance (100,000 cells per well). Sequential dilutions of NPs or CDs were incubated in 2% FBS DMEM with viruses at a multiplicity of infection (MOI) of 0.005 pfu/cell for 1h at 37°C prior to the infection of the cells or 2 h at 37°C. After the infection, the cells were washed with fresh medium and covered with medium containing 0.5% wt/v methyl cellulose in 2% FBS-DMEM to limit virus spread though the medium and incubated at 37°C, 5% CO₂. Upon clear plaque formation (HSV1 – 2 days, HSV2 -1 day) the cells were washed with MilliQ and stained with 0.1% wt/v crystal violet in 20% v/v ethanol for 20min, washed with MilliQ and dried. Plaques in treated and untreated wells are counted to determine the percentage of infection and accordingly calculate the dose response. The effective concentration at which 50% (e.g. 90%) of all viruses are inhibited is called EC 50. Respective EC₅₀ and EC₉₀ values were calculated from the dose response curve by fitting a variable slope sigmoidal curve through regression analysis in Prism 7.0 (GraphPad Software, San Diego, California, U.S.A.).

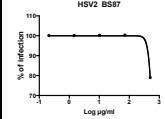
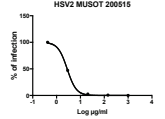
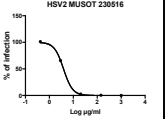
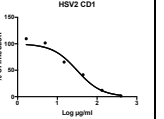
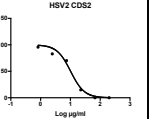
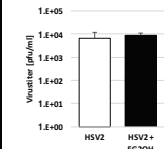
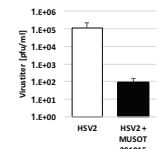
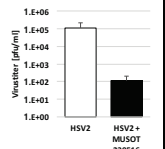
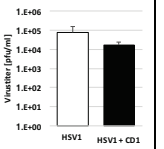
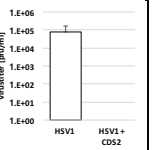
The virucidal effect of the test substances was evaluated in a microtiter virus yield reduction assay¹⁴⁷. Briefly, Vero cells were plated onto 96 well plates to form a monolayer of approx. 13,000 cells per well. Test substances (at a concentration of EC₉₀ or higher) and viruses (10⁴-

10^5 pfu, an MOI of 1-5 pfu/cell) were incubated for 1h at 37°C prior to infection. Pre-incubated viruses were sequentially diluted onto the cells down to highest dilution factor of 2×10^6 . After 2h of infection the cells were treated as described in the dose response assay – washed, covered with methyl cellulose, incubated until plaques formed, washed, stained, dried, counted. The viral titer was then calculated from wells where the test substance concentration was below the EC₅₀. Error bars in the virucidal test represent the standard deviation of all counts over a single virucidal plate.

Dose response and virucidal assay for the interaction of HPV with NPs were performed by V. Cagno and showed a clear virucidal effect for MUSOT 131008 and MUSOT BS NPs. Dose response and virucidal assay for the interaction of HSV2 with NPs were also performed by V. Cagno and showed a virustatic effect of heparin and MES and a clear virucidal effect for MUSOT 131008 as shown in Figure 1-7.

The tables following on the following pages summarize the results of the dose response and virucidal testing of all other particles and cyclodextrins studied for their interaction with HSV1 and HSV2 here.

Table 2: Dose response and virucidal assay of HSV2 to NPs

	EG2OH	MUSOT 200515	MUSOT 230516	CD1	CDS2
Dose response curve					
EC50 in µg/ml	613	2.78	3.9	31.1	10.7
EC90 in µg/ml	915	7.32	10.2	148.1	32.4
Virucidal activity at a dose of 200µg/ml					

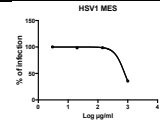
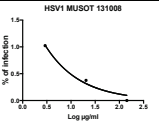
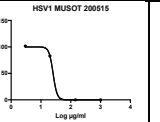
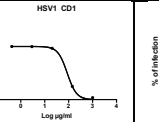
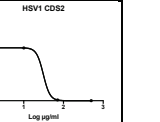
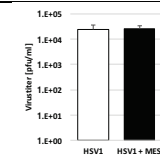
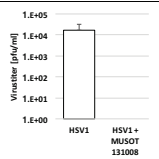
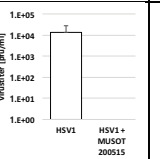
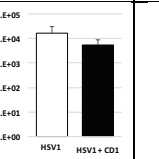
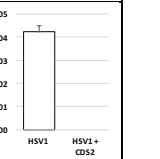
HSV2 viruses have been tested against a range of different particles and cyclodextrins. Anionic EG2OH NPs showed no reduction in virus infectivity nor any reduction of virus titer in the virucidal assay. These particles served as negative controls for electron microscopy. MUSOT 200515 and MUSOT 230516 particles showed a steep dose response curve with EC₉₀

concentrations of about 10µg/ml, which would be approximately 45 nM. Tested at a concentration of 200µg/ml that is well above the EC₉₀ all three particles exhibited a virucidal effect when tested on approximately 50,000 viruses. At substantially higher virus loading 20 µg MUSOT 200515 were shown to irreversibly inhibit 50,000 -100,000 viruses in different experiments (data not shown). Two different cyclodextrins were tested for their antiviral effect on HSV2 and all inhibited the viruses. The subsequent virucidal test, though, showed that only CDS2 blocked the viruses irreversibly. CD1 could be diluted off the virus and a fully infective virus was released.

The results of the antiviral testing on HSV1 are presented in Table 3. Short ligand MES particles showed only a minor effect on the viruses at high doses. The dose-response curves on HSV1 were largely shifted to higher concentrations leading to EC₉₀ values of well above 1mg/ml for MES. Thus, the virucidal test at 0.2mg/ml naturally yielded no reduction of virus titer. The MUSOT particles studied showed a dose response comparable to that on HSV2, though shifted to higher doses as well. Whilst MUSOT 200515 showed an EC₅₀ of 2.78 on HSV2 the EC₅₀ for HSV1 was shifted to 25.7.

Although a concentration of 0.2mg/ml is above the EC₉₀ of all MUSOT particles tested on HSV1 in the evaluation of the virucidal activity only MUSOT 131008 showed a 4 log reduction. The log reduction of CDS2 at 0.2mg/ml was only of 1.2 at 0.2mg/ml. Therefore, several virucidal test were repeated at higher concentrations and yielded clear virucidal effects for MUSOT 230516, MUSOT 131008 and CDS2. CD 1 tested at 1mg/ml was again diluted off the virus in the virucidal sequential dilution showing that its antiviral effect is merely virustatic, not virucidal.

Table 3: Dose response and virucidal assay for HSV1

	MES	MUSOT 131008	MUSOT 200515	CD1	CDS2
Dose response curve					
EC ₅₀ in µg/ml	~790	0.001	25.7	117.2	31.1
EC ₉₀ in µg/ml	~3000	0.06	35.6	346.1	47.6
Virucidal					
Virucidal dose	200µg/ml	200µg/ml	1000µg/ml	1000µg/ml	1000µg/ml

While a dose response is performed at an approximate virus to NP ratio of 5 viruses per μg of NPs in 200 μl of total volume, a virucidal test is typically performed with 2500 viruses per μg of NPs in 100 μl . The results of the dose-response can be considered a good orientation for the concentration to choose for the virucidal, but it might be taken into consideration that a certain number of NPs is necessary to irreversibly inhibit a virus.

Different characteristics of NPs, for example median diameter and solubility, can vary across identical preparations. This issue is often termed batch-to-batch variability. Consequently, the influence of the NPs size and OT ratio on the virucidal activity on MUSOT-NPs was tested and showed that in a range of mean core diameters from 2.1 to 3.0 nm size does not affect the NP's virucidal activity. Neither does the OT ratio. OT ratios from 11% to 34% did not correlate with the NPs' ability to irreversibly inhibit HSV2.

The time course of the virucidal effect as evaluated in a separate virucidal experiment depicted in Figure 3-3 showing that a virus titer reduction of 3 logs can already be reached after 30 min at a concentration of 200 $\mu\text{g}/\text{ml}$.

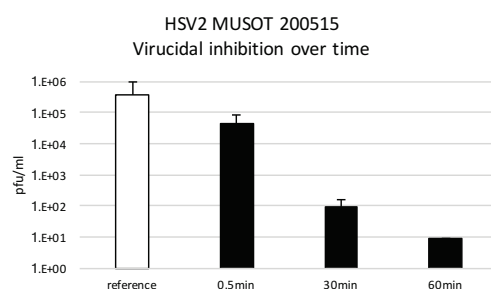


Figure 3-3: Virucidal assay of HSV1 with 230516 NPs over a time frame of 1h. A log reduction higher than 3 logs can be achieved after 30min.

Table 4 summarizes the results of the virological testing of the different NPs and cyclodextrins that were used in the course of this study.

Table 4: Summary of antiviral and virucidal properties of NPs and Cyclodextrins

	Antiviral	Virucidal
EG2OH	✗	✗
MES	✓	✗
MUSOT BS	✓	✓
MUSOT 131008	✓	✓
MUSOT200515	✓	✓
CD1	✓	✗
CD2 and CDS2	✓	✓

3.4 Transmission electron microscopy

3.4.1 Dry transmission electron microscopy

Viruses were incubated with NPs in a setup comparable to the virucidal setup and drop cast onto a glow discharged carbon coated 400 mesh-Copper grid and left to adhere in a humidified chamber for 5 min. Then the grids were washed on a 20 μ l drop of MilliQ and stained with 0.5% Uranyl acetate. Images were taken on a Tecnai Spirit BioTWIN Transmission electron microscope at an acceleration voltage of 80kV at magnifications of 30,000-50,000x.

3.4.2 Cryo electron microscopy and tomography

For cryo electron microscopy (CryoEM) Viruses were treated with NPs and deposited onto a lacey or quantifoil R2/2 on Copper 300mesh grid inside a FEI vitrobot Marc IV, then blotted and immediately vitrified in liquid ethane. The samples were continuously kept frozen below -170°C and imaged in a Gatan 626 single tilt cryo tomography holder using a FEI Tecnai F20 Cryo 200kV transmission electron microscope (TEM) equipped with a 4k by 4k FEI Eagle CD camera at magnifications of 30,000-50,000x in Low Dose mode at an exposure of 4-10electrons/ \AA^2 with a defocus of 1.5 to 2 μm .

The association of NPs and viruses has been counted and classified. The virus morphology has been evaluated. Image processing of the 2D projection images in ImageJ¹⁴⁸ included size measurements of capsids, virus envelopes as well as enumerating NPs on virus envelopes as shown in Figure 3-4.

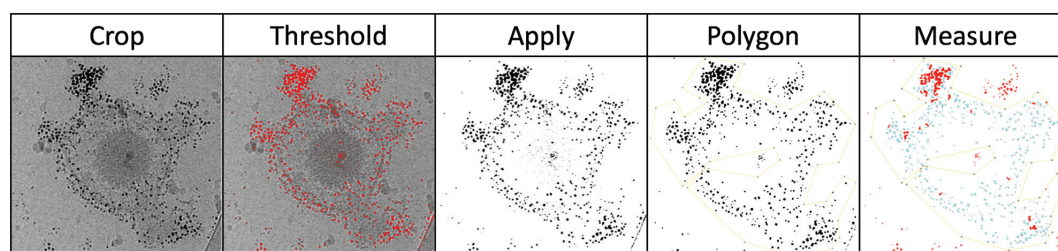


Figure 3-4: NP enumeration on virus envelopes in ImageJ: the cryoEM micrograph was cut to a region of interest, a threshold to choose all NPs was applied, to remove small densities from ethane droplets or the virus capsid the thresholded areas were eroded and then dilated one, then a polygon was drawn around the NPs attached to the viruses and the size and number of the particle was measured for particles with an area above 0.5 nm^2 and a circularity above 0.6.

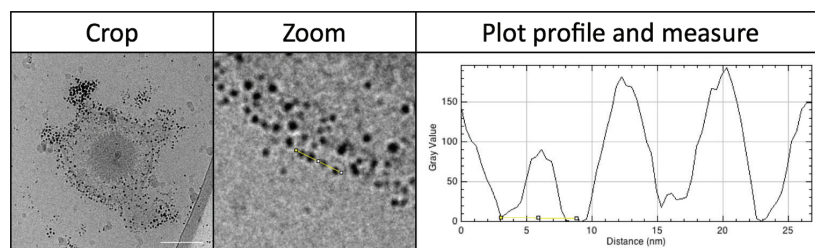


Figure 3-5: Measurement of NP distance from viral envelope as well as NP particle to particle distance in ImageJ: the cryoEM micrograph is cropped and then zoomed to a region of interest, then the line profile over NPs lining up on the side of the virus that appear to roughly be at the same focus are plotted, and the centre to centre distance between NPs is measured.

Cryo-Electron-Tomography (CryoET) the samples have been tilted from -60° to $+60^\circ$ in 2° increments at a total electron dose of electrons/ \AA^2 using the Tecnai Imaging & Analysis software. Tilt series were aligned and tomograms reconstructed using etomo of IMOD¹⁴⁹. The tomograms were further processed in ImageJ¹⁴⁸ to produce grouped Z slices of the reconstructed tomograms by averaging 10 nm in height per slice, 3D gaussian blurring was applied for increased contrast.

The authors contributions in this thesis cover a large part of the virological testing and all cryoEM studies as well as the according analyses.

Chapter 4 Overall virus – nanoparticle association

The previously described studies have been solely based on the cytopathic effect that the viruses exerted onto cells and limited EM observations. This chapter presents results to answer the first research question: Can the treatment of viruses with antiviral or virucidal NPs be correlated to detectable morphologies or morphological damage to the viruses? We examined the differences between the association of virustatic and virucidal NPs to different HSPG-dependent viruses in their near-native solution state using cryoEM. In a qualitative and quantitative study of the treated virus populations, we aimed to establish differential association characteristics and morphologies of virustatic and virucidal NPs on viruses.

4.1 Cryo electron microscopy of HPV-NP-interaction

The first virus imaged in CryoEM upon interaction with virucidal MUSOT NPs was human papilloma-16 pseudovirus (HPV) at has been presented in the introduction on page 60. It was evident from the images that NPs and capsids co-localize and form different patterns. Four generally different appearances of capsid–NP associations have been identified and quantified: capsids without NPs, capsids with single NPs, capsids with clusters of NPs and fully NP-covered capsids. The relative abundance of each of those classes has been quantified for the interaction of HPV with the different classes of NPs presented in Table 4: Summary of antiviral and virucidal properties of NPs and Cyclodextrins (page 56).

The non-virus interacting NP EG2OH showed almost uniquely viruses free of NPs. Two different virucidal MUSOT-NPs on the other hand largely associated with the viral capsids. Upon 5 min incubation with MUSOT BS the viral capsids were only up to 20% free of NPs. 20% of the viruses are associated with single NPs, 20% with clustered NPs and 40% were fully covered. The proportion of the latter class increased to 81% upon prolonged incubation for 45 min. Upon treatment with MUSOT 131008, no virus remained free of NPs and more than 80% of the viruses were directly fully covered. The size of the fully covered viruses was

88 ± 21 nm, which compares well with that of the virus capsids 65 ± 8 nm, suggesting that the virus capsids are potentially covered by at least a monolayer of NPs.

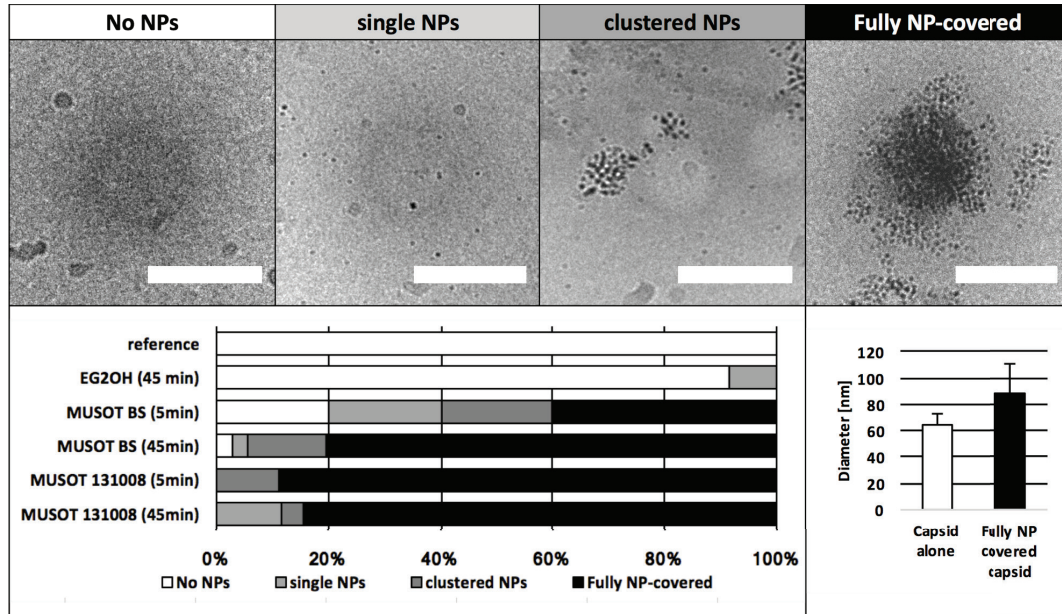


Figure 4-1: CryoEM of HPV-NP association. Top panel: CryoEM images of HPV-NP association showing representative images of the different categories of NP-virus association that have been quantified. Bottom panel: quantification of HPV-NP association for three different NPs (10-50 viruses classified per sample). The Scale bar is 100nm.

HPV pseudovirus proved to be, not only very unstable but also the achieved concentrations were low so that only a small number of viruses could be imaged (10 to 50 viruses per condition). Additionally, imaging of HPV was impeded by the density gradient based on opti-prep, an electron-dense medium that largely decreases the attainable contrast of the virus under CryoEM. Consequently, conclusions from HPV imaging can only conclude that virucidal NPs do numerously attach to and fully cover viruses.

4.2 Cryo electron microscopy of Herpesviridae

Herpes simplex viruses belong to a more complex class of HSPG-dependent viruses. As described in on page 40 following. Herpes viruses consist of an outer envelope studded with glycoproteins, tegument proteins and capsid proteins enclosing the double stranded DNA. CryoEM studies were conducted on two different batches of HSV2 and one batch of HSV1. Figure 4-2 shows different virus morphologies of HSV1 and HSV2 a and b as imaged in CryoEM. The viruses clearly present an icosahedral capsid of about 120 nm in diameter. The enveloped virus has an approximate diameter of 200 ± 47 nm for HSV1 and 180 ± 49 nm for HSV2b. The bottom panel depicts the respective proportion of capsids only and envelopes

capsids. Both viruses show an approximate 1:1 ratio between capsids only and full enveloped viruses, except in the batch HSV2a where only free capsids could be observed.

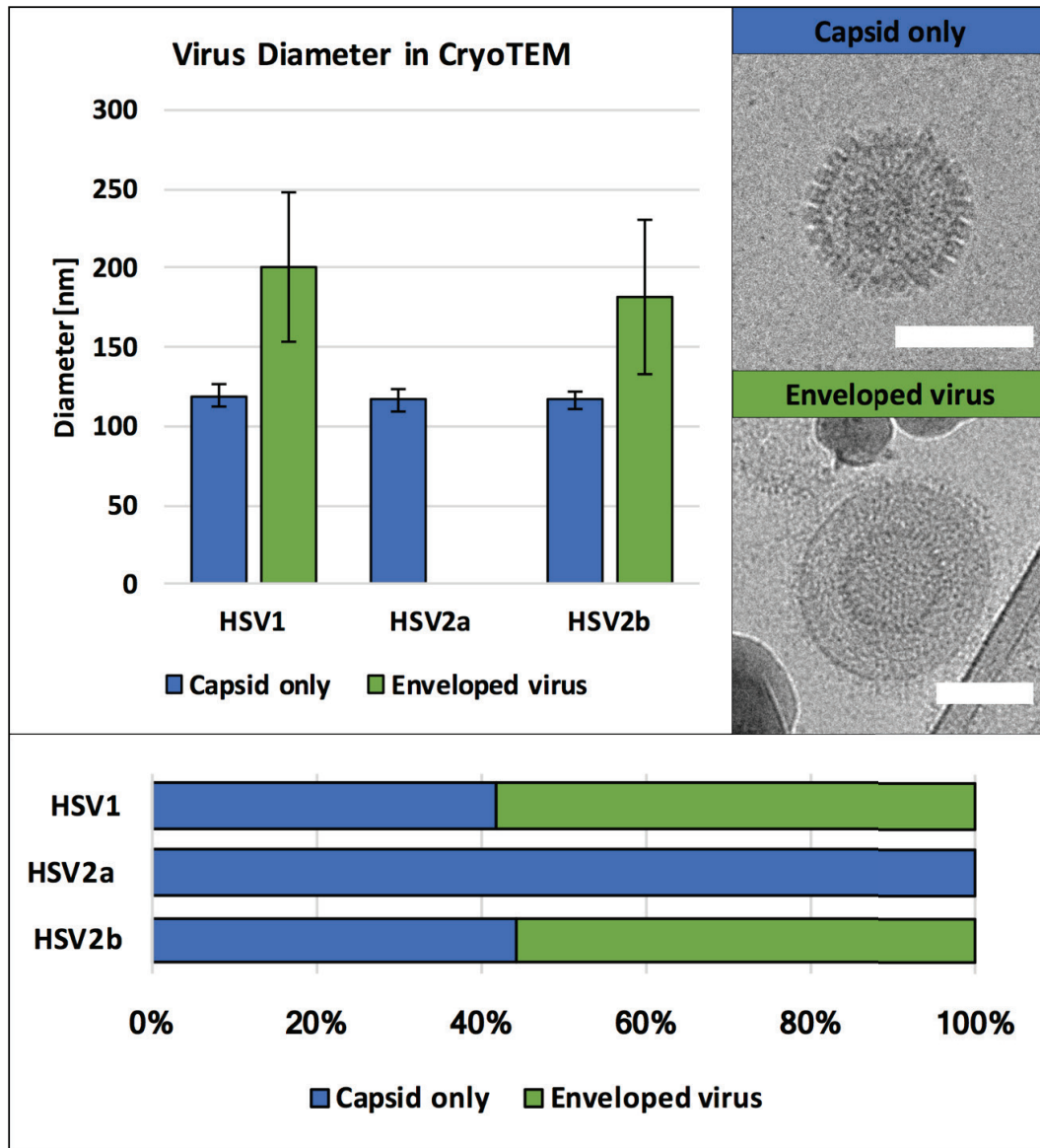


Figure 4-2: CryoEM micrographs and diameter of capsid only and fully enveloped viruses in HSV1 and two HSV2 batches (top) Quantification of the relative abundance of virus capsids and fully enveloped virus by virus and batch (bottom). The scale bar is 100 nm.

4.3 Cryo electron microscopy of HSV2-NP interaction

NPs again avidly associated to viruses. In order to systematize the observations in CryoEM, we categorized the different morphologies of virus-NP interactions as follows: viruses free of NPs, viruses co-localizing with one up to 50 single NPs with an emphasis on single NPs.

When NPs clustered on the viruses they were placed in a separate category. The last category comprises all viruses that appeared fully covered with NPs. Representative CryoEM micrographs per category are depicted in Figure 4-3.

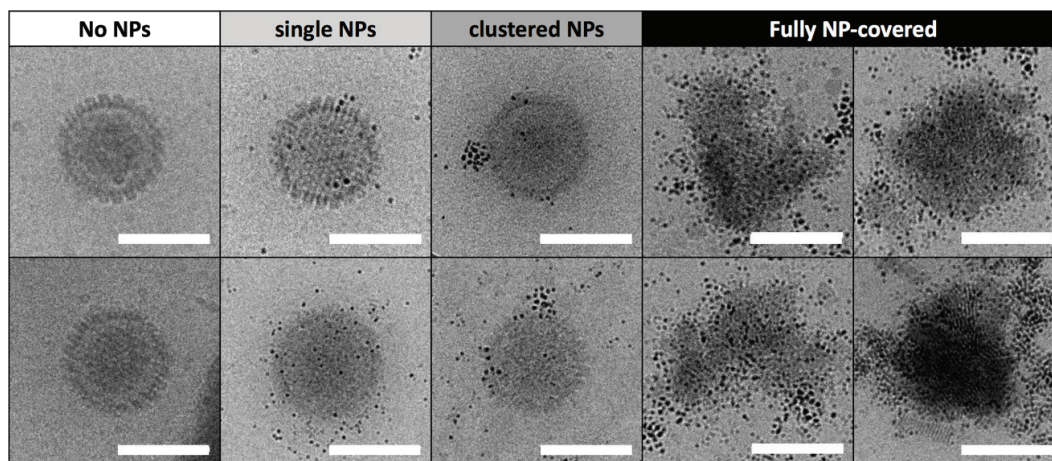


Figure 4-3: Representative CryoEM images for the different general classes of NP- virus association as observed in incubation durations, ranging from 5 min to 2h. The scale bars are 100 nm.

Based on this categorisation the relative proportion of the different classes has been determined as shown in Figure 4-4. The incubations have been performed in a manner comparable to that of a virucidal test with pre-incubation for 1h at 37°C. Different abundances per category clearly highlighted a difference in virus interaction between virustatic and virucidal NPs.

Reference samples as well as the non-virus inhibiting EG2OH predominantly show no or only single NPs co-localizing with the virus capsids. A comparable association pattern applies for the virustatic MES NPs. Virucidal MUSOT NPs on the other hand seem to avidly associate with the viruses showing predominantly fully NP-covered viruses.

In line with the virology results indicating a time dependence of the virucidal effect as can be seen from Figure 3-3, shorter incubation times were tested and viruses associated with MUSOT 131008 were tested after 5, 15 and 30 min of incubation at 37°C. No virus remained free of NPs, even starting at the shortest incubation time of 5 min. Rates of fully covered viruses present are 74% at 5min, 61% at 15min, 76% at 30 min and 39% at 90 min of incubation. Fully clustered viruses appeared to bundle even at short incubation times, hence the rate of fully covered NPs with time should be evaluated with caution, as it is likely to be underestimated (see Figure 4-4d)

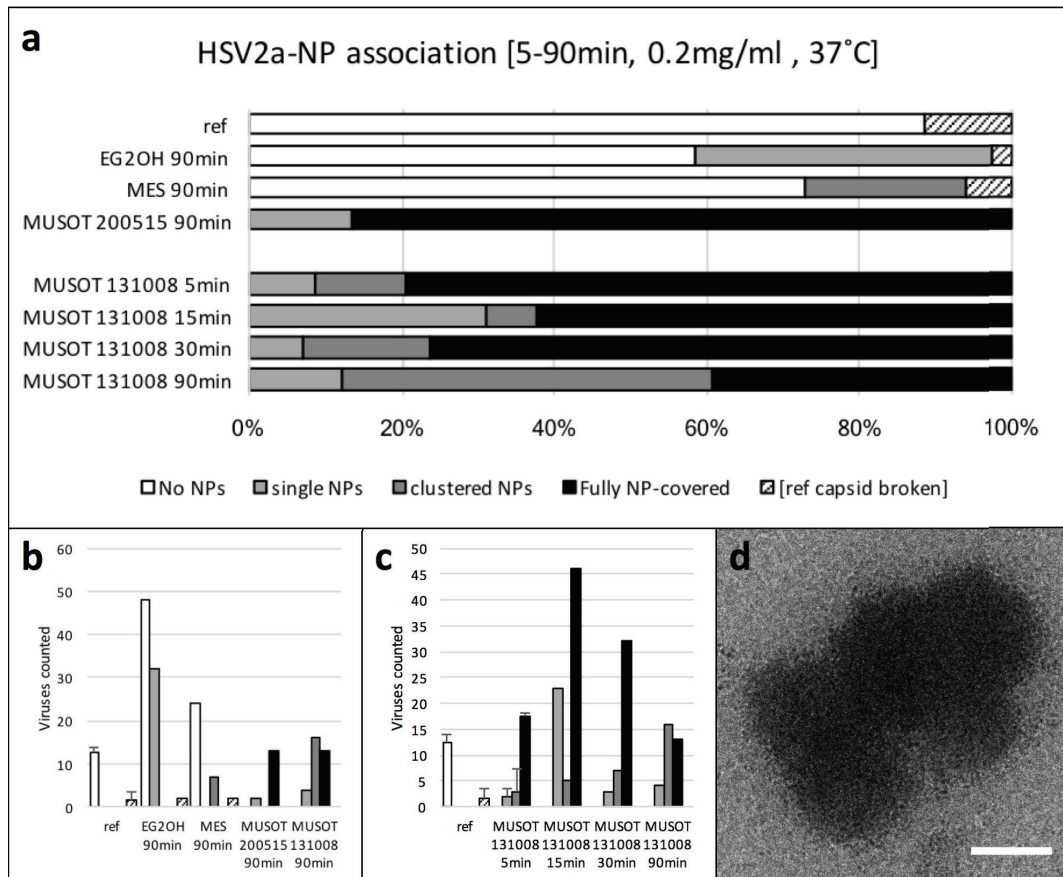


Figure 4-4: Quantification of NP-HSV₂ association for different NPs at a concentration of 0.2mg/ml incubated with NPs from 5 min to 90 min at 37°C. Per data set at least 30 viruses have been classified, the counts are displayed in (b) and (c). (d): cluster of fully covered viruses after 5 min of incubation with MUSOT. The scale bar is 100 nm.

The high degree of NP association to the viruses after only 5 min of incubation suggests a rapid binding and full coverage. The following experiments therefore focussed on the immediate interaction between NPs and viruses. Figure 4-5 shows that the association of virucidal NPs with viruses happens as quickly as within 0.5 min. Virucidal MUSOT 131008 and MUSOT 200515 fully covered more than 25% of all viruses counted and no virus remained free of NPs. Virustatic MES NPs, on the other hand only showed an association to HSV₂ virions as single or clustered NPs. Even at increased concentration of virustatic MES particles (1mg/ml), only an association of single NPs (43%) and clustered NPs (17%) became apparent.

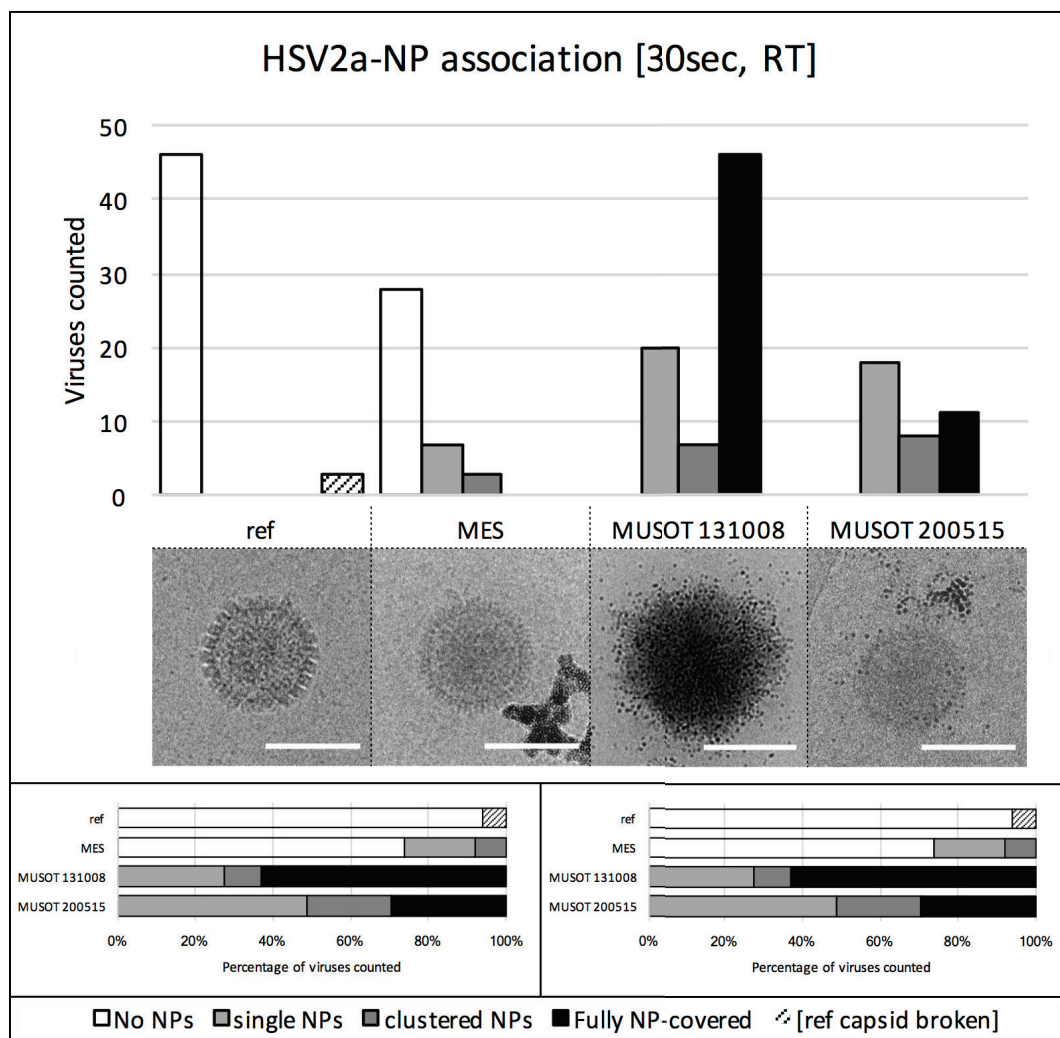


Figure 4-5: Quantification of NP-HSV2 association for different NPs at a concentration of 0.2mg/ml incubated with NPs for 0.5 min at RT before plunging into liquid ethane. Top: virus counts for the different association classes with example pictures of Virus-NP interaction per NP sample. Scale bars are 100 nm. Bottom: ratio representation of the different virus NP associations per NP after 30sec of contact of NP and virus: left comparison of different NPs at a concentration of 0.2mg/ml, right: comparison of two different MES concentrations.

Figure 4-6 summarizes all HSV2-NP association classes and their respective proportions over time from short (0.5min) to long time scale (90min) comparable to the tests performed in the virucidal assays. It can be seen that over time, particles do associate with viruses independently of their virucidal properties. EG2OH that initially seemed to not associate to the viruses, showed 36% of viruses with single NPs co-localized in the images after 90 min of incubation. In the MES sample, it was apparent that the proportion of viruses that initially associated with single NPs evolved to have formed NP clusters. The MES-clusters, as depicted in Figure 4-5, appeared both in solution and on the viruses, suggesting a mere co-localisation with the clusters. MUSOT 131008 NPs showed an immediate strong association

to the viruses leaving no virus free of NPs. Even after only 0.5 min of incubation all viruses presented with at least single NPs associated to them. The fluctuations in the percentage of single NP associated, clustered NP associated and fully covered viruses might predominantly be due to the aggregation of fully covered viruses with themselves over time as shown previously in Figure 4-4. MUSOT 200515 particles were generally less prone to aggregation and associated progressively over time from almost half of the viruses with single NPs, to 22% with NP clusters and 20% fully covered to an 87% full coverage after 90min and 13% presenting as associated with single NPs.

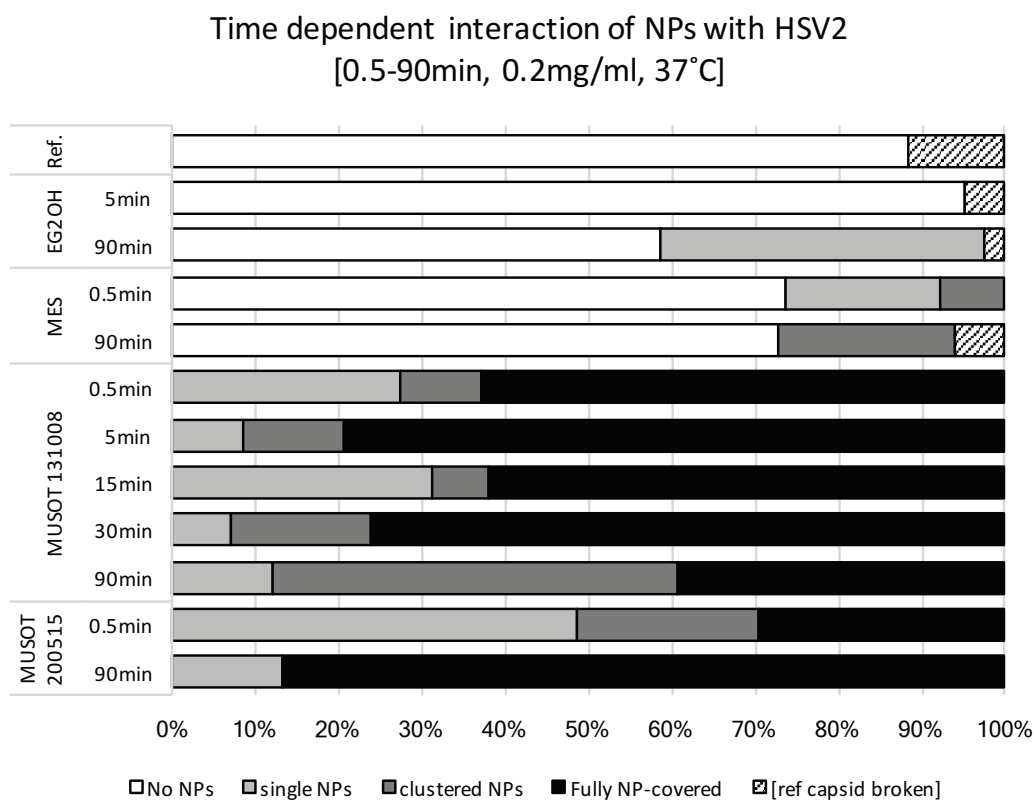


Figure 4-6: Quantification of NP-HSV2 association for different NPs at a concentration of 0.2mg/ml incubated with NPs for 0.5 min to 90 min.

Interestingly, the immediate incubation of NPs and viruses showed that NPs not only cover the viruses, but also influence the virus morphology. Figure 4-7 summarizes the different morphologies of HSV2 that have been observed and afterwards quantified: intact capsids, distorted, opened and broken capsids as well as enveloped viruses, though most viruses in this HSV2 batch were envelope-free.

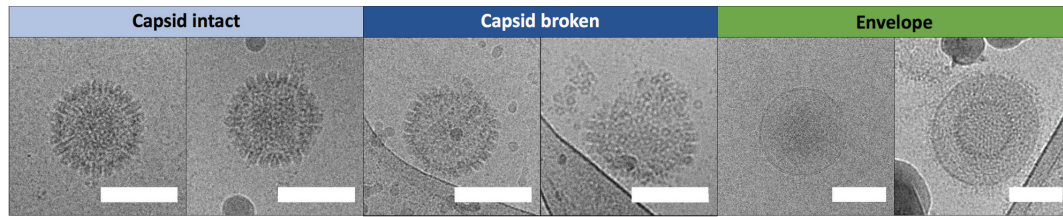


Figure 4-7: Representative pictures of virus morphologies identified in CryoEM. Scale bars are 100 nm.

The proportion of the respective morphologies changes largely upon NP treatment, see comparative Figure 4-8. The reference showed 88% of intact and 12% of broken capsids as well as 4% of enveloped viruses, from 30 viruses counted in 2 samples.

It is not possible to evaluate the morphology of all viruses in our samples, because an excessive number of NPs can conceal the underlying virus. This is an issue especially when using the highly virus-avid MUSOT batch 131008 that consistently showed more than 60% of all viruses as fully covered and hence left only a small proportion of all viruses for morphological inspection. Figure 4-8 shows both the full virus counts of intact capsids, broken capsids, enveloped viruses and fully covered viruses as well as the relative proportions of intact and broken capsids and envelopes.

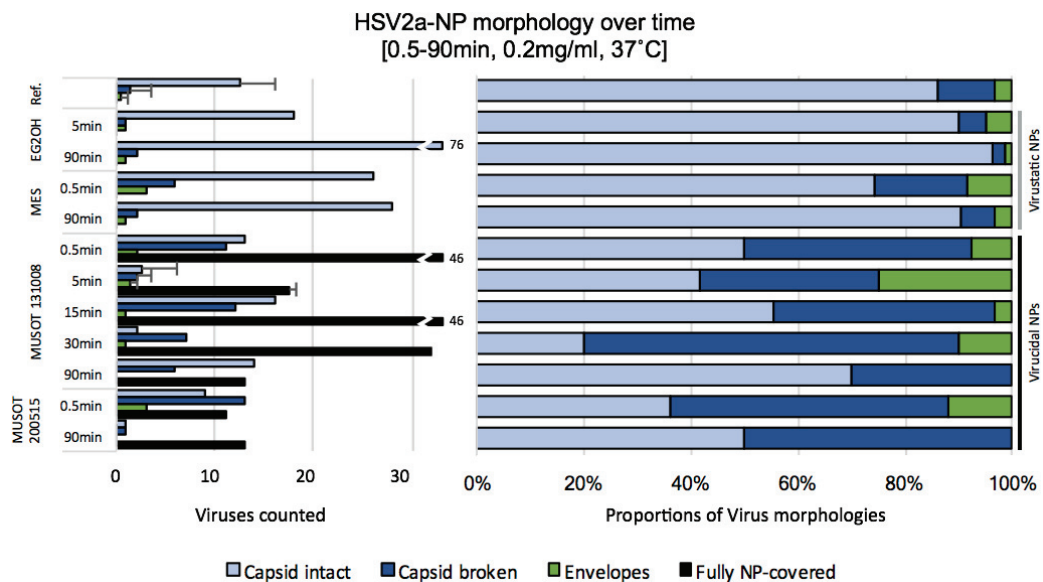


Figure 4-8: CryoEM quantification of different virus morphologies after 30sec incubation of HSV2a with 0.2mg/ml NPs. Left: Virus counts, error bars are standard deviations of the mean. Right: Relative proportions of the different virus morphologies in observable samples (all but fully-covered viruses)

The non-virus inhibiting EG2OH NP and the virustatic MES NP showed a low number of broken capsids comparable to that of the reference samples between 3% (EG2OH 90min)

and 17% (MES 0.5min) of the viruses. Incubations with MUSOT particles in contrast showed an up to three times increased number of broken capsids: MUSOT 131008 42%(30sec), 33% (5min), 41% (15min), 70% (90min) and MUSOT 200515 52% (30sec), 50% (90min) of observable viruses, that is the total of viruses minus fully-covered viruses. The countable number of capsids in several MUSOT samples was very low, but a general trend to a high proportion of broken capsids can be observed. In summary, when counting all MUSOT treated viruses 60 intact capsids, 54 broken capsids, 10 enveloped viruses and 196 fully NP covered viruses were imaged.

As introduced above the first HSV2 batch only showed a small number of enveloped viruses. NP treatments appear to impart a colloidal stability to the envelopes so that upon imaging immediately after NP treatment more envelopes can be observed in the MES and MUSOT200515 treated samples. At later time points the evaluation of this effect was impeded because the viruses were progressively fully-covered. The size of the fully-covered viruses was 122 ± 31 nm, only slightly larger than that of the naked virus capsids ($116 \text{ nm} \pm 7$ nm) as measured from CryoEM images in ImageJ. To conclude the study on HSV2 we re-tested the NPs on a second HSV2 batch that was richer in envelopes as shown in Figure 4-2. We were able to reproduce similar NP-association patterns as with HSV2a. The results of HSV2 incubation with 0.02mg/ml and 0.2mg/ml of MUSOT 131008 are shown in Figure 4-9.

At a concentration of 0.2mg/ml MUSOT 131008 particles show a lower proportion of fully covered viruses, but no virus is free of NPs. The immediate association of a 10 times lower concentration of these particles showed, as expected, lower NP-virus association. 4% of the viruses even remained free of NPs, 90% of the viruses associated with single NPs (in contrast to 30% in the 0.2mg/ml sample), none associated with clusters and 6% of the viruses were fully covered. Morphologically, a decreased number of enveloped viruses as well as an increased number of broken capsids could be observed in the NP-treated samples as illustrated in Figure 4-9. While the reference sample showed roughly the same number of non-enveloped as enveloped viruses, the NP-treated samples only showed 17% (0.02mg/ml) or 28% (0.2mg/ml) of the viruses enveloped. Regarding broken capsids both NP-treated samples presented a ratio of almost 1:1 whereas the proportion of broken capsids in the reference sample is 1:8. By comparing the two NP concentrations, a clear progression towards more clustered and fully covered viruses was observed, whereas at the lower NP concentration, a higher number of broken capsids was present. Most broken capsids in the 0.02mg/ml sam-

ple showed only single NPs mostly below 5 NPs attached, in the high concentration incubation on the other hand broken capsids were associated with 20 or more single NPs or clustered NPs. This increase as well as the decreased proportion of broken capsids upon treatment with 0.2mg/ml of NPs suggests that an initially broken capsid is readily fully covered, if a sufficient number of NPs is available to cover the viruses.

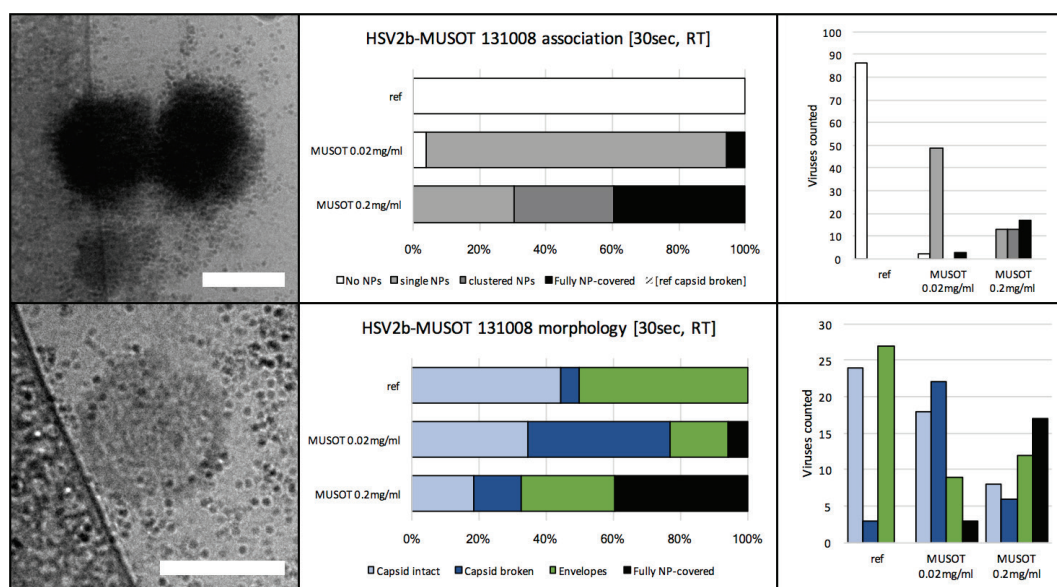


Figure 4-9: CryoEM quantification of HSV2b association and morphology upon immediate treatment with MUSOT 131008. Left: representative CryoEM micrographs showing two fully NP covered viruses (top) and a broken capsid with non-agglomerated NPs (bottom) (Scale bars are 100 nm). Centre: relative proportions of different virus-NP association classes (top) and virus morphologies (bottom). Right: counts of NP-virus association classes and virus morphologies

4.4 Cryo electron tomography of HSV2-NP interaction

The images presented so far only represent a 2D projection of a 3D object, one dimension cannot be evaluated, therefore we studied the three-dimensional NP association to the viruses in several cryo electron tomography (CryoET) experiments. The following pictures show grouped Z-slices of about 8 nm thickness through HSV2 tomograms as explained in the Materials and Methods. Single images of the full tomograms were averaged over a range of 10 nm in z to obtain the images shown below. A 3D Gaussian Blur has been applied to increase contrast. The image montage representation was assembled to show 15 slices of 8 nm thickness to encompass the entire virus capsid volume to better evaluate the NP association at all depth levels.

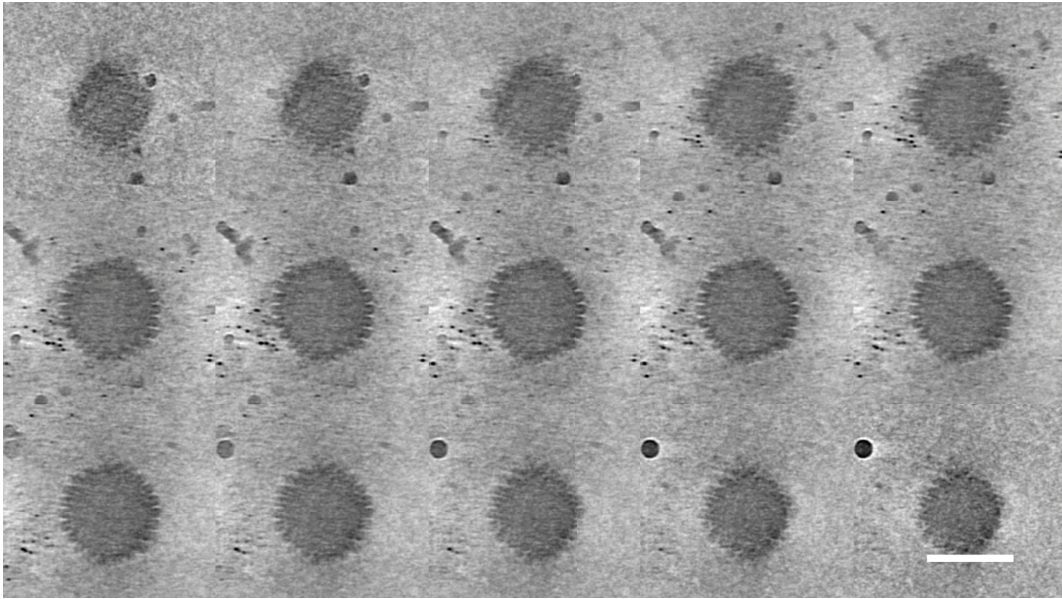


Figure 4-10: Grouped (22) z-slice montage of a CryoET reconstruction of HSV2 incubated for 1h with MUSOT 131008 particles, Tomogram acquired by Dr. Ricardo Guerrero-Ferreira. Scale bar is 100 nm

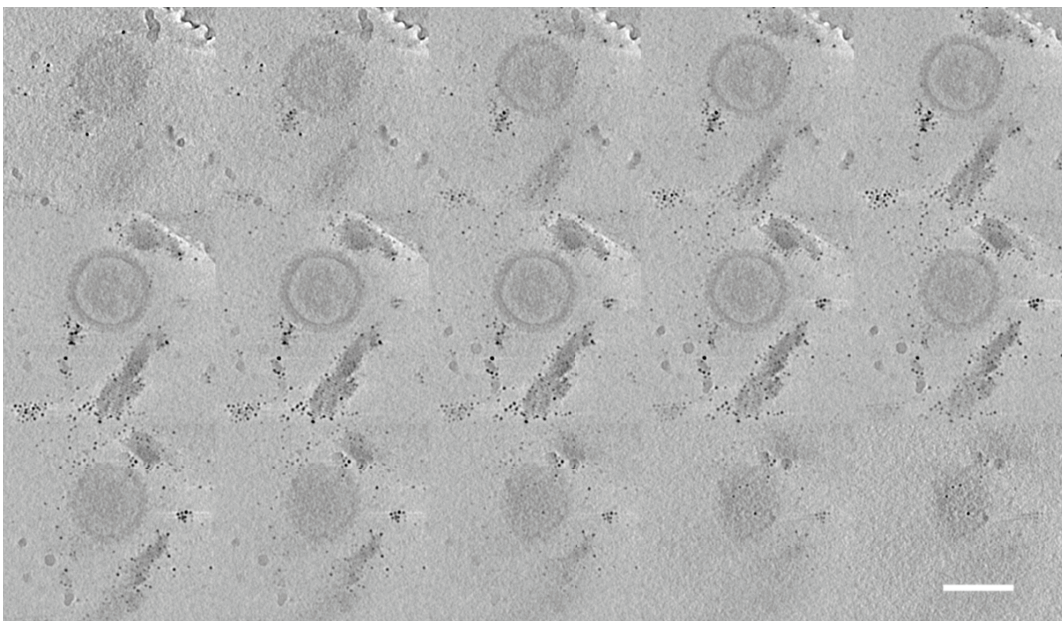


Figure 4-11: Grouped (13) z-slice montage of a CryoET reconstruction of HSV2 incubated for 1h with MUSOT 131008 particles, Tomogram acquired by Dr. Ricardo Guerrero-Ferreira. Scale bar is 100 nm

Figure 4-10 and Figure 4-11 provide clear evidence that MUSOT 131008 NPs localize close to the virus capsids and are not merely superimposed. Both tomograms have been acquired after 1h incubation of HSV2a with 0.2mg/ml MUSOT NPs. Figure 4-10 is representative of the class of viruses associated with single NPs; Figure 4-11 depicts the association of a cluster

of NPs to a viral capsid. Moreover, the sheet-like aggregates typical for MUSOT 131008 can be observed on the lower right of every image in Figure 4-11. Figure 4-12 supports the 2D observation of the fully NP-covered viruses and confirms that these are round in three dimensions instead of mere flat sheets of NP aggregates that can be found in NP samples.

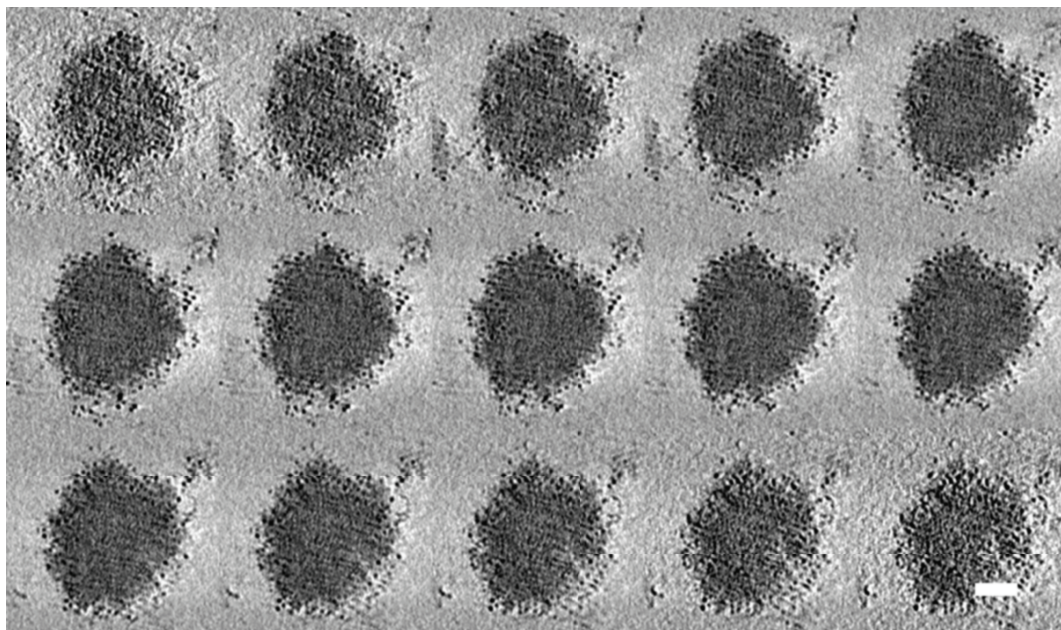


Figure 4-12: Grouped (10) z-slice montage of a CryoET reconstruction of HSV2 incubated for 30sec with MUSOT 131008 particles. Scale bar is 100 nm.

4.5 Cryo electron microscopy of HSV1-NP interaction

The third virus studied in interaction with NPs was HSV1. As in the case of HPV and HSV2, MUSOT NPs exerted a virucidal effect on HSV1. As was pointed out above, HSV1 presents a considerably higher proportion of enveloped viruses than HSV2a. Although CryoEM is a technique that imparts low stresses on the sample, a lot of broken envelopes were imaged, especially in the reference sample. The proportions are presented in Figure 4-13. NP-treated viruses overall showed 30% more intact envelopes and up to 80% less broken viruses than the reference, suggesting that NPs impart a colloidal stability to the virions. Upon presence of EG2OH in solution, the proportion of broken viruses was reduced to 4%. For MUSOT 131008, only non-fully covered viruses could be evaluated and showed an equal distribution of intact, protruded and broken viruses. Interestingly, 91% of all MUSOT 200515 treated viruses showed protrusions of the viral envelope as presented in Figure 4-13 f.

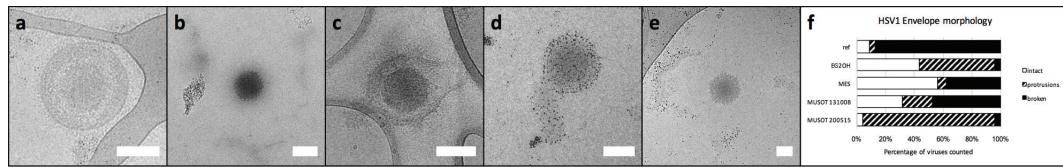


Figure 4-13: Representative images of different envelope morphologies counted in HSV1 samples treated with different NPs: (a) intact envelope (b,e) broken envelope, (c,d) protruded envelope; (a,b) reference images, (c,d,e) MUSOT 200515 treated viruses.

Representative CryoEM images of the association of NPs with HSV1 envelopes after 30sec of incubation are shown in Figure 4-14. Both the appearance as well as the overall proportions of NP association to HSV1 compare well to the effects observed previously on HSV2. While non-virucidal EG2OH NPs as well as virustatic MES NPs only marginally co-localize with the viruses, the virucidal NPs fully cover the viruses. Yet for the two different MUSOT batches imaged the coverage of the virus envelopes is very different. MUSOT 131008 particles cluster much more densely on the viruses than MUSOT200515 particles. MUSOT 131008 as well as several other MUSOT particles frequently show sheet-like aggregates - as highlighted by an arrow in Figure 4-14 - upon incubation with biological specimens such as viruses, red blood cells or amyloid fibres. In high resolution STEM these have been imaged as superlattices of ordered clusters. The presence of NP clusters is difficult to address, they have been observed in batches occasionally. We believe that these sheets cover fully these viruses rendering them electron dense. We have never seen such aggregates in MUSOT200515 and therefore assume a NP-virus association as shown on the very right in Figure 4-14 as the equivalent of a fully-covered MUSOT131008 virus and quantified these as such.

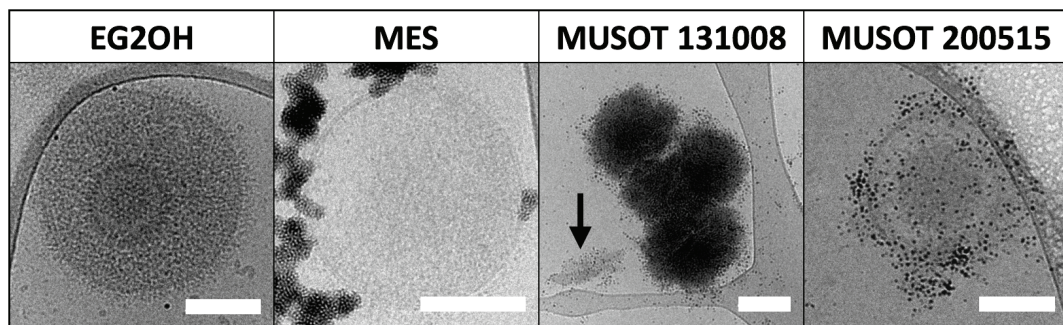


Figure 4-14: Representative CryoEM micrographs of the most represented classes in the interaction of HSV1 with non-virus inhibiting EG2OH, virustatic MES and virucidal MUSOT 131008 and 200515. Scale bars are 100 nm.

The quantification of the respective association classes of NPs to viruses is provided in Figure 4-15 (b). At 0.2mg/ml virucidal MUSOT 131008 and 200515 particles showed no virus without NPs and displayed full-coverage rates of 91 and 94% respectively. The incubation

with 0.02mg/ml of MUSOT 131008 shows that the number of NPs in the incubation limits this quick full coverage. A ten times reduced amount of NP results in a largely decreased proportion of immediately fully covered HSV1 virions (91% \rightarrow 23%), comparable to the effect seen previously on HSV2 (see Figure 4-9). This supports the hypothesis, that once an ample amount of NPs is available broken viruses quickly become fully covered.

Morphologically the HSV1-NP association differs significantly from that of HSV2 (Figure 4-15). MUSOT 131008 shows a comparable profile to that on HSV2 with an even higher rate of full coverage of 91%. Interestingly, the previously described difference in aggregation propensity between the two MUSOT batches is relevant regarding their interaction with the viral envelopes. Upon treatment with MUSOT 200515 76%, the fully-covered envelopes can be clearly be identified. The dense coverage with small aggregates seen in MUSOT 131008 leaves this conclusion only for 6% of the entire sample. The incubation of 0.02mg/ml of MUSOT 131008 NPs on HSV1 showed an overall comparable trend to the morphologies observed on HSV2 (see Figure 4-9), in which 18% of the capsids were intact, 49% broken, 9% of the envelopes were intact and 22% of the viruses were fully covered.

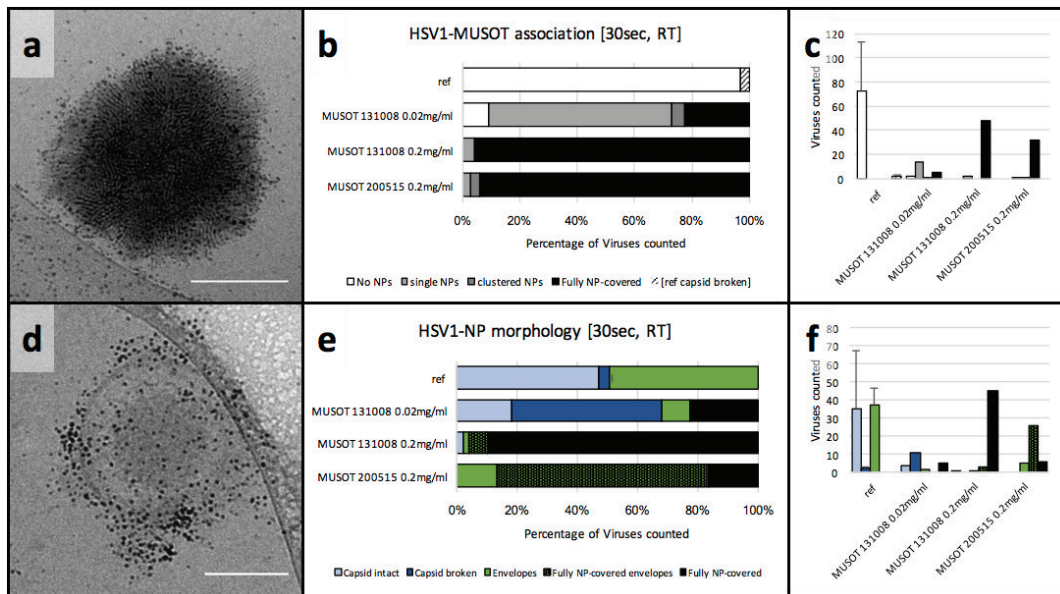


Figure 4-15: Quantification of HSV1-NP association and morphologies after 0.5 min incubation with MUSOT NPs (a) MUSOT 131008 fully covered virus (b) HSV1-MUSOT association quantified (c) counts of (b). (d) MUSOT 200515 fully covered virus (e) HSV1-MUSOT morphology quantified (f) counts of (e). Scale bars are 100 nm.

The imaging of the long-term association of NPs with HSV1 was limited, because prolonged incubation significantly reduced the number of viruses visible on the cryo grid. The thin ice-layer provides an inherent bias to the measurement as only objects up to 400 nm can be

adequately visualized. This happens because thick ice absorbs too many electrons, which reduces the contrast and can create black areas on the grid. It was only possible to image the HSV1 NP interaction at a short time frame of 10 min with a lower concentration of 0.02mg/ml. The results of this experiment are shown in Figure 4-16. MES and MUSOT 131008 NP association to HSV1 as well as their respective morphology was evaluated from CryoEM images. MES NPs in this sample largely presented as clusters both in solution as well as next to the viruses (48%) (see also Figure 4-14 middle). 37% of the viruses remained free of NPs and 16% appeared fully covered. The percentages in this case should be considered with caution because the total virus count was low (19 viruses quantified). MUSOT 131008 on the other hand only presented as 85% fully covered, but with some less dense coverage showing that 10 out of the 81 fully-covered viruses were enveloped.

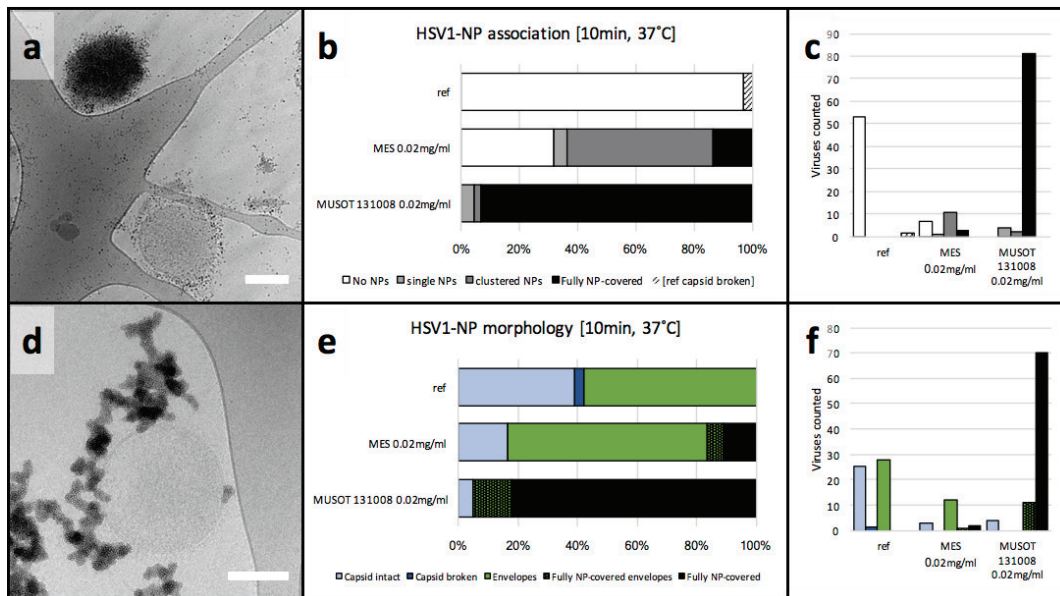


Figure 4-16: CryoEM quantification of HSV1 association and morphology upon immediate treatment with MES or MUSOT 131008; Left: (a) image of two fully-covered MUSOT viruses, one densely covered, one less covered enabling the observation of the enclosed virus envelope, (d) HSV1 treated with MES co-localizing with MES clusters (Scale bars are 100 nm); Centre: Relative proportions of HSV1-MUSOT association (b) and morphology (e) after 10 min of incubation at 37°C; Right: according counts of association (c) and morphology (f)

To summarize the results on densely fully-covered viruses, Figure 4-17 shows the respective sizes of the virus capsids, envelopes and fully-covered viruses. For both viruses, the size of the fully-covered viruses spanned the entire size distribution of the viruses. For HSV1 the size distribution appeared bimodal with a peak around the size of the capsids ($\sim 120 \text{ nm} \pm 5 \text{ nm}$) and another peak around that of the enveloped virus (HSV1: $200 \pm 47 \text{ nm}$, HSV2: $180 \pm$

50 nm). The size distribution of fully covered HSV2a was centred around the capsids diameter, but showed a number of fully covered viruses at sizes up to 40 nm below that of the intact capsids as well as single fully covered particles up to 230 nm in diameter.

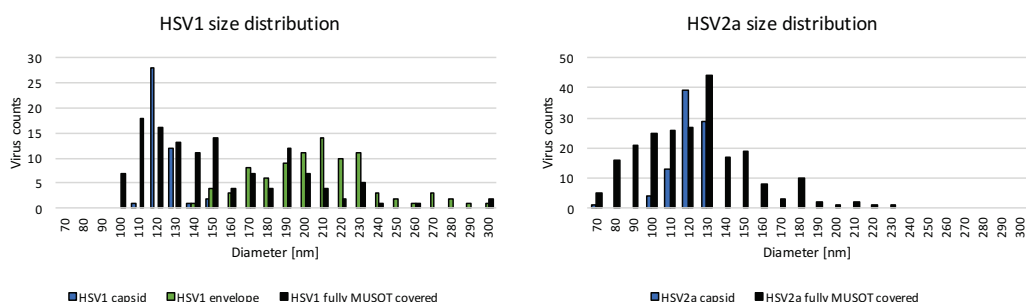


Figure 4-17: Comparison of capsid, enveloped and fully covered virus diameter for HSV1 and HSV2, 262 and 314 viruses were measured, respectively 3.9 nm

4.6 Discussion

In this chapter, we aimed to establish a protocol to evaluate the antiviral and virucidal activity of different NPs through CryoEM by examining the differences between the association of virustatic and virucidal NPs to different HSPG-dependent viruses in their near-native solution state.

Very little was found in the literature on imaging the interaction of antiviral NPs with viruses. The key limitation of the studies found that only negative staining of viruses treated with antiviral NPs has been performed. In the current project, we support initial studies on dry TEM using CryoEM that is substantially less prone to artefacts that arise from sample drying, aggregation and heavy metal stains. In CryoEM, samples are visualized in a thin 200-400 nm of vitrified ice that preserves the solvated state of the visualized structures. Great care has been taken to preserve fragile structures well by preparing grids in a humidified chamber to minimize evaporation, by optimizing the blotting setup as well as the general procedures for sample handling and imaging. Potential artefacts from occasional formation of excessively thick ice, cubic ice in the samples, ethane or water droplets frozen onto the ice or damages to the radiation-sensitive sample can be minimized, but not fully avoided. These challenges are taken into consideration in the interpretation of the images. A further limitation that should be considered is the high number of broken virus envelopes. The CryoEM procedure appears to impart a stress on the envelopes making them burst even in reference samples. The reason a the commonly used stabilizer sucrose is not applicable in

our study is that initial virological experiments showed that sucrose interferes with the virucidal effect of our NPs. Also reported procedures such as a grid pre-treatment with polylysines have not proven useful for the scope of this study. Although a polylysine grid pre-treatment resulted in largely intact virus envelopes on the grid they were not applicable to this study as the polylysines induced heavy aggregation of NPs.

For the interpretation of the results of this study, one procedural limitation has to be taken into account: the total volume of CryoEM samples is 3.5 μl of viruses treated usually with 0.2mg/ml of NPs. To obtain a reasonable number of viruses on the TEM grid, the highest concentration of viruses possible is used resulting at a high virus-to-NP ratio of about 45,000 viruses per μg of NPs ($\sim 3 \times 10^{15}$ NPs). In the plaque assays though, the virus-to-NP ratio is 0.1-1 pfu/ μg of NPs for a dose response test, and 5000 viruses per μg of NPs in the virucidal tests. In all experiments, the virus concentrations are determined by experimental constraints: in a dose response setup, the number of plaques is limited by the size of the plate used to perform the test – in our case, 24-well plates that can accommodate not more than 50-100 plaques well-separated and countable. In the virucidal assay on the other hand, higher virus concentrations are required to sequentially dilute virus and the putative virucidal substance. For EM studies, classically high virus concentrations up to 10^9 pfu/ml are used to acquire many virions per picture. For CryoEM, often sucrose gradients are used to concentrate the viruses, but sucrose stabilizes the viruses and this interferes with the scope of this study that aims to visualize the damaging effect of the presented virucidal NPs. Preliminary tests also showed a decreased virucidal efficacy upon pre-treatment of viruses with sucrose. A virus titer log reduction of 3.9 was scaled down to 1.6 upon virus pre-treatment with sucrose. We therefore performed CryoEM experiments directly on the viral stock solutions (HPV: 10^6 ffu/ml, HSV2a: 3×10^5 pfu/ml, HSV2b and HSV1: 10^6 pfu/ml). The NP concentration tested in the virucidal assays was 0.2mg/ml. The virucidal tests were performed at a pfu per μg of NP ratio of 2500. To yield a similar ratio in a CryoEM experiment on the virus stock a 20-fold increased NP concentration would be necessary, but a NP concentration of 4mg/ml is a pitch-black solution that does not allow for any virus to be visualized. The imaging conditions in this cryo setup hence presents the best compromise between an unaltered virus solution and well-dispersed NPs. In turn, this limits the number of viruses that can be imaged per sample as usually only single viruses were observable per field of view and low dose imaging is both time consuming as well as limited by contaminations of the column on prolonged imaging on ice.

4.6.1 Association of nanoparticles with viruses

In this study, we compare the NP association and morphology of different viruses upon treatment with non-virus inhibiting EG2OH NPs, virustatic MES NPs and virucidal MUSOT NPs. Overall we could observe that viruses treated with non-virus inhibiting EG2OH particles present as free of NP or associated with single NPs. This finding was consistent over all viruses tested: HPV (Figure 4-1), HSV2 batch a and b (Figure 4-4 and Figure 4-9) and HSV1 (Figure 4-15).

The treatment of viruses with virustatic MES particles mostly showed viruses free of NPs. Both single MES NPs and clusters of MES NPs have been found associated with viruses: to at most 30% of the for HSV2 capsids, but up to 60% for HSV1 full virions. Incubation with a 5x increased concentration of MES particles increased the number of NP associated viruses. This could be attributed to more binding, but also to more NPs floating in solution ready to superimpose on viruses.

Virucidal NPs on the other hand, showed a clear tendency to associate numerous onto the viruses. Predominantly viruses associated with clusters of NPs as well as with fully NP-covered viruses. A high propensity of fully NP covered viruses has been seen with all viruses tested: HPV (Figure 4-1), HSV2 batch a and b (Figure 4-4 and Figure 4-9) and HSV1 (Figure 4-15). Differences in the aggregation behaviour of the NPs greatly influence the appearance of the fully covered viruses ranging from electron dense black objects where no internal structure can be visualized, as in the case of MUSOT 131008, to a more dispersed NP-attachment on the viruses, as in the case of MUSOT 200515. The MUSOT 131008 batch presented dense sheet-like aggregates (Figure 4-14 arrow) in solution that also appeared to cover the viruses and thus formed a much denser coverage of the fully-covered viruses. MUSOT 200515 a more recently prepared NP batch did not present these features in solution and neither was it found on the viruses.

To ascertain whether or not the NP-virus association is not merely non-contact, superimposed NPs and viruses in the 2D projection of the EM image, we verified their co-localisation using CryoET. We confirmed a close co-localisation of NPs and viruses in 3D as well as the fully NP covered viruses are 3D round objects.

We further observed that the association of virucidal MUSOT NPs to viruses is progressive in nature. This finding supports the idea that different categories of NP-virus association actually represent stages of gradual NP coverage: stage 1 includes all viruses without NP

attachment, stage 2 viruses associated with single NPs, stage 3 viruses associated with clusters of NPs and stage 4 fully NP-covered viruses as presented below in Figure 4-18.

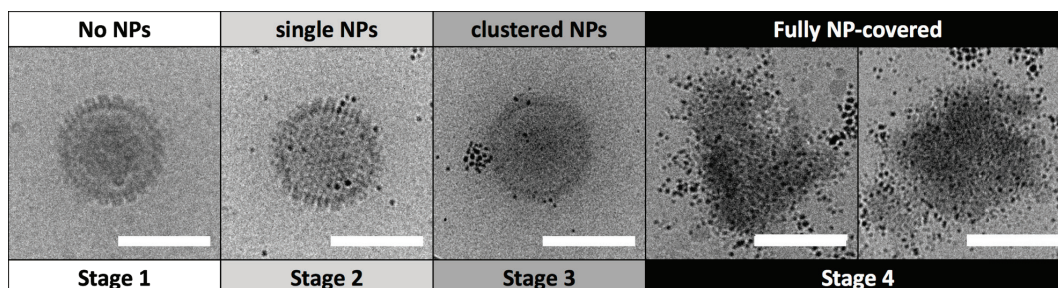


Figure 4-18: Stages of virus-NP association. Scale bar 100 nm.

These stages have been found consistently in all viruses imaged: HPV, HSV2 and HSV1 and in our interpretation, relate clearly to the virustatic and virucidal action of the different NPs as seen from the antiviral and virucidal testing presented in the Materials and Methods. Stages 2 and 3 show the first stages of NP attachment, hence possibly the appearance of a transient binding, a virustatic effect. Stage 4 on the other hand showed fully covered viruses having partly lost their structural integrity, which we interpret as the imaging of the virucidal endpoint.

The hypothesis that fully NP covered viruses correspond to the virucidal endpoint is further supported considering that the CryoEM has been performed at NP concentrations below a full virucidal effect. The progression from 63% to 79% of full coverage for HSV2 treated with MUSOT 131008 for 0.5 and 5 min, respectively, showed that this concentration of NPs is sufficient to fully cover the majority of viruses (compare Figure 4-6). The following long-term differences in the extent of full coverage (44% at 15min, 77% at 30 min and 40% at 90min) can be attributed to two phenomena. As explained fully MUSOT 131008 covered viruses appear to cluster substantially after 5min. If those clusters exceed a size of 500 nm it is not possible to image them anymore and the probability of them being removed in the blotting process increases further upon increased cluster size. Fully NP covered viruses deplete a lot of NPs, which can explain the higher proportion of single NP and clustered NP associated viruses in the 90 min sample. Possibly at later time points there are no longer enough NPs left to fully cover the remaining viruses at a low initial concentration of NPs. High proportions of fully covered NPs even at sub-virucidal concentrations point to the universality of the progression towards the final stage of the virucidal effect which we define as the fully NP covered viruses seen under CryoEM. The observation of virus envelopes fully

covered by NPs, as shown for MUSOT 200515 particles in Figure 4-15, and in the size distribution of the fully covered viruses in Figure 4-17, indicates that the full NP coverage represents a virucidal NP association phenomenon, not only for non-enveloped viruses such as HPV, but also for enveloped viruses such as HSV. Overall these results support the hypothesis that fully NP covered viruses present the imaging of the final virucidal.

4.6.2 Morphology of nanoparticle treated viruses

In order to understand how full coverage takes place we studied the initial effects of the NPs on the viruses to elucidate how the stable virus capsid that initially only associates to single NPs progressively becomes fully covered by NPs. An inspection of the morphology of the viruses revealed that the proportion of viruses imaged presenting broken capsids increased significantly upon NP treatment. Figure 4-8 presents an overview of the virus morphologies imaged. In a careful evaluation of the morphologies, fully-covered viruses cannot be evaluated because their electron dense NP coverage conceals any internal structures: we therefore evaluated the morphology of the remaining viruses. Considering that in certain samples the number of non-fully covered viruses is very low, care had to be taken to interpret the remaining viruses whose morphology could be evaluated.

HSV2a treated with virustatic MES NPs or a reference amount of water showed a high proportion of intact capsids and only some (3-17%) broken capsids. Viruses treated with virucidal MUSOT NPs on the other hand presented with proportions of broken capsids ranging from 32 to 70% as presented in Figure 4-8. Interestingly, the proportion of broken capsids was even higher for samples treated with 10 times lower amounts of NPs as shown in Figure 4-9. The reduced amount of MUSOT NPs resulted in a smaller proportion of fully covered viruses (6%), but a vast proportion of the viruses associated with single NPs (91%) and 4% remained bare of NPs. The viruses associated with single MUSOT NPs showed the following capsid morphologies: 42% intact capsids [16 counted] and 57% broken capsids [22 counted]. At the standard concentration used the ratio of broken to intact capsids was higher (6 broken capsids with single NPs [3] and clustered NPs [3] versus 4 intact capsids with single NPs), but the low counts of capsids visible comparable to the viruses fully covered limits the statistical relevance of these counts. A comparable pattern of NP association and virus morphology was established for HSV1 virions in contact with MUSOT NPs (see Figure 4-15): whereas at 0.02mg/ml MUSOT 131008 concentration 4 intact (2 with and 2 without NPs) and 11 broken capsids (10 with single NPs attached and 1 with a NP cluster) could be imaged, the sample at 0.2 mg/ml only showed one single intact capsid in 53 viruses imaged. Viral

capsids are metastable supramolecular structures, with a precisely defined 3D structure. These grant viruses exceptional colloidal stability that enables them to open only upon contact with its target. If the capsid structure is perturbed, the stability of the system is affected, which leads to a loss of this inert structure in the presence of other interfaces. This can explain why NPs aggregate and accumulate more readily onto the damaged viruses leading to fully NP covered viruses. Based on the observed progression from high ratios of broken capsids to high ratios of fully covered viruses we deduced that initially broken capsids immediately get covered by NPs in case there is an ample amount of particles available in solution.

4.6.3 Summary

Despite limitations regarding the virus counts and the attainable NP concentration in CryoEM, we were able to establish that viruses treated with virucidal NPs break and become progressively fully covered by NPs, which we interpret as the morphology of the virucidal endpoint.

Based on these observations on the virus populations, the following chapter will further study the details of the NP – virus interaction on a single virus level and study the location and distribution of NPs on broken capsids as well as on envelopes.

Chapter 5 An in-depth study of the nanoparticle virus interaction

The previous chapter confirmed our hypothesis that we can find a correlation between the treatment of viruses with virucidal MUSOT NPs and their morphology. We showed that both full virus coverage with NPs and broken viruses correlate with a virucidal NP treatment, even at the earliest time points. In this chapter, we perform an in-depth analysis of the association of the virucidal NPs to the envelope and capsid of herpes simplex viruses. The research question is: Can a mechanism for the interaction of virucidal NPs with viruses be hypothesised?

Therefore, I will detail the interactions of NPs with the envelopes of HSV as well as with the HSV capsids, and will discuss these results with respect to the current understanding of virus structures and their function in virus infectivity to hypothesize a mechanism for the virucidal action of MUSOT NPs.

5.1 Cryo electron microscopy of nanoparticle association to viral envelopes

In order to understand the early steps of the virucidal mechanism, we studied the CryoEM micrographs taken of virucidal MUSOT NPs and herpes simplex viruses after 30sec of incubation, before freeze plunging.

Upon interaction of MUSOT NPs with the viral envelope, several observations have been made. NPs decorate the envelope, but do not attach directly at the lipid bilayer of the envelope, nor do they distribute evenly over the entire envelope. The following section is focussed on the study of these interactions.

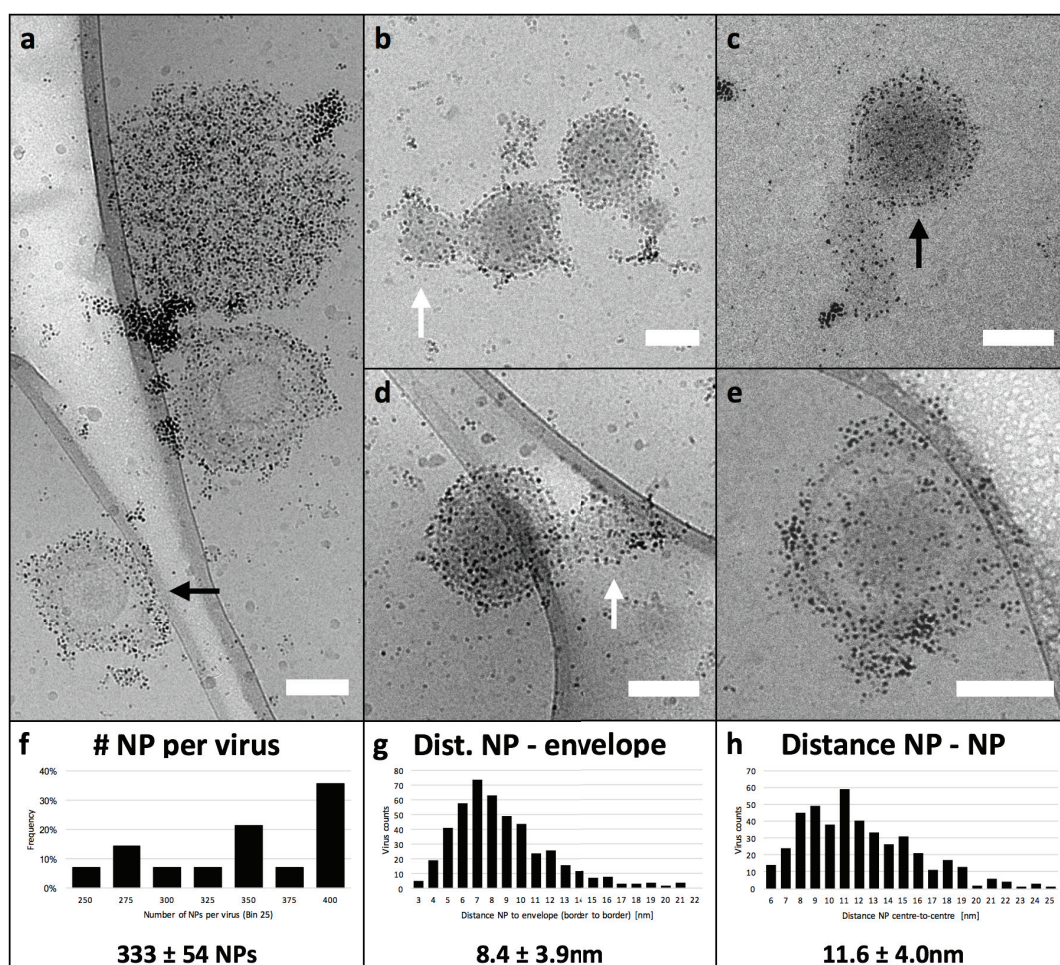


Figure 5-1: CryoEM images of MUSOT200515 (0.2mg/ml) immediate association to HSV1 envelopes showing intact viruses (a, e) as well as viruses with long protrusions (b, c and d); areas of thicker glycoprotein coverage are marked with a black arrow, envelope protrusions are marked with a white arrow. Scale bars are 100 nm. (f-h) Quantification of MUSOT 200515 distribution on the virus envelope: number of NPs per fully covered enveloped virus (g), border-to-border distance of NP and envelope (f); centre-to-centre distance of NPs on the virus envelope (h)

Figure 5-1 contains an overview of HSV1 virions immediately upon interaction with MUSOT 200515 particles. NPs associate all around the envelope, but in a more spaced fashion than in the case of MUSOT 131008 particles, so that the virus underneath is not completely concealed. The arrangement of the NPs on the virus envelope was analysed, focusing on: their distance from the envelope, the number of NPs per virus and the NP centre-to-centre distance on the virus envelope. The results of these quantifications are presented in Figure 5-1 (g-h). The distance between the rim of the NPs and the virus envelope was measured for 466 MUSOT 200515 NPs on 20 virus envelopes and plotted in Figure 5-1g. 71% of MUSOT 200515 NPs were located between 5 and 10 nm away from the virus envelope. The most frequently observed distance was 7 nm, but overall distances ranged from 3 nm to 25 nm with

an average of 8.4 ± 3.9 nm. NPs covered the viruses at a high density: the number of particles was counted on 11 viruses that provided sufficient contrast to clearly threshold NPs from the virus in the background (see Figure 5-1f). Between 237 and 395 NPs with an average of 333 ± 54 NPs bound to the virus envelope were counted from the 2D projection images of the enveloped viruses. The total number of particles attached to the three-dimensional virus is likely to be slightly higher, especially on densely covered viruses in which the probability that NPs superimpose each other is higher. Not only do distances between the envelope and NP show a repetitive pattern, but so do the NP core-to-core distances between NPs that line up on the virus envelope. The NP arrangement on densely covered viruses shows an average centre-to-centre NP distance of 11.6 ± 4.0 nm. The most frequently observed distance is 11 nm (13%), followed by 9 nm (11%) and 8 nm (10%) as can be seen from Figure 5-1 (left).

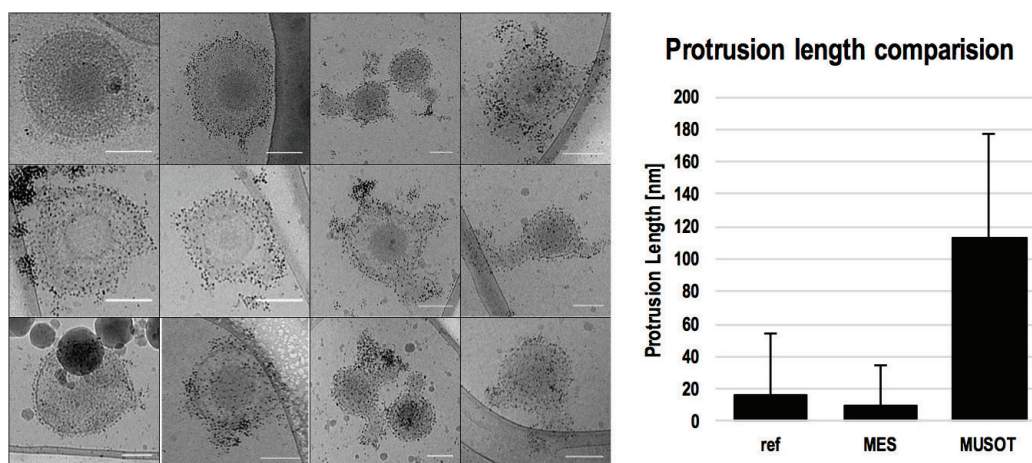


Figure 5-2: Membrane protrusions after treatment with MUSOT 200515 NPs for 0.5min; (Left) CryoEM micrographs of protruded viruses. Scale bars are 100nm. (Right) Comparison of the protrusion lengths between reference viruses, MES treated viruses and MUSOT treated viruses

We furthermore observed that the viruses treated with MUSOT-NPs showed long protrusions. Protrusions in viruses treated with MUSOT NPs show a dense decoration with single as well as clustered NPs. Reference samples or MES treated samples on the other hand only showed short protrusions that are not densely decorated with NPs. Increasing protrusion length furthermore reduced the average radius of the envelope around the capsid.

A more detailed analysis on a single virus level was performed based on the CryoEM micrograph presented in Figure 5-3. HSV2 batch b was treated with 0.02mg/ml of MUSOT 131008 for 30sec before plunge freezing. The virus showed a comparably low number of NPs bound to the virus, therefore left more space to study the exact position of those NPs.

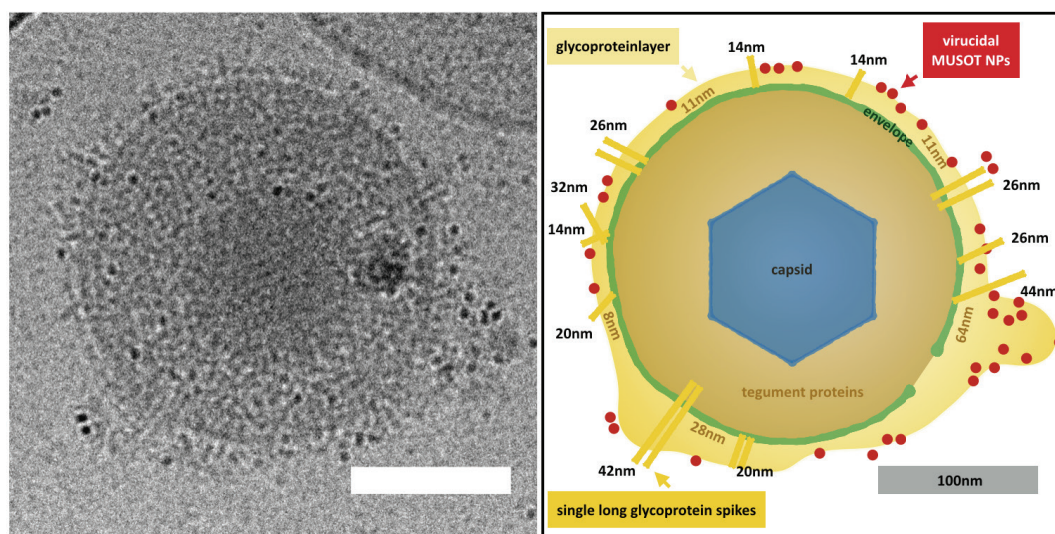


Figure 5-3: CryoEM image of 0.5 min MUSOT 131008 treated HSV2 with well resolved viral glycoproteins. Left: HSV1 after 30sec of incubation with 0.02mg/ml of MUSOT 131008 NPs. Right: colour coded representation of the same picture: capsid blue, tegument proteins light brown, envelope green, glycoprotein layers light yellow including its respective thickness at different parts of the circumference of the virus in light brown. Individually distinguishable glycoproteins are labelled yellow, their length extending outside the virus envelope is written in black, NPs at the outer rim of the viruses glycoprotein layers have been labelled in red. Scales bars are 100 nm.

The cryoEM micrograph clearly showed all key constituents of the virus: the DNA arranged inside the capsid, the dense layer of tegument proteins, the virus envelope and studded glycoproteins. The original image and a colour coded scheme of that image are depicted in Figure 5-3. Structures visible inside the capsid are due to the circular arrangement of the DNA inside HSV1 capsids. The tegument proteins appear dense and internally structured showing different densities that seem to connect the capsid and the envelope. The dark structure visible next to the capsid cannot be unambiguously determined. Glycoproteins are studded on the virus envelope or appear to emerge from it connecting to the tegument proteins under the virus envelope. The glycoproteins cover the entire virus envelope forming a layer of varying thickness on two different sides of the virus. In the top part of the virus the glycoprotein layer appears 8 to 11 nm thick; on the bottom part the overall glycoprotein layer thickness is between 20 and 29 nm. One part of the glycoprotein layer appears to distend outwards to 64 nm with an apparent density at the end of the distention. Single glycoproteins emerge as long spikes (14 nm to 42 nm) from the glycoprotein layer, mostly perpendicularly, but in several cases lower angles. Different lengths and directions of single glycoproteins visible have been highlighted in the cartoon next to the original CryoEM image depicted in Figure 5-3

On the enveloped viruses, the NPs distributed discretely at a distance of 8-10 nm from the viral envelope. On the other hand, more clustered NPs were located on regions of a glycoprotein layer thickness of more than 20 nm. In the cartoon, NPs at the outer rim of the glycoprotein layer have been highlighted in red to underline the different distances of the NPs from the virus envelope. A cluster of NPs co-localized with a part of the glycoprotein coat that appeared to protrude: near this area a part of the virus envelope appears less clearly outlined than on the rest of its circumference. The potentially opened area is shown in the colour coded representation as a gap. Densities next to this area cannot ultimately be assigned to glycoproteins or out of focus NPs from this single image, but we interpret this area as an early stage of the protrusions presented in Figure 5-3.

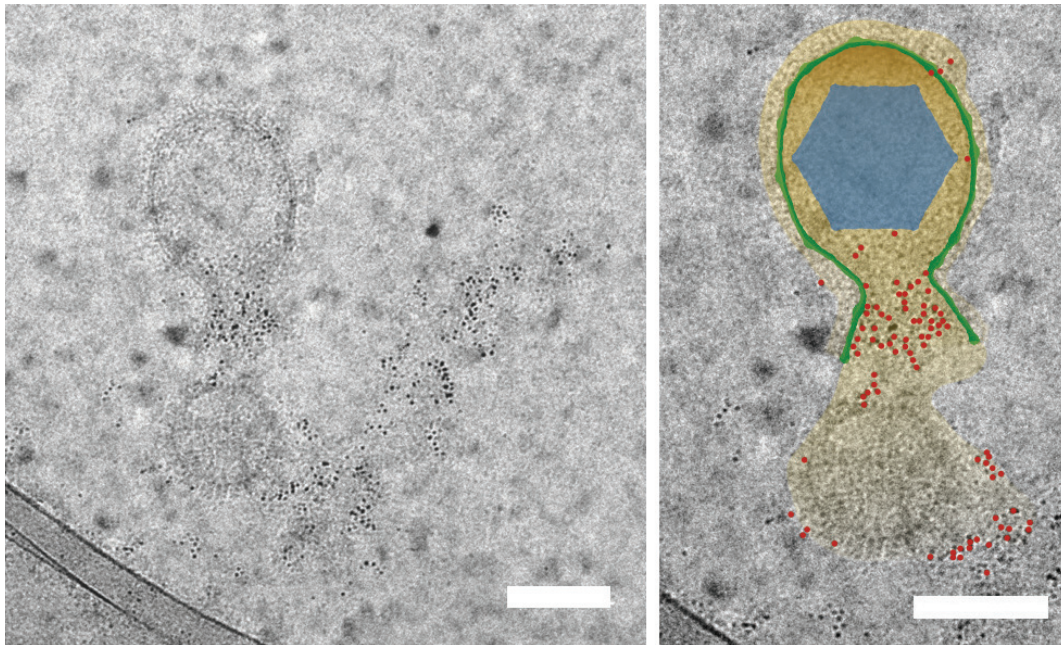


Figure 5-4: HSV1 enveloped virus 30sec after incubation with 0.2mg/ml MUSOT 131008 showing a virus capsid expelled out of the virus envelope. Left: original CryoEM micrograph, Right: zoomed, colour coded representation of the same picture: capsid blue, tegument proteins light brown, envelope green, glycoprotein layer light yellow, NPs have been labelled in red. Scales bars are 100 nm.

A potentially later stage of the aforementioned envelope opening is illustrated in Figure 5-4 that depicts a capsid that was expelled from the virus envelope. HSV1 was incubated with 0.2mg/ml MUSOT 131008 NPs for 30sec and then plunge frozen. The grainy ice in the background of the image indicated partial formation of cubic ice. Figure 5-4 shows the imaging of an opened virus envelope. The area where the viral envelope opened is densely covered with NPs. The tegument proteins appeared to extend out of the envelope and remained partly attached to the expelled capsid. Around these tegument proteins expelled together

with the capsid a substantial number of NPs were found. Close proximity of the capsid as well as the high curvature of the lipid membrane suggest that the virus was frozen immediately upon expelling the capsid.

5.2 Cryo electron microscopy and tomography of the interaction of nanoparticle with viral capsids

The then liberated capsids as well associate with virucidal NPs that appear to alter the capsids structure. Figure 5-5 shows representative pictures of capsid alterations visible in these samples. A detailed observation of the breaking and broken capsids showed that irrespective of the virucidal NP batch or herpes simplex virus tested NPs appear to attach to capsid vertices (f,g,k,p,r,n,s), rather than the sides of the capsids. Frequently aggregates of NPs at the capsid vertices have been observed (b,d,e,g).

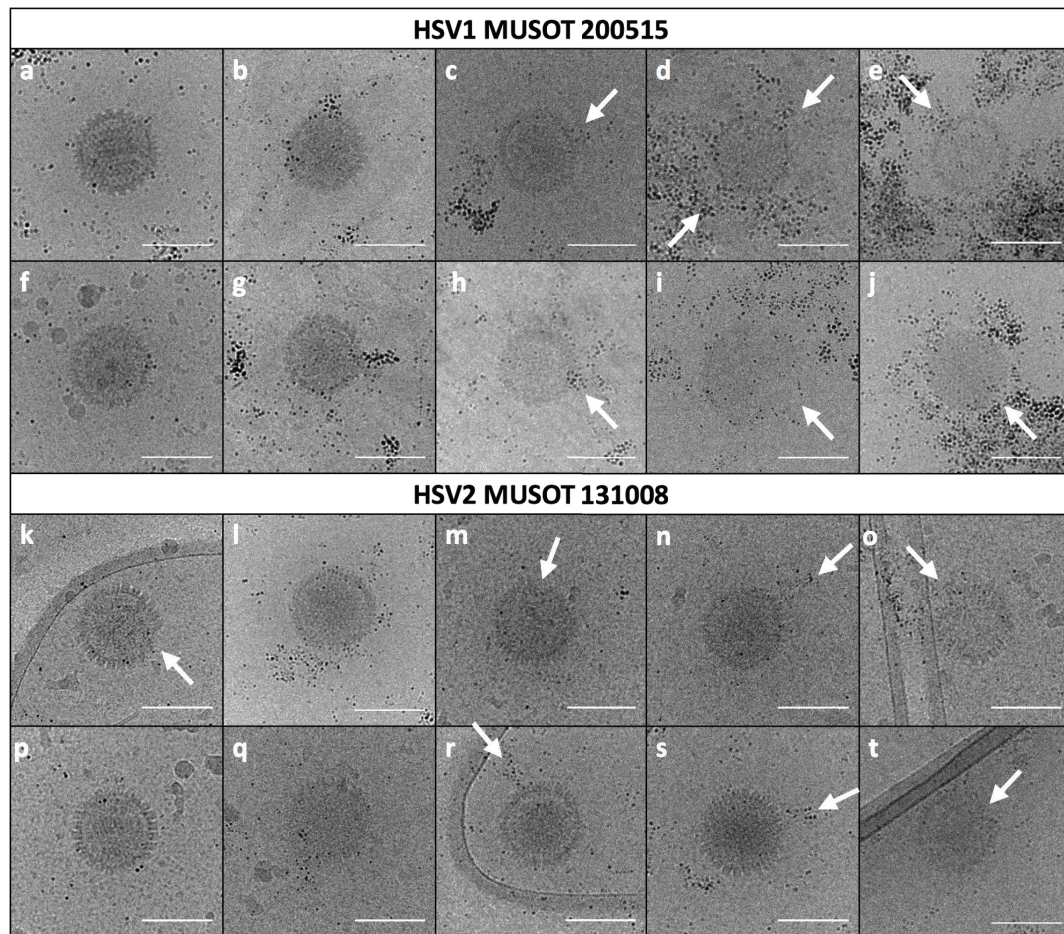


Figure 5-5: CryoEM of breaking and broken capsids: (a-j) HSV1 treated with MUSOT 200515 0.2mg/ml for 0.5 min at RT; (k-t) HSV2 treated with MUSOT 131008 0.2mg/ml for 0.5 min at RT. Scale bars are 100 nm

Moreover particles did not only cluster, but frequently appeared lined up in the direction of the vertex opening (c,e,g,h,n,p,r,s). In a number of images it was evident that these lines of particles were connected to a deformed, elongated capsid vertex that formed an elongated opening (d,g,h,n,r,s). On a number of capsids the overall shape appeared altered (c,l,m,p,o,t), including impressions (c) or missing densities (i,k,m,o,t) loss of angular arrangement of the capsid proteins (t,i) and capsid inflation (i). Images such as Figure 5-5 (h,i,o) that show a capsids with decreased internal electron density can be assumed to be an opened emptied capsids, from which DNA has already been released¹³³. This opening of the capsid can, not only be observed in a 2D projection CryoEM image, but also in 3D using CryoET. To this end, tilt-series of broken capsids were acquired, aligned and tomograms reconstructed. The images in Figure 5-6 and Figure 5-7 present a montage of grouped z-slices of about 10 nm in height through the capsid from the bottom of the capsid (top left) to be top of the capsid (bottom right).

Figure 5-6 depicts a virus with clustered NPs attaching to the lower part of the viral capsid (labelled by an arrow) apparently distorting the capsid at that region. It is apparent that the capsid is opened at the bottom vertex (black arrows) and NPs integrated as well into the top of the capsid (white arrows). White streaks are due to the shading effect that the electron-dense gold core of the NPs imparts when the sample is tilted; the dense particles hide information behind them, hence the area appears as a white streak in the reconstructed tomogram. In other tomograms with fiducial markers (15 nm citrate or ProteinA coated gold NPs) this phenomenon also occurs, but classically, a region of interest is chosen in which fiducial markers are distant enough not to conceal the object. In our images though the NPs are not only fiducial markers for the tomogram reconstruction, but also part of the objects of interest.

The later stage of the virucidal effect is presented in Figure 5-7: an opened virus capsid where the rim of the remaining capsid proteins at the site of breakage appears to be lined by MUSOT 200515 NPs. The opened capsid does not present the angular arrangement of the capsid proteins that formed the icosahedral shell.

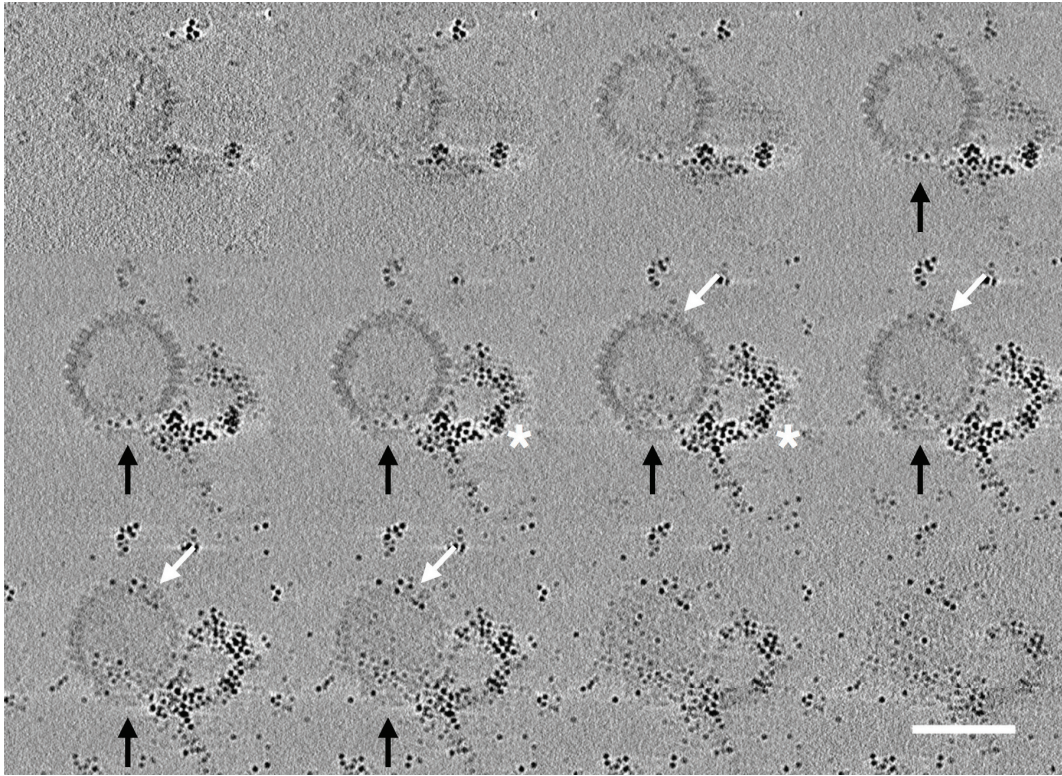


Figure 5-6: Grouped z-slice montage of a CryoET reconstruction of HSV2 incubated for 30sec with MUSOT 200515 particles, white and black arrows indicate areas where the NPs are integrating into the capsid and distort the capsid, small black asterisks highlight striations due to the NPs electron density shading effect in the tilt image acquisition. Scale bar is 100 nm



Figure 5-7: Grouped z-slice montage of a CryoET reconstruction of HSV2 incubated for 30sec with MUSOT 200515 particles. Scale bar is 100 nm

We hypothesize that the insertion of NPs at the capsid vertex destabilizes the capsid arrangement sufficiently to eventually liberate the tightly packed DNA out of the capsid. We suggest that this process starts from the insertion of single NPs at one of the 12 vertexes of the icosahedral capsid and following aggregation of NPs further destabilizes the capsid protein assembly until it bursts and releases its DNA.

5.3 Discussion

Chapter 4 proposed that the full coverage of the viruses by MUSOT NPs is the final stage of the virucidal effect of these NPs. This chapter focussed on an in-depth examination of the action of the virucidal MUSOT NPs on capsids and on the virus envelope, to elucidate how these NPs affect the morphology of the viruses, hence their function.

CryoEM offers tremendous advantages in the imaging of biological samples, yet again general limitations, as outlined extensively in Chapter 2 as well as at the beginning of the discussion of Chapter 4, have to be taken into account in the evaluation of the obtained micrographs. For the in-depth evaluation of these micrographs several further considerations have to be taken into account in the interpretation of the images. In single particle analysis, it is well-known that biological specimens tend to adopt an orientation towards the carbon of the TEMgrid. In cryoEM on holey carbon this effect is less pronounced, but viruses have been found to preferentially locate near the carbon rim of the holes. It cannot be excluded that they adopt a preferential orientation concealing a part of the information, especially when 2D images are evaluated. To evaluate the interaction between capsid proteins with NPs, the high difference in contrast between gold particles and the soft constituents of the viruses creates difficulties in analysing the images. NPs have a high molecular mass, hence high amplitude contrast and can be imaged close to focus. The light elements that make up the viruses on the other hand necessitate a high defocus (-2 to $-3\ \mu\text{m}$) to be visualized in phase contrast. The thus necessary compromise in focus renders the allocation of NPs to specific regions on the capsid more challenging. Moreover, when NPs are imaged with a $1.5\ \mu\text{m}$ defocus, strong Fresnel fringes form as a white rim around the NPs that can conceal other underlying structures such as parts of a capsid.

The analyses in this chapter are based on a range of cryoEM micrographs. The interpretation of these images must consider that these are 2D representations of three dimensional viruses. Accordingly counts of electron-dense objects such as gold NPs can be slightly under-

estimated by the superposition of these in 3D, particularly on a densely-covered virus. Measurements of distances between structures on the images are likely to be underestimated, as their exact distance in z-height on the 3D object is not known. The thickness of the fresnel fringes around the NPs was used as an orientation to perform measurements of NP distances at roughly comparable z-height to limit the underestimation of distances measured. Regarding the distances measured between envelope and NPs the same limitation was taken into account. The distance was thus measured between the outer rim of the envelope and the particles located there, still the distance of a NP located on the envelope, but at higher z-height would be shorter than the real distance in 3D. This limitation particularly applied to particles located close to the envelope. A detailed evaluation of different morphologies of the envelope upon treatment with the NPs would be highly interesting, but statistical information can only be gained after an optimisation of the cryoEM procedure to yield higher ratios of intact envelopes in the reference samples.

A further biological limitation to consider in this part of the study is that, per se, the HSV capsid is not infective. This disadvantage is outweighed by: (1) the capsid size that is amenable to imaging and (2) because HSV is a readily available member of the herpesviridae family, which represents a good model to investigate the interaction between NPs and viral capsids. It would have been ideal to directly study the NP-capsid association on a non-enveloped HSPG-dependent virus such as HPV rather on a sample rich in non-infective HSV capsids, but the preparation of HPV samples in an optiprep gradient impossibilitated the visualisation of these viruses under cryoEM. And (3) on a long-term perspective the direct effects on HSV capsids could be of high interest when the capsids themselves are targets, as for example in a therapeutic approach on latently infected neurons.

5.3.1 Nanoparticle interaction with viral envelopes

Turning now to the experimental results we examined position and distribution of virucidal MUSOT 200515 and 131008 NPs on the surface of HSV1 and HSV2 viruses. For the study of these interactions it was pivotal that the viruses were not fully concealed by the NPs. Hence incubations with MUSOT 131008 NPs, that were more aggregation-prone due to more tiny clusters in the NP batch (as outlined on page 70), were performed on short term at low concentration (0.02mg/ml). MUSOT 200515, on the other hand, did not aggregate on the viruses in a way that fully concealed the virus, hence the fully covered virucidal endpoint could be studied on these NPs.

Fully MUSOT 200515 covered HSV1 virions depicted in Figure 5-1 showed that the virucidal NPs do not directly associate to the viral envelope, but localize at a distance of 8.4 ± 3.9 nm from the surface of the viral envelope bilayer. The distances of NPs to the virus envelope agree with the length of different viral glycoproteins: gC 24 nm⁸⁸, gD 8 nm⁸⁸, gH/gL 8 nm¹⁵⁰ and gB 10 nm in prefusion-conformation and 14 nm in postfusion-conformation⁴⁰. The importance and function of glycoproteins in the viral infection cycle has been introduced in Chapter 2.1.5. The distance-distribution of MUSOT 200515 NPs on virus envelopes centres around a distance of 7 to 9 nm off the virus envelope. Fewer particles were located further from the envelope at distances up to 21 nm. This suggests a binding of the NPs to the shorter glycoproteins: gB, gD and gH/gL.

The number of NPs bound to the virus surface has been quantified and showed, on average, 333 ± 54 NPs bound per virus envelope. Grünewald et al. counted 600-750 spikes on the viral envelope that they attribute to glycoproteins per HSV1 in a CryoEM reconstruction of the full virion¹⁷. Therefore we suggest that NPs bind to every second glycoprotein on the viral envelope. The glycoprotein spacing on the virus has been reported to be 13 nm on the proximal pole and as small as 9 nm at the distal pole. The spacing of virucidal MUSOT NPs on the virus envelope was measured to be on average 11.6 ± 4.0 nm, yet as introduced above this value is likely underestimated for short distances. Comparable to the glycoprotein spacing differences on proximal and distal pole of viruses different densities of NPs have been observed on viruses e.g. in Figure 5-1 (e). The theoretical spacing of 330 NPs on a sphere of 200 nm diameter would be approximately 19 nm. By comparing real and theoretical spacing of NPs calculated based on the number of NPs per virus and its diameter, an underestimation factor of about two could be determined from five viruses. The average distances between NPs measured on the virions support the hypothesis that NPs bind every second glycoprotein. It can therefore be summarized from the study of densely MUSOT 200515 covered viruses that the virucidal NPs bind numerous and densely to the glycoprotein layer of the viral envelope, covering on average half of the there presented glycoproteins.

The study of the NP association to two single viruses (Figure 5-3, Figure 5-4) supports the hypothesized interaction with short glycoproteins on the viral envelope. A schematic representation of the binding we hypothesize is depicted in Figure 5-8 as will be detailed in the following. As explained in Figure 5-3 MUSOT 131008 NPs predominantly associated to the virus envelope layer at a distance between 8 and 10 nm on the proximal pole and up to 20 nm at the distal pole of the virus. A clustering of the NPs was observed at the protrusion

that extends as far as 64 nm off the virus surface. Single long glycoprotein spikes emerging more than 20 nm out of the glycoprotein layer do not seem to be associated to NPs, which suggests a preferential binding to the short glycoproteins. Judging from the abundance, length and angle of those spikes it can be assumed that these are 20-40 nm long gC spikes, that has been deemed non-essential for the virus entry. The 8-10 nm short glycoproteins gB, gD and gH/gL are essential, as is their organisation. It has been reported that the organisation of different glycoproteins onto different poles of the virus serves the purpose to keep large, bulky glycoproteins far away from the entry associated short glycoproteins gB, gD and gH/gL to avoid steric hindrance¹³⁶. Figure 5-8 summarizes the allocation of the different densities imaged on the virus envelope to glycoproteins.

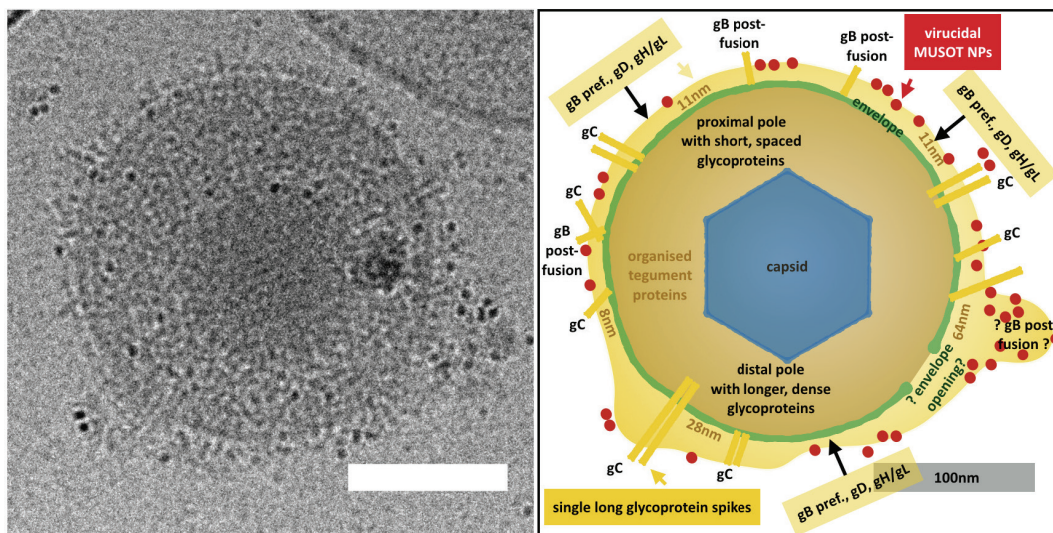


Figure 5-8: Schematic representation of the aforepresented CryoEM of an HSV1 virion after 30sec of treatment with 0.02mg/ml of MUSOT 131008: Left: CryoEM image of 0.5 min MUSOT 131008 treated HSV2 with well resolved viral glycoproteins, Right schematic representation of the proposed glycoproteins virucidal MUSOT NPs bind to; The scale bar is 100 nm.

To summarise virucidal MUSOT NPs have been found to preferentially bind to gB, gD and gH/gL. The number of virucidal NPs bound per virus in the case of abundant MUSOT 200515 NPs was high enough to cover half of all glycoproteins on the viral envelope. Based on these observations we suggest that by multivalently, irreversibly binding to vital viral glycoproteins virucidal MUSOT NPs firstly impose steric hindrance and can act as spacers to hinder the establishment of stable binding and membrane fusion.

Secondly, we propose that the strong binding of virucidal NPs to viral glycoproteins leads to the induction of conformational changes in the viral glycoproteins. The function of the short

glycoproteins gD, gH/gL and gB is to exert a force onto the membranes of virus and cell to induce membrane fusion. As introduced in Chapter 2.5 after initial gC binding to HSPG gD approaches the membranes of the cell and the virus. Then the gH/gL complex pulls the membranes together to induce membrane fusion. This initial fusion pore is stabilised by gB to form a stable envelope opening through which the viral capsid enters the cell. T-shaped gB in post-fusion form could clearly be identified by Mordehai et al. on the merged membranes after membrane fusion as depicted in Figure 5-9. The high curvature of regions rich in postfusion gB highlights the force gB exerts on the membrane.

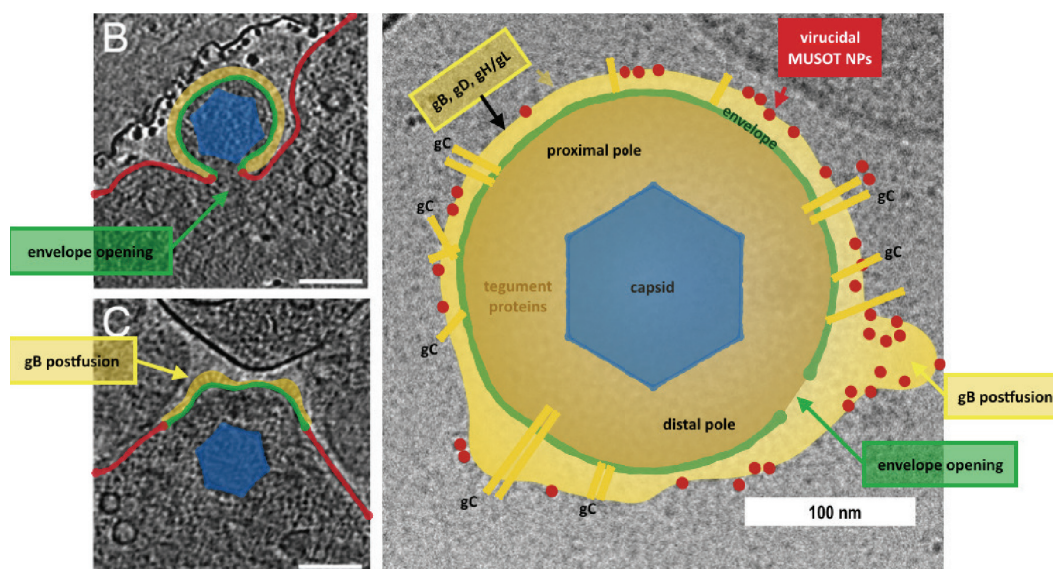


Figure 5-9: Left: Membrane fusion pore reproduced from Maurer et al.¹³⁶ with colour coding: capsid blue, virus envelope green line, viral glycoproteins yellow, cell membrane red line; Right: schematic representation of NP decorated virus with gB postfusion rich region and envelope opening highlighted.

We hypothesise that the action of virucidal NPs on the virus envelope glycoproteins induces comparable conformational changes leading to protruded region in the glycoprotein coat of the virus and suggest that the observed opening of the envelope could be induced by the action of the glycoprotein conformational change and clustering.

5.3.2 Hypothesized mechanism for virucidal NP action

Based on the results of the NP association to viral envelopes and viral capsid we propose the following mechanism for the virucidal action of MUSOT-NPs. We hypothesise that the association of NPs to viral glycoproteins induced conformational changes leading to the formation of membrane distortions and protrusions is sufficient to destabilise the viral envelop enough to eventually expel the viral capsid. The viral capsid in turn as well interacts with

the virucidal NPs showing a sufficient destabilization to open the capsid and liberate the enclosed DNA. Further progressive coverage with NPs then leads to the morphology of the virucidal endpoint that has been established in the previous Chapter. In the following paragraphs, I am going to detail the separate steps of the hypothesized virucidal mechanism.

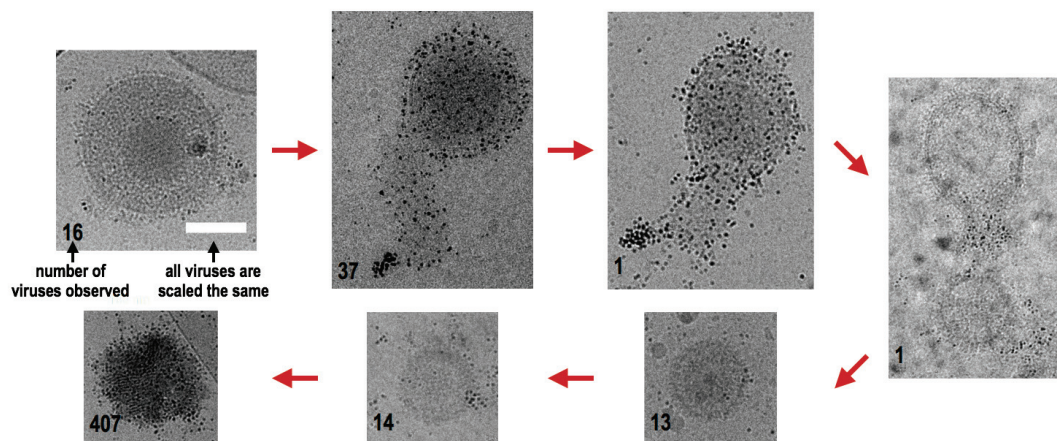


Figure 5-10: CryoEM micrographs of the hypothesized mechanism for the action of virucidal NPs on viruses showing different stages of NP-virus interaction from the initial association of NPs to the virus to the formation of protrusions that open to liberate the capsid that in turn is opened and decorated by virucidal NPs. The small number at the lower left of each image indicates the total number of images in which such a morphology has been imaged. All images have been obtained after 0.5 min short incubation of virucidal NPs with HSV1. The Scale bar is 100nm.

5.3.2.1 Nanoparticle binding and formation of membrane protrusion

We propose that starting from the initial binding of NPs to the viral glycoproteins conformational changes are induced in the viral glycoproteins leading to the formation of membrane protrusions. In samples treated with virucidal NPs these protrusions were both longer than in reference samples and densely decorated with NPs. Stannard et al.⁸⁸ described membrane protrusions as rich in gB, which could suggest binding of virucidal NPs to gB. The gB trimer in its prefusion conformation presents a central cavity of a width of approximately 4 nm. This cavity is flanked by the domain containing the hydrophobic, charged fusion loops that stabilize the membrane merging and could structurally present an ideal binding pocket for amphiphilic NPs. An image of the two conformations of the protein are depicted in Figure 2-11. The binding of virucidal NPs to the exposed part of the metastable prefusion-gB could trigger a conformational change of gB to its postfusion form which exerts a force onto the membrane as illustrated in Figure 5-9 inducing high membrane curvature. How the domains arrange during the conformational change is still debated, as is the effect this would have on the virus envelope if this were to happen numerous by a concerted induction through NPs. Evidence as to the membrane curvature changing action of gB can be found

both in the post-membrane fusion conformations imaged by Maurer et al.¹³⁶ as well as in the size distribution of extracellular vesicles enriched in gB that Mordehai et al.¹³⁷ utilized for their 3D structure study in gB. Vesicles with post-fusion gB were smaller, showing a higher curvature than those with pre-fusion gB. This protein additionally shows a high propensity to form clusters¹³⁹ and thereby further drives the membrane fusion process during virus infection. Membrane breakage as depicted in Figure 5-4 where an event of capsid expulsion from the viral envelope was imaged could be based on excessive NP binding to said gB and the induction conformational changes of this protein lacking its cellular counterpart. The propensity of gB to cluster could further drive this process to lead to the formation of glycoprotein clusters and membrane protrusions that exert a sufficient force onto the membrane to induce its breakage. The then liberated capsid again interacts with the NPs in solution.

5.3.2.2 *Capsid-nanoparticle interaction*

Quantitative image analysis presented in Chapter 4 showed that the proportion of broken capsids in viruses treated with virucidal NPs is substantially increased: from 10% in the HSV2 reference sample to 46% over all capsids counted in MUSOT treated on HSV2, see Figure 4-8. Hence, the possibility that some images show NPs that attached to already broken viruses cannot be completely excluded. As in previous experiments, higher counts, based for example, on a higher initial virus concentration, would facilitate the interpretation of the results. This is especially relevant when analysing broken or non-stabilized capsids which we suspect to be short-lived structures as has been reported for unstabilized viral procapsids in solution¹²⁸. As in the previous interpretation of the effects of NPs on the viral envelope the interpretation of the NP effects on viral capsids is based on images that have been categorized from different samples at short (0.5 min) incubation time.

From the images presented in Figure 5-5 we propose the following sequence of events leading to the breaking of the capsid and fully NP covered virucidal endpoint: association of NPs to capsid vertices followed by NP clustering and lining up at capsid vertices to the deformation and opening of the vertices as presented in Figure 5-11.

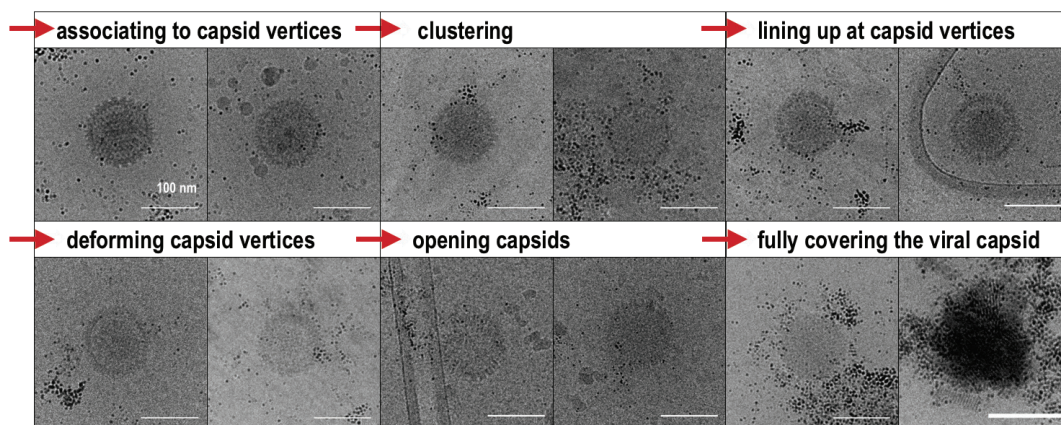


Figure 5-11 Hypothesised sequence of NP-capsid association events leading to the eventual breakage and full NP coverage of broken capsids. Scale bars are 100nm.

We have observed that particles predominantly attack the virus pentons (Figure 5-5 b and e) rather than the virus hexons. A capsid opened by the NPs at more than one site has only been observed twice (Figure 5-5 d and Figure 5-6). We hypothesise that this observation of a single point where NP attachment starts, is linked to structural details of the capsid. The icosahedral capsid is built of the major capsid protein VP5 arranged in pentons and hexons that are packed primarily by electrostatic interactions¹⁵¹. The capsid structure of HSV has been described in detail in Chapter 2.1.5. The pentons are more spaced than the hexons, hence the channel formed by the protein pentons is wider¹⁵¹. One of the 12 pentons is occupied by the portal protein that is of particular importance in the viral life-cycle as it is both responsible for the loading of the DNA from the nucleus into the capsids as well as the ejection out of the capsid into the nucleus¹³⁰. Clustering and lining up of NPs on capsid vertices are most likely linked to tegument and portal proteins on the virus capsids. We hypothesize that once the particles interact with the metastable capsid, it causes irreversible structural modifications in the capsid such as elongations and deformations. The CryoET slices represented in Figure 5-6 and Figure 5-7 show empty capsids devoid of their DNA at different stages of capsid degradation. Whereas the first virus depicted still shows a polyhedral structure, the second virus is round with a large opening on the capsid.

Compared to the capsid thickness of 15 nm¹³¹ the MUSOT NPs have a core diameter around 2.8 nm, and a hydrodynamic radius of 5-6 nm: thus, large enough to disrupt the capsid upon insertion. Excessive aggregation and the insertion of virucidal NPs into the penton or the portal protein could create enough distortion to destabilize the electrostatic binding of the capsid proteins, or that of the small part of the protein that plunges the penton channel, to

induce the ejection of the DNA that is confined in the capsid at high pressure $\sim 18 \text{ atm}^{132}$. The concept that multivalent binding of NPs to a viral capsid can exert a force onto the capsid of has as well been proposed based on simulations of one of our collaborators⁷⁷.

An intact virus is a supramolecular assembly that, through evolution, has developed remarkable colloidal stability in complex biological fluids⁵. This allows viruses to avoid establishing deleterious interfaces and activates only upon recognizing its target host. However, once the viral structure is damaged, the NPs adsorb avidly onto the broken virus.

To summarize the capsid – NP interaction we propose that MUSOT NPs fit between the capsid proteins at the vertices of the icosahedral capsid. There, there located, penton channels and the portal protein of the virus present anchoring points for the NPs where they are able to establish multivalent binding to induce local distortions that destabilize the metastable capsid sufficiently to release their DNA and hence become irreversibly inactivated. Once the viral structure is damaged, the NPs adsorb avidly onto the broken virus leading to the fully NP covered morphology of the virucidal endpoint.

5.3.2.3 Summary of the hypothesized virucidal mechanism

Figure 5-12 summarizes the hypothesized mechanism of virucidal NPs on enveloped and non-enveloped viruses:

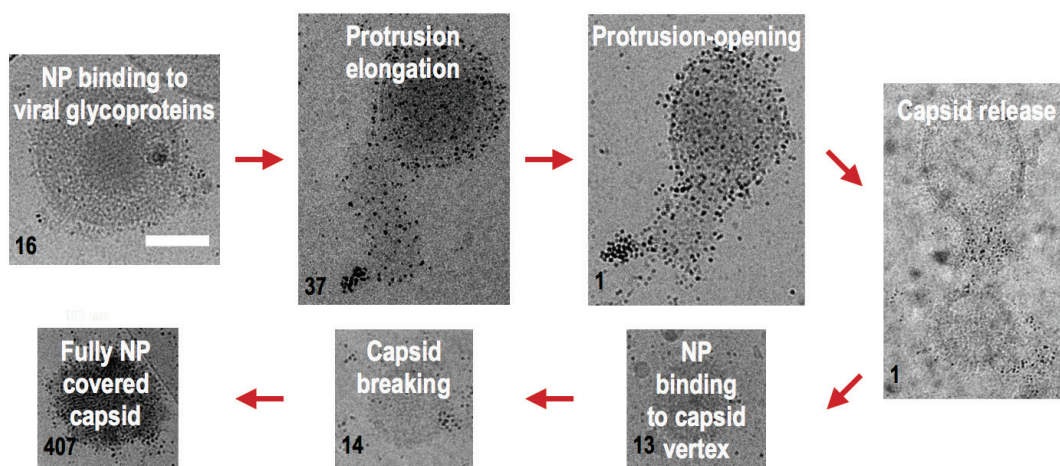


Figure 5-12: Hypothesized virucidal mechanism

Chapter 6 Conclusion

6.1 Achieved results

This study set out to determine whether the treatment of viruses with broad-spectrum antiviral NPs can be correlated to detectable morphological damage to the viruses imaged by Electron Microscopy. Therefore, we examined the differences between the association of virustatic and virucidal NPs to different HSPG-dependent viruses in their near-native solution state using CryoEM. By employing qualitative and quantitative assessments of the treated virus populations we established differential association characteristics and morphologies of virustatic and virucidal NPs on viruses.

We found that virustatic NPs only attach in low numbers and without significant progression over time: we interpret this binding to be only transient. Virucidal NP on the other hand attach to viruses in high number and show a clear progression towards fully NP covered viruses, which we interpret as the imaging of a the final virucidal effect. This effect could be imaged both on HPV, HSV1 and HSV2 as well as with two different virucidal MUSOT NPs. In a further examination of the association of single NPs with viruses, we identified determinants of the interaction of virucidal NPs with herpes simplex viruses to conclude a mechanism for the virucidal action of MUSOT NPs. We found that NPs appear to interact with proteins vital to the viral infection cycle. On the viral envelope we propose that the stable multivalent binding of numerous NPs exerts a force onto the viral envelope leading to envelope breakage. The released capsids in turn as well interact with NPs and we propose that the interaction of viruses with the major capsid protein of HSV destabilizes the metastable capsids sufficiently to release the enclosed DNA.

This project provided an opportunity to advance the field of antivirals. It is the first study to provide a solution-state visualisation of the interaction of viruses and virucidal NPs. The in-depth study further offers important insight into the association of single NPs with viral proteins, of capsid and envelope and that could govern the development of new antiviral therapies.

6.2 Future development

For future studies, we propose two focus areas: one on the mechanism underlying the virucidal properties of these NPs and another aiming towards the *in-vivo* use to treat viral infections. Here especially potential side effects stemming from the similarity of the presentation of sulfonates on the NPs surface to heparin has to be considered.

6.2.1 A deeper mechanistic study

For a deeper study of the protein-NP interactions an exhaustive CryoET study should be conducted to reconstruct the internalisation of virucidal NPs between capsids proteins, or to demonstrate the conformational changes in the glycoproteins. In such a study both the virus titer and the CryoEM procedure should be optimized to obtain a sufficiently high number of viruses per image and tomogram at high virus quality. Therefore, a study of cryoprotectants that could be used in CryoEM, but do not interfere with the virucidal effect to be imaged would be required. Virus pre-treatment with sucrose for example rendered the virucidal action either less effective or prohibited viruses from effectively binding. A combined ultracentrifugation and ultrafiltration protocol could both concentrate the viruses and remove residual sucrose from the viruses. Additionally, CryoEM sample preparation setup to reliably have a high proportion of perfect round viruses in the reference is important for an unbiased evaluation of the morphological effects NPs exert on the virus membranes.

Preliminary experiments where the virus-NP pre-incubation has been conducted at 4°C contrary to the incubation at 37°C showed that the previously observed virucidal effect of MUSOT NPs only manifests as virustatic upon pre-incubation at 4°C as shown in Figure 6-1.

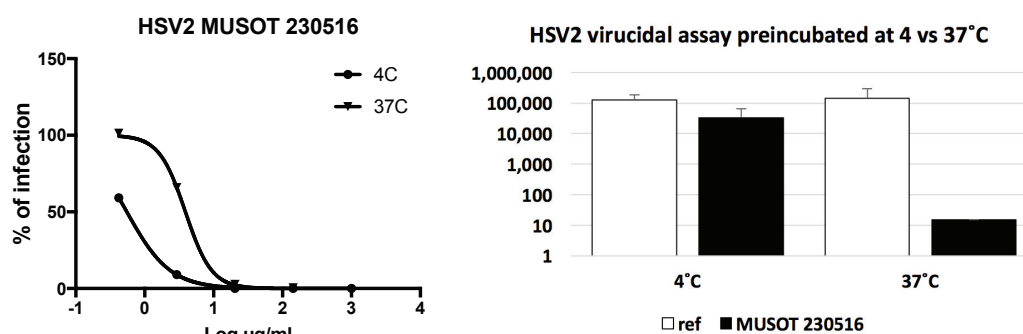


Figure 6-1: Dose response and virucidal assay testing the temperature influence on NP-virus pre-incubation. Left: Dose response of MUSOT 230516 at 37°C and 4°C. Right: HSV2 pre-incubated with MUSOT 230516 at 4°C and 37°C.

We propose that this effect supports the hypothesized mechanism. For a conformational change to be induced or a membrane to be distorted energy is necessary that is not provided at 4°C. The additionally reduced mobility of lipids at 4°C could explain why not virucidal effect could be observed when the virucidal testing is performed at 4°C. An investigation, if this observation can be connected to an according NP-virus association and morphology in CryoEM could greatly support the proposed mechanism of conformational changes from metastable to stable systems.

For a further biological and virological evaluation of the virucidal effect of NPs a quantification of the liberation of the major capsid protein VP5 from the viruses could be tested to support the hypothesis of virus envelope opening upon virus action. Additionally, the DNA release¹³² could be quantified to support the concept of capsid opening, initial tests showed that for this to work, concentrated virus samples would be necessary to obtain a measurable amount of DNA.

6.2.2 Towards application as a pharmaceutical active agent

Nanotherapeutics have, for now, only made it through FDA approval in the form of liposomes, polymer based platforms (predominantly involving poly-ethylene glycols PEG) or nanocrystalline active substances¹⁵². Metallic NPs have only recently made it into clinical trials predominantly in the form of iron and iron oxide NPs as contrast agents or enhanced iron supplements. Although a lot of research effort is invested into gold NPs, none have been FDA approved to date.¹⁵³

Therefore, our research group invested into translating the virucidal design principle established on gold NPs onto different materials, namely on iron NPs as presented in Cagno et al. [submitted]⁷⁷ and on cyclodextrins. Cyclodextrins show low cytotoxicity, do not elicit an immune response and are widely used in pharmacology to enhance the bioavailability of active substances¹⁵⁴. β -cyclodextrin, as received, is FDA approved in several drug formulations and made the FDA list of Generally Regarded as Safe (GRAS) food additives¹⁵⁴. A commercially available short linker sulfonated β -CD, termed CD₁, showed an antiviral response in the dose response assay, but released infective viruses again upon dilution, i.e. showed only a virustatic effect (see Table 2). Samuel Jones replicated the supramolecular design we employed on the NP on cyclodextrin by functionalizing β -CD with 11 carbon long hydrophilic chains terminated with sulfonates. The virological testing of this molecule, termed

CDS2 showed a steep dose response curve and the virucidal assays could confirm the virucidal action of CDS2, confirming a successful design replication. The virustatic action of the short-linker CD1 and the virucidal action of the long-linker CDS2 were shown both on HSV1 and HSV2 as presented in the characterization in the Materials and Methods on page53.

A first CryoEM study on the morphologies of viruses after 0.5 min of incubation with 0.02mg/ml virucidal CD2 showed a high proportion of broken capsids as depicted in Figure 6-1. CDS2 treated viruses show a markedly increased proportion of broken capsids: 44% for 0.02mg/ml and $33 \pm 3\%$ for 0.2mg/ml. Morphologies upon CDS2 0.2mg/ml treatment have been counted in two separate samples.

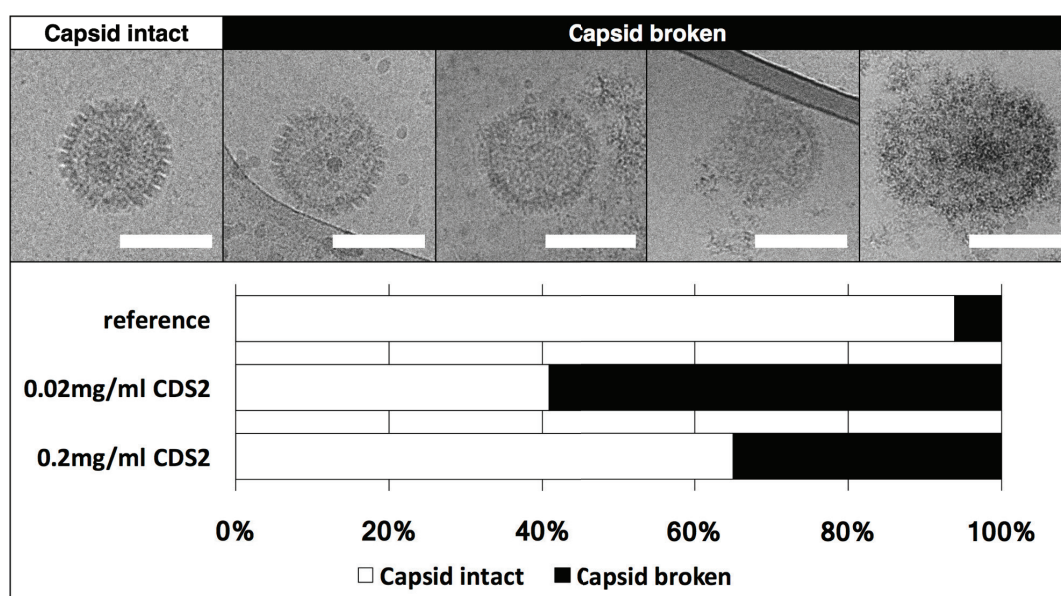


Figure 6-2: CryoEM imaging and quantification of HSV2 capsid morphology immediately after treatment with CDS2 (approximate incubation time below 0.5 min): the top panel shows representative CryoEM images of intact versus broken capsids; the diagram below shows the ratio of intact vs. broken capsids for a reference sample versus samples treated with 0.02mg/ml CDS2 or 0.2mg/ml CDS2. The scale bar is 100 nm

The interaction of HSV1 with the virucidal CDS2 and virustatic CD1 was comparable to that seen in HSV2 viruses. The proportion of broken capsids increases from 3% in the reference sample to 15% in the CD1 sample, further to 13% upon exposure to 0.02g/ml CDS2 to 20% for a high concentration of CDS2 of 0.2mg/ml as depicted below in Figure 6-3. On a closer observation of the glycoprotein arrangement on the envelope periodicities comparable in size to those for CD crystals have been observed and could hint towards a possible cross-linking of the proteins through CDS2.

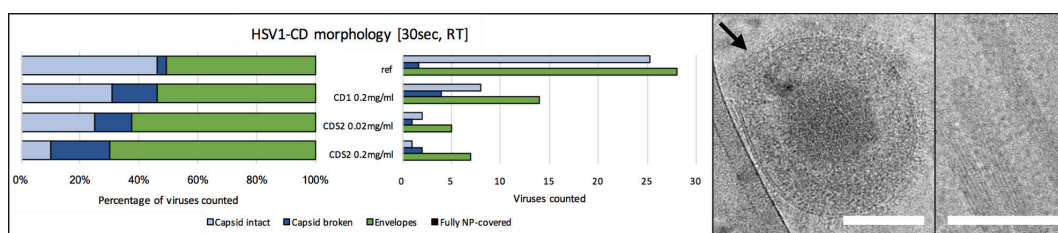


Figure 6-3: Diagrams of counts of the CryoEM HSV1 morphology after treatment with the virustatic CD1 and virucidal CDS2 for 0.5 min at RT (Left), CryoEM micrograph of HSV1 incubated for 30sec with 0.02mg/ml CDS2 after 30sec, an area of increased glycoprotein organisation is highlighted by a black arrow (middle), CD2 crystals observed in a less soluble production of sulfonated cyclodextrins. Scale bar is 100 nm

Nonetheless for an antiviral substance or nanomaterial to be relevant, it must perform its role in an infected living organism. Although the morphological studies presented in this thesis showed a novel way of approaching this complex problem, its relevance will ultimately be judged by its efficacy as a tool against viral infections. As described in the introduction, little can be offered to victims of viral infections, that can be fatal, not only to individual patients, but to entire populations.

To summarize this work showed that, by tuning the surface chemistry on gold NPs and cyclodextrins, viral activity could be manipulated along with the observation of drastic morphological alterations *in-vitro*. These findings pave the way for both *in-vivo* research towards broad spectrum antiviral treatments and also to further fundamental *in-vitro* studies that can reveal otherwise unanticipated viral vulnerabilities.

References

1. Lozano, R. *et al.* Global and regional mortality from 235 causes of death for 20 age groups in 1990 and 2010: a systematic analysis for the Global Burden of Disease Study 2010. *Lancet* **380**, 2095–2128 (2012).
2. Smil, V. The next 50 years: Fatal discontinuities. *Population and Development Review* (2005).
3. Dye, C. After 2015: infectious diseases in a new era of health and development. *Philosophical Transactions of the Royal Society B: Biological Sciences* **369**, 20130426–20130426 (2014).
4. Smith, K. F. *et al.* Global rise in human infectious disease outbreaks. *Journal of The Royal Society Interface* **11**, 20140950 (2014).
5. Flint, S. J., Enquist, L. W., Racaniello, V. R. & Skalka, A. M. *Principles of Virology: Vol. 1 and 2, 4th edition. 1 and 2*, (ASM Press, 2004).
6. Loze, P. M. *et al.* Vaccines are different: A systematic review of budget impact analyses of vaccines. *Vaccine* (2017).
7. Fine, P., Eames, K. & Heymann, D. L. Herd Immunity: A Rough Guide. *Clin Infect Dis* **52**, 911–916 (2011).
8. Fine, P. E. Herd immunity: history, theory, practice. *Epidemiol Rev* **15**, 265–302 (1993).
9. Greenwood, B. The contribution of vaccination to global health: past, present and future. *Philos. Trans. R. Soc. Lond., B, Biol. Sci.* **369**, 20130433–20130433 (2014).
10. De Clercq, E. Antivirals: past, present and future. *Biochemical Pharmacology* **85**, 727–744 (2013).
11. Pelliccia, M. *et al.* Additives for vaccine storage to improve thermal stability of adenoviruses from hours to months. *Nature Communications* **7**, 13520 (2016).
12. Mateu, M. G. Virus engineering: functionalization and stabilization. *Protein Eng. Des. Sel.* **24**, 53–63 (2011).
13. Doerschuk, P. C., Gong, Y., Xu, N., Domitrovic, T. & Johnson, J. E. Virus particle dynamics derived from CryoEM studies. *Current Opinion in Virology* **18**, 57–63 (2016).
14. Hampson, K. *et al.* Rabies Exposures, Post-Exposure Prophylaxis and Deaths in a Region of Endemic Canine Rabies. *PLOS Neglected Tropical Diseases* **2**, e339 (2008).
15. Rappuoli, R., Mandl, C. W., Black, S. & De Gregorio, E. Vaccines for the twenty-first century society. *Nature Reviews Immunology* (2011).
16. Koelle, D. M. & Corey, L. Herpes Simplex: Insights on Pathogenesis and Possible Vaccines. *Annu. Rev. Med.* **59**, 381–395 (2008).
17. Grünewald, K. *et al.* Three-dimensional structure of herpes simplex virus from cryo-electron tomography. *Science* **302**, 1396–1398 (2003).

18. Schmid, M. F. *et al.* A Tail-like Assembly at the Portal Vertex in Intact Herpes Simplex Type-1 Virions. *PLOS Pathogens* **8**, e1002961 (2012).
19. Whitley, R. J. & Roizman, B. Herpes simplex virus infections. *The Lancet* **357**, 1513–1518 (2001).
20. Brady, R. C. & Bernstein, D. I. Treatment of herpes simplex virus infections. *Antiviral Research* **61**, 73–81 (2004).
21. Brown, Z. A. *et al.* The acquisition of herpes simplex virus during pregnancy. *New England Journal of Medicine* **337**, 509–515 (1997).
22. Greenberg, M. S. *et al.* A comparative study of herpes simplex infections in renal transplant and leukemic patients. *J. Infect. Dis.* **156**, 280–287 (1987).
23. Kaye, S. & Choudhary, A. Herpes simplex keratitis. *Prog. Retin. Eye Res.* **25**, 355–380 (2006).
24. Sauerbrei, A., Bohn, K., Heim, A. & Hofmann, J. Novel resistance-associated mutations of thymidine kinase and DNA polymerase genes of herpes simplex virus type 1 and type 2. *Antiviral Therapy* (2011).
25. Bacon, T. H., Boon, R. J., Schultz, M. & Hodges-Savola, C. Surveillance for Antiviral-Agent-Resistant Herpes Simplex Virus in the General Population with Recurrent Herpes Labialis. *Antimicrobial Agents and Chemotherapy* **46**, 3042–3044 (2002).
26. De Clercq, E. Strategies in the design of antiviral drugs. *Nat Rev Drug Discov* **1**, 13–25 (2002).
27. Martinez, J. P., Sasse, F., Brönstrup, M., Diez, J. & Meyerhans, A. Antiviral drug discovery: broad-spectrum drugs from nature. *Natural Product Reports* **32**, 29–48 (2015).
28. Christ, F. *et al.* Rational design of small-molecule inhibitors of the LEDGF/p75-integrase interaction and HIV replication. *Nature Chemical Biology* **6**, 442–448 (2010).
29. Christ, F. & Debyser, Z. The LEDGF/p75 integrase interaction, a novel target for anti-HIV therapy. - PubMed - NCBI. *Virology* **435**, 102–109 (2013).
30. Bonhoeffer, S., May, R. M., Shaw, G. M. & Nowak, M. A. Virus dynamics and drug therapy. *Proceedings of the National Academy of Sciences of the United States of America* **94**, 6971–6976 (1997).
31. Chen, E. C., Miller, S. A., DeRisi, J. L. & Chiu, C. Y. Using a Pan-Viral Microarray Assay (Virochip) to Screen Clinical Samples for Viral Pathogens. *Journal of Visualized Experiments : JoVE* (2011).
32. Vigant, F., Santos, N. C. & Lee, B. Broad-spectrum antivirals against viral fusion. *Nature Reviews Microbiology* **13**, 426–437 (2015).
33. Alex M Agelidis, D. S. Cell entry mechanisms of HSV: what we have learned in recent years. *Future virology* **10**, 1145–1154 (2015).
34. Pöhlmann, S. & Simmons, G. *Viral entry into host cells*. **790**, (Springer New York, 2013).
35. Rusnati, M. *et al.* Sulfated K5 Escherichia coli polysaccharide derivatives: A novel class of candidate antiviral microbicides. **123**, 310–322 (2009).
36. Liu, J. & Thorp, S. C. Cell surface heparan sulfate and its roles in assisting viral infections. *Med Res Rev* **22**, 1–25 (2002).
37. Spillmann, D. Heparan sulfate: Anchor for viral intruders? *Biochimie* **83**, 811–817 (2001).
38. Deepak Shukla, P. G. S. Herpesviruses and heparan sulfate: an intimate relationship in aid of viral entry. *Journal of Clinical Investigation* **108**, 503–510 (2001).
39. WuDunn, D. & Spear, P. G. Initial interaction of herpes simplex virus with cells is

- binding to heparan sulfate. *J. Virol.* **63**, 52–58 (1989).
40. Zeev-Ben-Mordehai, T. *et al.* Two distinct trimeric conformations of natively membrane-anchored full-length herpes simplex virus 1 glycoprotein B. *PNAS* **113**, 4176–4181 (2016).
41. Rider, C. C. The potential for heparin and its derivatives in the therapy and prevention of HIV-1 infection. *Glycoconj. J.* **14**, 639–642 (1997).
42. Dogra, P. *et al.* Novel Heparan Sulfate-Binding Peptides for Blocking Herpesvirus Entry. *PLoS ONE* **10**, e0126239 (2015).
43. Cagno, V. *et al.* Highly sulfated K5 Escherichia coli polysaccharide derivatives inhibit respiratory syncytial virus infectivity in cell lines and human tracheal-bronchial histocultures. *Antimicrobial Agents and Chemotherapy* **58**, 4782–4794 (2014).
44. Witvrouw, M. & De Clercq, E. Sulfated Polysaccharides Extracted from Sea Algae as Potential Antiviral Drugs. *General Pharmacology: The Vascular System* **29**, 497–511 (1997).
45. Harden, E. A., Falshaw, R., Carnachan, S. M., Kern, E. R. & Prichard, M. N. Virucidal activity of polysaccharide extracts from four algal species against herpes simplex virus. - PubMed - NCBI. *Antiviral Research* **83**, 282–289 (2009).
46. Taylor, D. L. *et al.* Potent inhibition of human immunodeficiency virus by MDL 101028, a novel sulphonic acid polymer. *Antiviral Research* **28**, 159–173 (1995).
47. Donalisio, M. *et al.* Inhibition of human respiratory syncytial virus infectivity by a dendrimeric heparan sulfate-binding peptide. *Antimicrobial Agents and Chemotherapy* **56**, 5278–5288 (2012).
48. Sepúlveda Crespo, D., Ceña Díez, R., Jiménez, J. L. & Ángeles Muñoz Fernández, M. Mechanistic Studies of Viral Entry: An Overview of Dendrimer-Based Microbicides As Entry Inhibitors Against Both HIV and HSV-2 Overlapped Infections. *Med Res Rev* **37**, 149–179 (2017).
49. McCormack, S. *et al.* PRO2000 vaginal gel for prevention of HIV-1 infection (Microbicides Development Programme 301): a phase 3, randomised, double-blind, parallel-group trial. *Lancet* **376**, 1329–1337 (2010).
50. Pirrone, V., Wigdahl, B. & Krebs, F. C. The rise and fall of polyanionic inhibitors of the human immunodeficiency virus type 1. *Antiviral Research* **90**, 168–182 (2011).
51. Van Damme, L. *et al.* Lack of effectiveness of cellulose sulfate gel for the prevention of vaginal HIV transmission. *N. Engl. J. Med.* **359**, 463–472 (2008).
52. Galus, A. *et al.* Hexagonal-shaped chondroitin sulfate self-assemblies have exalted anti-HSV-2 activity. *Carbohydrate Polymers* **136**, 113–120 (2016).
53. Lembo, D. *et al.* Auto-associative heparin nanoassemblies: A biomimetic platform against the heparan sulfate-dependent viruses HSV-1, HSV-2, HPV-16 and RSV. *European Journal of Pharmaceutics and Biopharmaceutics* **88**, 275–282 (2014).
54. Lembo, D. & Cavalli, R. Nanoparticulate delivery systems for antiviral drugs. *Antivir. Chem. Chemother.* **21**, 53–70 (2010).
55. Galdiero, S. *et al.* Silver Nanoparticles as Potential Antiviral Agents. *Molecules* **2011**, Vol. 16, Pages 8894–8918 **16**, 8894–8918 (2011).
56. Khandelwal, N., Kaur, G. & Kumar, N. Application of silver nanoparticles in viral inhibition: A new hope for antivirals. *Dig. J. of Nanomat. & Biomat.* (2014).
57. Lara, H. H., Ayala-Núñez, N. V., Ixtapan-Turrent, L. & Rodríguez-Padilla, C. Mode of antiviral action of silver nanoparticles against HIV-1. *Journal of Nanobiotechnology* **8**, 1 (2010).
58. Lara, H. H., Garza-Treviño, E. N., Ixtapan-Turrent, L. & Singh, D. K. Silver nanoparticles are broad-spectrum bactericidal and virucidal compounds. *Journal of Nanobiotechnology* **9**, 30 (2011).

59. Zheng, Y., Cloutier, P., Hunting, D. J. & Sanche, L. Radiosensitization by Gold Nanoparticles: Comparison of DNA Damage Induced by Low and High-Energy Electrons. *Journal of Biomedical Nanotechnology* **4**, 469–473 (2008).
60. de Souza e Silva, J. M. *et al.* Viral Inhibition Mechanism Mediated by Surface-Modified Silica Nanoparticles. *ACS Appl. Mater. Interfaces* **8**, 16564–16572 (2016).
61. Bergstrom, D. E. *et al.* Polysulfonates derived from metal thiolate complexes as inhibitors of HIV-1 and various other enveloped viruses in vitro. *Antivir. Chem. Chemother.* **13**, 185–195 (2002).
62. Baram-Pinto, D., Shukla, S., Perkas, N., Gedanken, A. & Sarid, R. Inhibition of Herpes Simplex Virus Type 1 Infection by Silver Nanoparticles Capped with Mercaptoethane Sulfonate. *Bioconjugate Chemistry* **20**, 1497–1502 (2009).
63. Bowman, M.-C. *et al.* Inhibition of HIV fusion with multivalent gold nanoparticles. *Journal of the American Chemical Society* **130**, 6896–6897 (2008).
64. Bastian, A. R. *et al.* Cell-free HIV-1 virucidal action by modified peptide triazole inhibitors of Env gp120. *ChemMedChem* **6**, 1335–9–1318 (2011).
65. Ekblad, M. *et al.* A highly lipophilic sulfated tetrasaccharide glycoside related to muparfostat (PI-88) exhibits virucidal activity against herpes simplex virus. *Antiviral Research* **86**, 196–203 (2010).
66. Shogan, B., Kruse, L., Mulamba, G. B., Hu, A. & Coen, D. M. Virucidal Activity of a GT-Rich Oligonucleotide against Herpes Simplex Virus Mediated by Glycoprotein B. *J. Virol.* **80**, 4740–4747 (2006).
67. Steinmann, J. Some principles of virucidal testing. *Journal of Hospital Infection* **48**, S15–S17 (2001).
68. Siddharta, A. *et al.* Virucidal Activity of World Health Organization–Recommended Formulations Against Enveloped Viruses, Including Zika, Ebola, and Emerging Coronaviruses. *J. Infect. Dis.* (2017).
69. Rabenau, H. F., Steinmann, J., Rapp, I., Schwebke, I. & Eggers, M. Evaluation of a Virucidal Quantitative Carrier Test for Surface Disinfectants. *PLoS ONE* **9**, e86128 (2014).
70. Abe, M., Kaneko, K., Ueda, A., Otsuka, H. & Shiosaki, K. Effects of several virucidal agents on inactivation of influenza, Newcastle disease, and avian infectious bronchitis viruses in the allantoic fluid of chicken eggs. *Jpn. J. Infect. Dis.* (2007).
71. Chan, Y. F. & Abu Bakar, S. Virucidal activity of Virkon S on human enterovirus. *Med. J. Malaysia* **60**, 246–248 (2005).
72. Cusi, M. G. & Fanigliulo, D. Virucidal activity of a novel non-alcoholic combination of disinfectants. *Journal of Chemotherapy* **28**, 140–142 (2016).
73. Tyler, R., Ayliffe, G. A. J. & Bradley, C. Virucidal activity of disinfectants: studies with the poliovirus. *Journal of Hospital Infection* **15**, 339–345 (1990).
74. Bultmann, H., Girdaukas, G., Kwon, G. S. & Brandt, C. R. The Virucidal EB Peptide Protects Host Cells from Herpes Simplex Virus Type 1 Infection in the Presence of Serum Albumin and Aggregates Proteins in a Detergent-Like Manner. *Antimicrobial Agents and Chemotherapy* **54**, 4275–4289 (2010).
75. Chen, N., Zheng, Y., Yin, J., Li, X. & Zheng, C. Inhibitory effects of silver nanoparticles against adenovirus type 3 in vitro. *Journal of Virological Methods* **193**, 470–477 (2013).
76. Atukorale, P. U. Amphiphilic gold nanoparticles: mechanisms for interaction with membranes and applications in drug and vaccine delivery. (2014).
77. Cagno, V. *et al.* Broad-spectrum Non-toxic Antiviral Nanoparticles with a Virucidal Inhibition Mechanism (submitted). *Nature Materials* (2017).

78. Huang, R., Carney, R. P., Stellacci, F. & Lau, B. L. T. Colloidal Stability of Self-Assembled Monolayer-Coated Gold Nanoparticles: The Effects of Surface Compositional and Structural Heterogeneity. *Langmuir* **29**, 11560–11566 (2013).
79. Huang, R., Carney, R. P., Stellacci, F. & Lau, B. L. T. Protein–nanoparticle interactions: the effects of surface compositional and structural heterogeneity are scale dependent. *Nanoscale* **5**, 6928–6935 (2013).
80. Huang, R., Carney, R. P., Ikuma, K., Stellacci, F. & Lau, B. L. T. Effects of Surface Compositional and Structural Heterogeneity on Nanoparticle–Protein Interactions: Different Protein Configurations. *ACS nano* **8**, 5402–5412 (2014).
81. Knoll, M. & Ruska, E. Das Elektronenmikroskop. *Z. Physik* **78**, 318–339 (1932).
82. Kausche, G. A., Pfankuch, E. & Ruska, H. Die Sichtbarmachung von pflanzlichem Virus im Übermikroskop. *Naturwissenschaften* **27**, 292–299 (1939).
83. Williams, R. C. & WYCKOFF, R. W. G. ELECTRON SHADOW MICROGRAPHY OF THE TOBACCO MOSAIC VIRUS PROTEIN. *Science* **101**, 594–596 (1945).
84. Sharp, D. G., Lanni, F. & Beard, J. W. The egg white inhibitor of influenza virus hemagglutination. II. Electron microscopy of the inhibitor. *J. of biol. chem.* **185**, 681–688 (1950).
85. Heinmets, F. Modification of Silica Replica Technique for Study of Biological Membranes and Application of Rotary Condensation in Electron Microscopy. *Journal of Applied Physics* **20**, 384–388 (2004).
86. Brenner, S. & Horne, R. W. A negative staining method for high resolution electron microscopy of viruses. *Biochim. Biophys. Acta* **34**, 103–110 (1959).
87. Robin Harris, J. & Horne, R. W. Negative staining: A brief assessment of current technical benefits, limitations and future possibilities. *Micron* **25**, 5–13 (1994).
88. Stannard, L. M., Fuller, A. O. & Spear, P. G. Herpes Simplex Virus Glycoproteins Associated with Different Morphological Entities Projecting from the Virion Envelope. *Journal of General Virology* **68**, 715–725 (1987).
89. Goldsmith, C. S. & Miller, S. E. Modern uses of electron microscopy for detection of viruses. - PubMed - NCBI. *Clinical Microbiology Reviews* **22**, 552–563 (2009).
90. Kapikian, A. Z. *et al.* Visualization by immune electron microscopy of a 27-nm particle associated with acute infectious nonbacterial gastroenteritis. *J. Virol.* **10**, 1075–1081 (1972).
91. Lin, Y. *et al.* Probing the structure of the SARS coronavirus using scanning electron microscopy. *Antiviral therapy* (2004).
92. Porter, K. R. & Blum, J. A study in microtomy for electron microscopy. *The Anatomical Record* **117**, 685–709 (1953).
93. Glauert, A. M., Rogers, G. E. & Glauert, R. H. A new embedding medium for electron microscopy. *Nature* (1956).
94. Watson, M. L. Staining of Tissue Sections for Electron Microscopy with Heavy Metals. *The Journal of Cell Biology* **4**, 727–730 (1958).
95. Mettenleiter, T. C. Herpesvirus assembly and egress. *J. Virol.* **76**, 1537–1547 (2002).
96. Martin, N. *et al.* Virological synapse-mediated spread of human immunodeficiency virus type 1 between T cells is sensitive to entry inhibition. *J. Virol.* **84**, 3516–3527 (2010).
97. Adrian, M., Dubochet, J., Lepault, J. & McDowell, A. W. Cryo-electron microscopy of viruses. *Nature* (1984).
98. Dubochet, J. & McDowell, A. W. Vitrification of pure water for electron microscopy. *Journal of Microscopy* **124**, 3–4 (1981).
99. Dubochet, J. *et al.* Cryo-electron microscopy of vitrified specimens. *Quarterly Reviews of Biophysics* **21**, 129–228 (1988).

100. Dubochet, J., Lepault, J., Freeman, R., Berriman, J. A. & Homo, J. C. Electron microscopy of frozen water and aqueous solutions. *Journal of Microscopy* **128**, 219–237 (1982).
101. McDowall, A. W. *et al.* Electron microscopy of frozen hydrated sections of vitreous ice and vitrified biological samples. *Journal of Microscopy* **131**, 1–9 (1983).
102. Erickson, H. P. & Klug, A. Measurement and Compensation of Defocusing and Aberrations by Fourier Processing of Electron Micrographs. *Philosophical Transactions of the Royal Society of London B: Biological Sciences* **261**, 105–118 (1971).
103. Knapek, E. & Dubochet, J. Beam damage to organic material is considerably reduced in cryo-electron microscopy. *Journal of molecular biology* (1980).
104. Newcomb, C. J., Moyer, T. J., Lee, S. S. & Stupp, S. I. Advances in cryogenic transmission electron microscopy for the characterization of dynamic self-assembling nanostructures. *Current Opinion in Colloid & Interface Science* **17**, 350–359 (2012).
105. Grassucci, R. A., Taylor, D. & Frank, J. Visualization of macromolecular complexes using cryo-electron microscopy with FEI Tecnai transmission electron microscopes. *Nature Protocols* **3**, 330–339 (2008).
106. Grassucci, R. A., Taylor, D. J. & Frank, J. Preparation of macromolecular complexes for cryo-electron microscopy. *Nature Protocols* **2**, 3239–3246 (2007).
107. Crick, F. H. & Watson, J. D. Structure of small viruses. *Nature* **177**, 473–475 (1956).
108. Harrison, S. C., Olson, A. J., Schutt, C. E., Winkler, F. K. & Bricogne, G. Tomato bushy stunt virus at 2.9 Å resolution. *Nature* **276**, 368–373 (1978).
109. Rossmann, M. G. *et al.* Structure of a human common cold virus and functional relationship to other picornaviruses. *Nature* **317**, 145–153 (1985).
110. Crowther, R. A. Procedures for Three-Dimensional Reconstruction of Spherical Viruses by Fourier Synthesis from Electron Micrographs. *Philosophical Transactions of the Royal Society of London B: Biological Sciences* **261**, 221–230 (1971).
111. Chang, J., Liu, X., Rochat, R. H., Baker, M. L. & Chiu, W. Reconstructing virus structures from nanometer to near-atomic resolutions with cryo-electron microscopy and tomography. *Advances in experimental medicine and biology* **726**, 49–90 (2012).
112. Saxton, W. O., Baumeister, W. & Hahn, M. Three-dimensional reconstruction of imperfect two-dimensional crystals. *Ultramicroscopy* **13**, 57–70 (1984).
113. Ke, X. *et al.* Three-dimensional analysis of carbon nanotube networks in interconnects by electron tomography without missing wedge artifacts. *Microsc. Microanal.* **16**, 210–217 (2010).
114. Lasker, K. *et al.* Molecular architecture of the 26S proteasome holocomplex determined by an integrative approach. *PNAS* **109**, 1380–1387 (2012).
115. Danev, R., Buijsse, B., Khoshouei, M., Plitzko, J. M. & Baumeister, W. Volta potential phase plate for in-focus phase contrast transmission electron microscopy. *PNAS* **111**, 15635–15640 (2014).
116. Meyer, R. R. & Kirkland, A. I. Direct electron detector. *United States Patent* (2011).
117. Kühlbrandt, W. The Resolution Revolution. *Science* **343**, 1443–1444 (2014).
118. Schweitzer, A. *et al.* Structure of the human 26S proteasome at a resolution of 3.9 Å. *PNAS* **113**, 7816–7821 (2016).
119. Dubochet, J., McDowall, A. W., Menge, B., Schmid, E. N. & Lickfeld, K. G. Electron microscopy of frozen-hydrated bacteria. *Journal of Bacteriology* **155**, 381–390 (1983).
120. Hughes, L., Hawes, C., Monteith, S. & Vaughan, S. Serial block face scanning electron microscopy—the future of cell ultrastructure imaging. *Protoplasma* **251**, 395–401 (2013).

121. Knott, G., Rosset, S. & Cantoni, M. Focussed Ion Beam Milling and Scanning Electron Microscopy of Brain Tissue. *JoVE* e2588–e2588 (2011).
122. Korogod, N., Petersen, C. C. H. & Knott, G. W. Ultrastructural analysis of adult mouse neocortex comparing aldehyde perfusion with cryo fixation. *Elife* **4**, e05793 (2015).
123. Rigort, A. *et al.* Focused ion beam micromachining of eukaryotic cells for cryoelectron tomography. *PNAS* **109**, 4449–4454 (2012).
124. Plitzko, J. M., Rigort, A. & Leis, A. Correlative cryo-light microscopy and cryo-electron tomography: from cellular territories to molecular landscapes. *Current Opinion in Biotechnology* **20**, 83–89 (2009).
125. Kukulski, W., Schorb, M., Kaksonen, M. & Briggs, J. A. G. Plasma Membrane Reshaping during Endocytosis Is Revealed by Time-Resolved Electron Tomography. *Cell* **150**, 508–520 (2012).
126. Zhou, Z. H., Chen, D. H., Jakana, J., Rixon, F. J. & Chiu, W. Visualization of Tegument-Capsid Interactions and DNA in Intact Herpes Simplex Virus Type 1 Virions. *J. Virol.* **73**, 3210–3218 (1999).
127. Zhou, Z. H. *et al.* Seeing the Herpesvirus Capsid at 8.5 Å. *Science* **288**, 877–880 (2000).
128. Heymann, J. B. *et al.* Dynamics of herpes simplex virus capsid maturation visualized by time-lapse cryo-electron microscopy. *Nat Struct Biol* **10**, 334–341 (2003).
129. Cardone, G. *et al.* Visualization of the herpes simplex virus portal in situ by cryo-electron tomography. *Virology* **361**, 426–434 (2007).
130. Rochat, R. H. *et al.* Seeing the portal in herpes simplex virus type 1 B capsids. *J. Virol.* **85**, 1871–1874 (2011).
131. Newcomb, W. W. *et al.* The UL6 gene product forms the portal for entry of DNA into the herpes simplex virus capsid. *J. Virol.* **75**, 10923–10932 (2001).
132. Bauer, D. W., Huffman, J. B., Homa, F. L. & Evilevitch, A. Herpes Virus Genome, The Pressure Is On. *Journal of the American Chemical Society* **135**, 11216–11221 (2013).
133. Sae-Ueng, U. *et al.* Major capsid reinforcement by a minor protein in herpesviruses and phage. *Nucleic acids research* **42**, 9096–9107 (2014).
134. Harrison, S. C. Viral membrane fusion. *Nat. Struct. Mol. Biol.* **15**, 690–698 (2008).
135. Rey, F. A. Molecular gymnastics at the herpesvirus surface. *EMBO reports* **7**, 1000–1005 (2006).
136. Maurer, U. E., Sodeik, B. & Grünewald, K. Native 3D intermediates of membrane fusion in herpes simplex virus 1 entry. *PNAS* **105**, 10559–10564 (2008).
137. Zeev-Ben-Mordehai, T., Hagen, C. & Grünewald, K. A cool hybrid approach to the herpesvirus ‘life’ cycle. *Current Opinion in Virology* **5**, 42–49 (2014).
138. Heldwein, E. E. *et al.* Crystal structure of glycoprotein B from herpes simplex virus 1. *Science* **313**, 217–220 (2006).
139. Maurer, U. E. *et al.* The Structure of Herpesvirus Fusion Glycoprotein B-Bilayer Complex Reveals the Protein-Membrane and Lateral Protein-Protein Interaction. *Structure* **21**, 1396–1405 (2013).
140. Holthausen, D. J., Lee, S. H., Kumar, V. & Bouvier, N. M. An Amphibian Host Defense Peptide Is Virucidal for Human H1 Hemagglutinin-Bearing Influenza Viruses. *Immunity* **46**, 587–595 (2017).
141. Verma, A. *et al.* Surface-structure-regulated cell-membrane penetration by monolayer-protected nanoparticles. *Nature Materials* **7**, 588–595 (2008).
142. Jacob Silva, P. H. Discriminative adsorption of amphiphilic monolayer protected gold nanoparticles on amyloid fibers. 1–161 (2016).

-
143. Daniel, M. & Astruc, D. Gold nanoparticles: assembly, supramolecular chemistry, quantum-size-related properties, and applications toward biology, catalysis, and nanotechnology. *Chem. Rev* **104**, 293–346 (2004).
144. Carney, R. P. *et al.* Determination of nanoparticle size distribution together with density or molecular weight by 2D analytical ultracentrifugation. *Nature Communications* **2**, 335–8 (2011).
145. Haldar, B., Mallick, A. & Chattopadhyay, N. Supramolecular Inclusion in Cyclodextrins: A Pictorial Spectroscopic Demonstration. *Journal of chemical education* **85**, 429 (2008).
146. Donalisio, M. *et al.* In vitro anti-Herpes simplex virus activity of crude extract of the roots of *Nauclea latifolia* Smith (Rubiaceae). *BMC Complementary and Alternative Medicine* 2013 **13**:1 **13**, 266 (2013).
147. Prichard, M. N. *et al.* A microtiter virus yield reduction assay for the evaluation of antiviral compounds against human cytomegalovirus and herpes simplex virus. *Journal of Virological Methods* **28**, 101–106 (1990).
148. Schneider, C. A., Rasband, W. S. & Eliceiri, K. W. NIH Image to ImageJ: 25 years of image analysis. *Nature methods* **9**, 671–675 (2012).
149. Kremer, J. R., Mastronarde, D. N. & McIntosh, J. R. Computer visualization of three-dimensional image data using IMOD. *Journal of Structural Biology* **116**, 71–76 (1996).
150. Chowdary, T. K. *et al.* Crystal structure of the conserved herpesvirus fusion regulator complex gH-gL. *Nat. Struct. Mol. Biol.* **17**, 882–888 (2010).
151. Bowman, B. R., Baker, M. L., Rixon, F. J., Chiu, W. & Quirocho, F. A. Structure of the herpesvirus major capsid protein. *The EMBO Journal* **22**, 757–765 (2003).
152. Zhang, L. *et al.* Nanoparticles in medicine: therapeutic applications and developments. *Clin. Pharmacol. Ther.* **83**, 761–769 (2008).
153. Bobo, D., Robinson, K. J., Islam, J., Thurecht, K. J. & Corrie, S. R. Nanoparticle-Based Medicines: A Review of FDA-Approved Materials and Clinical Trials to Date. *Pharmaceutical Research* **33**, 2373–2387 (2016).
154. Davis, M. & Brewster, M. Cyclodextrin-based pharmaceuticals: past, present and future. *Nat Rev Drug Discov* **3**, 1023–1035 (2004).

Curriculum Vitae

CONTACT INFORMATION

Address	Marie Mueller / Chemin du Levant 3 / 1005 Lausanne, CH
mail	marie.mueller@mailbox.org
mobile	+41 78 605 10 34
LinkedIn	muellermarie

PERSONAL INFORMATION

Birthdate	05.02.1986
Nationality	German
Languages	(mother tongue); English (C2); French (C1); Dutch (A2)

EMPLOYMENT HISTORY

2011-2017	PhD thesis in Material Science and Engineering at the SUNMIL-Group at the École Polytechnique Fédérale de Lausanne (EPFL), CH "Broad-spectrum Antiviral Nanoparticles: a morphological CryoEM Study on the Interaction of Nanoparticles and Viruses" supervised by Prof. Francesco Stellacci
2014-2015	Teaching "Thermodynamics for Materials Science" Prof. Francesco Stellacci
2011	Master Thesis at the SUNMIL-Group at the EPFL, CH "Vaccine-delivery to dendritic cells with striped nanoparticles"
2009	Internship at the SuNMaG-Group at the Massachusetts Institute of Technology (MIT), Cambridge, MA, USA "Drug-delivery with striped nanoparticles"
2008	Bachelor Thesis at the Institute of Biomedical Engineering (IBMT), University of Rostock, DE "In vitro characterisation of clogging properties of stents in the GI tract"
2007	Research assistant for Biomaterials at the IBMT, University of Rostock, DE

EDUCATION

- 2008-2011 Biotechnology Diploma, Ecole supérieure de Biotechnologie, Strasbourg, FR
Trinational studies at Universities of Basel (CH), Strasbourg (FR), Freiburg and Karlsruhe (Germany); completed with a French “Diplôme d'Ingénieur” and a German “Diplom-Biotechnologe”
- 2010-2011 Master of Science in Biotechnology and therapeutic innovation, University of Strasbourg, FR
- 2008-2005 Bachelor of Science in Medical Biotechnology, University of Rostock, DE
- 2005 Abitur, European school Ernst-Moritz-Arndt Gymnasium, Bergen, DE

PUBLICATIONS

- 2017 “Broad-spectrum Virucidal Nanoparticles: Inducing Irreversible Viral Changes, a novel approach towards broad-spectrum virucidal drugs” [under review at Nature Materials]
Andreozzi, P., Cagno, V., D'Alicarnasso, M., Jacob Silva, P.H., **Mueller, M.**, Vallino, M., Weber, J., Vukovic, L., Janecek, E.R., Jones, S., Sanavio, B., Martinelli, C., Donalisio, M., Kral, P., Krol, S., Lembo, D., Stellacci, F.
- 2012 Dynamic Cellular Uptake of Mixed-Monolayer Protected Nanoparticles. *Biointerphases* 7, 3-11 (2012)
Carney, R.P.* , Carney, T.M.* , **Mueller, M.*** & Stellacci, F.

EXTRACURRICULAR COMMITMENT

- 2008-2013 Young European Biotech Network (YEBN)
2013 Chairwoman
2012 Vice-Chairwoman
2009-2011 Leader of the YEBN industrial PhD programme (iPhD)
2009-2011 Newsletter-editor
Active YEBN member since 2008
- 2008-2011 Nouvelle Génération des Biotechnologistes (NGB)
2011 Lead organizer of the Comm4Biotech Science communication congress
2008-2011 Co-founder of NGB and Vice-Chairwoman in charge of international communication

